Cardiac Tropomyosin D137L Mutation Decreases Structural Flexibility to Cause Systolic Dysfunction

BY

SUMEYYE YAR
B.S., Sabanci University, Istanbul, 2007
M.S., Rush University, Chicago, 2009

THESIS

Submitted as partial fulfillment of the requirements
for the degree of Doctor of Philosophy in Biochemistry and Molecular Genetics
in the Graduate College of the
University of Illinois at Chicago, 2013

Chicago, Illinois

Defense Committee:

R. John Solaro, Chair and Advisor
Vadim Gaponenko, Co-Advisor
Karen J. Colley
Michael Caffrey
Pradip Raychaudhuri
Tomoyoshi Kobayashi, Physiology and Biophysics

To Tunç
To my Family,
Past, Present, and Future,
Those who forged the way, Those who sustain me, and Those who will follow

ACKNOWLEDGMENTS

First and foremost, I am deeply grateful to my advisor, R. John Solaro, for believing in me, giving me excellent advice, providing me the space to explore my own curiosity, and for being an exceptional scientist. I feel incredibly lucky to have been able to spend years talking to and learning from someone so insightful, knowledgeable and generous.

I am indebted to Tomoyoshi Kobayashi for his constructive comments and his meticulous review of my work during every stage of this project, and more importantly, for his contagious passion for science. I am also deeply thankful to my co-advisor, Vadim Gaponenko, for never turning me away when I needed help, teaching me NMR and for providing me valuable scientific advice. I owe many thanks to rest of my committee members: Karen J. Colley, Pradip Raychaudhuri and Michael Caffrey, for their excellent guidance, comments and support.

My grateful recognition goes to Minae Kobayashi for helping me with DSC and NMR experiments and reviewing my work. I also want to thank Shamim Chowdhury for her friendship and her help with Echocardiography measurements. I would like to express my gratefulness to the current and former members of the Solaro lab., particularly Chad Warren for helping me out with all sorts of science related questions that I had over the years, Jillian Simon for her friendship and providing me feedback during the writing process of this dissertation, and Robert T. Davis 3rd for his help with cardiomyocyte measurements. I am also thankful for those friends, who cheered me up during the most demanding times at UIC, especially Burcu Beştaş, Adriana Russ, Julie Mouannes Kozaili, Esther Calderon, Tangy Wilder and Raghu Nagalingam.

My most heartfelt gratitude goes toward my parents, Abdurrahman and Fatma, and my brother, Fatih, and my sister in law, Ayten, and joy of my life, my little nephew, Toprak Kuzey, for their unwavering love and support throughout my life. The hardest part of my Ph.D. years has been to live thousands of miles apart from them. Thanks for always being there for me.

Above all, I am thankful to Tunç, my husband and fellow traveler in life, my best friend and favorite chef for inspiring me, keeping me smiling, and for sharing all the challenges in life with me. His love keeps me afloat.

SY

TABLE OF CONTENTS

TABLE OF CONTENTS (continued)

CHAPTER PAGE

TABLE OF CONTENTS (continued)

CHAPTER PAGE

LIST OF TABLES

LIST OF FIGURES

FIGURE PAGE

LIST OF FIGURES (continued)

FIGURE PAGE

LIST OF ABBREVIATIONS

A	Maximal velocity of blood slow in the late diastole
α-TM	alpha-Tropomyosin
ATP	Adenosine triphosphate
CM	Cardiomyopathy
CO	Cardiac output
C*p*	Heat capacity
CrP	Creatine phosphate
cTn	cardiac Troponin
cTnC	cardiac Troponin C
cTnI	cardiac Troponin I
cTnT	cardiac Troponin T
Cy	Cyanine dye
DCM	Dilated cardiomyopathy
DEAE-FF	diethylaminoethanol-fast flow
ΔH_{cal}	Calorimetric enthalpy of transition
DIGE	Difference in gel electrophoresis
d*P*/d*t*	The first derivative of the rate of pressure change over time
DSC	Differential scanning calorimetry
DTT	dithiothreitol
E	Maximal velocity of blood flow in the early diastole
EDP	End-diastolic pressure

LIST OF ABBREVIATIONS (continued)

EDPVR	End-diastolic pressure-volume relationship
EDTA	ethylenediaminetetraacetic acid
EDV	End-diastolic volume
EGTA	ethylene glycol tetraacetic acid
EF	Ejection fraction
ESPVR	End-systolic pressure-volume relationship
ESV	End-systolic volume
FPLC	Fast protein liquid chromatography
GAPDH	glyceraldehyde-3-phosphate dehydrogenase
HCM	Hypertrophic cardiomyopathy
Hr	High relaxing
HR	Heart rate
HSQC	Heteronuclear single quantum coherence
IV	Inter ventricular
IVRT	Isovolumetric relaxation time
LA	Left atrium
LV	Left ventricle
LVIDd	Left ventricular internal dimension in diastole
LVIDs	Left ventricular internal dimension in systole
MHC	Myosin heavy chain
MLC	Myosin light chain

LIST OF ABBREVIATIONS (continued)

Mon	Month
MOPS	3-(N-morpholino)propanesulfonic acid
MyBP-C	Myosin binding protein-C
n*H*	*Hill* coefficient
NMR	Nuclear magnetic resonance
NTG	Non-transgenic
P-	Phosphorylated
PCR	Polymerase Chain Reaction
PMSF	phenylmethylsulfonyl fluoride
PTM	Post translational modification
PV	Pressure-volume
S1	subfragment-1
SDS-PAGE	Sodium Sodecyl Sulfate Polyacrylamide Gel Electrophoresis
SL	Sarcomere length
SR	Sarcoplasmic Reticulum
SV	Stroke volume
TG	Transgenic
Tm	Transition temperature
WT	Wild Type
$[Ca^{2+}]i$	Intracellular Calcium concentration
2D	Two dimensional

SUMMARY

The general objective of the experiments carried out in this thesis was to fill major gaps in our understanding of how thin filament control mechanisms translate to regulation of cardiac function. Filling these gaps is essential to understanding and treating acquired and familial cardiac disorders linked to sarcomeric protein mutations. Here we focused on α-tropomyosin (α-TM) as a nodal point in control of the thin filament state. Structural flexibility of α-TM represents a significant, but poorly understood property, in the control of thin filament state and cardiac function. In this study, we specifically addressed the following: (i) the implications of the D137L mutation on the global structural flexibility of α-TM and (ii) the effects of D137L mutation on cardiac function. A highly integrative study employing a range of approaches from recombinantly expressed proteins to ejecting heart of a novel transgenic mouse model was carried out in order to address these objectives.

α-TM is a coiled-coil protein that cooperatively binds along the actin filaments and serves as a nodal point in control of calcium regulated cardiac muscle dynamics. α-TM has a conserved, charged residue (Asp137) located in the hydrophobic core of its coiled-coil structure. This is distinct to the α-TM coiled-coil in that the residue is found at a position typically occupied by a hydrophobic residue. In a previous *in vitro* study, which substituted this Asp137 residue with a more expected canonical Leu, it was demonstrated that Asp137 destabilizes a local region in the middle of α-TM, inducing a more flexible region that is important for modulating the cooperative activation of the thin filaments. In the first part of this thesis, we extended these earlier findings and demonstrated that the D137L mutation decreased structural flexibility of α-TM, which was a global effect that caused long-range structural rearrangements.

We know next to nothing of the relative significance of α-TM flexibility in sarcomeric control mechanisms *in vivo.* Therefore in the second part of this study, we investigated implications of α-TM flexibility on *in situ* cardiac function of a novel transgenic mouse model expressing α-TM-D137L in the heart. To our knowledge, our findings are the first to show that a marked decrease in α-TM's structural flexibility due to substitution of Asp137 with Leu depressed systolic parameters of cardiac contraction and ultimately led to a phenotype similar to dilated cardiomyopathy in α-TM-D137L transgenic mouse heart.

α-TM molecules undergo calcium and myosin dependent regulatory relocations, azimuthally, over the surface of the actin filaments during cardiac muscle contraction and relaxation. Structural flexibility of α-TM is thought to have a key role in these relocations. Our results demonstrated that expression of α-TM-D137L in transgenic mouse hearts depressed calcium dependent activation of thin filaments. However, there was no change in the strongly bound cross-bridge dependent activation in skinned fiber preparations. Therefore we proposed a mechanism that the decreased flexibility of α-TM-D137L impede calcium dependent relocation of α-TM on actin resulting in a delay in time sensitive activation and relaxation processes of cardiac muscle, which eventually lead to systolic dysfunction in transgenic mouse hearts.

Collectively, this work has shed light on a functionally important structural characteristic of α-TM and suggested a possible association between flexibility of α-TM and cardiac disorders. A change in flexibility of α-TM has been previously reported for some cardiomyopathy linked α-TM mutations. While α-TM-D137L mutation is not associated with inherited cardiomyopathies, our findings provide unique insights into our understanding of both how disease-linked α-TM

point mutations can significantly alter the dynamic properties of α-TM, as well as, how altering α-TM flexibility can have a significant effect on calcium-dependent thin filament regulation and ultimately on cardiac function.

I. INTRODUCTION AND BACKGROUND

Parts of this research were originally published in Journal of Biological Chemistry. **Yar, S**., Chowdhury, S. A., Davis, R. T., 3rd, Kobayashi, M., Monasky, M. M., Rajan, S., Wolska, B. M., Gaponenko, V., Kobayashi, T., Wieczorek, D. F., and Solaro, R. J. Conserved Asp-137 Is Important for both Structure and Regulatory Functions of Cardiac alpha-Tropomyosin (alpha-TM) in a Novel Transgenic Mouse Model Expressing alpha-TM-D137L. *J Biol Chem.* (2013); 288, p.16235-16246.

Awareness of the role of alpha-tropomyosin (α-TM) in the regulation of heart function is growing. Studies in the field are mainly directed towards understanding mechanisms at both structural and physiological levels in order to develop therapeutic strategies for the treatment of TM-linked cardiac disorders. In this study, we focused on understanding the role of flexibility of α-TM, which is a hotly debated structural property in regulating cardiac function.

A. General Introduction to Tropomyosin

TMs are ubiquitous, highly conserved proteins that constitute a family of actin-binding proteins regulating actin filament function in both muscle and non-muscle cells. In non-muscle cells TM functions in an extraordinary array of cellular functions such as cell motility, cell shape, cell adhesion, vesicle transport, endocytosis, exocytosis, cytokinesis, and membrane function (1). In muscle cells, TM has a more defined function to regulate interactions between thin and thick filaments and hence the contraction of muscle (2). Although TM function is better understood in muscle, where it was first discovered in the 1940's (3,4), more than 40 isoforms of TM have been identified in different tissues (1). TM gene structure and generation of distinct

isoforms by alternative splicing and by utilization of alternative promoters are extensively reviewed elsewhere (2,5-7).

In vertebrate striated muscle, there are four main TM isoforms: α-TM, β-TM, γ-TM and κ-TM, however γ-TM is not expressed in cardiac cells. While β-TM is expressed during developmental stages in the embryo, α-TM, which is the main subject of this thesis, is the predominant isoform in adult human and mouse cardiac muscle (6,8). Although there is almost 100% α-TM expression in adult mouse hearts, in a recent study it was shown that there is 90-94% α-TM, 3-5% β-TM, and 3-5% κ-TM expression in adult human hearts (9,10). α-TM is essential for cardiac development and function as demonstrated by knockout of the α-TM gene resulting in embryonic lethality in mice at 10-14 days, corresponding to the development of the myocardium (11,12).

α-TM has an uninterrupted α-helical parallel coiled-coil structure along its entire length in which two α-helices associate to form a supercoil. A repeating pattern of hydrophobic residues in the first and the fourth positions of succeeding groups of 7 residues pack in a "knobs" into "holes" fashion to hold two chains together. TM molecules associate end-to-end to form continuous filaments and bind along the actin filaments.

From a clinical point of view, mutations in the cardiac α-TM gene are directly linked to cardiomyopathies (CMs), dilated cardiomyopathy (DCM) and hypertrophic cardiomyopathy (HCM) (13). It is still unclear how single mutations within the α-TM gene translate to cardiac diseases. However studies on the mechanisms using mouse models and biochemical approaches are promising.

B. Regulation of Cardiac Muscle Contraction and Tropomyosin

Cardiac muscle contraction is initiated by a depolarizing current within the cardiomyocyte, leading to an action potential that lasts about 300 msec. The coupling between this action potential and contraction is called "excitation-contraction coupling" (Figure 1). Ca^{2+} has an essential role in this process. When the cardiomyocyte is depolarized, small amounts of Ca^{2+} ions enter the cell through voltage-gated L-type Ca^{2+} channels located throughout the t-tubule system (14). This Ca^{2+} entry is sensed by ryanodine receptors on the surface of the sarcoplasmic reticulum (SR), triggering opening of the ryonodine receptors and a subsequent release of larger amounts of Ca^{2+} from the SR. This process is called "Ca^{2+}-induced-Ca^{2+} release" (15). During this process, intracellular Ca^{2+} concentration ($[Ca^{2+}]_i$) increases from around 100 nM to a micromolar range. Free intracellular Ca^{2+} interacts with myofilaments, leading to shortening of the myocyte and resultant muscle contraction. During repolarization, Ca^{2+} is transported out of the cytosol via SR ATPase located on the SR and Na^+/Ca^{2+} exchangers located on sarcolemma bringing $[Ca^{2+}]_i$ back to diastolic levels. While these two processes are the main means for Ca^{2+} removal from the cytosol, mitochondrial Ca^{2+} uptake and Ca^{2+} pumps located on plasma membrane also contribute in reducing cytosolic Ca^{2+} during transition diastole. This decrease in cytosolic $[Ca^{2+}]$ leads to cardiomyocyte relaxation. One should note that abnormalities in cardiomyocyte Ca^{2+} handling are commonly observed in cardiac diseases.

At the myofilament level, force generation during cardiac muscle contraction results from adenosine triphosphate (ATP) coupled cyclic interactions between the myofilament proteins myosin and actin. During this process, cardiac troponin (cTn), the Ca^{2+} receptor, exerts its effects indirectly on actin filaments by acting on TM, which regulates actin-myosin interactions. cTn is

a heterotrimeric protein complex composed of cardiac troponin-C (cTnC), the Ca^{2+}- binding unit that has one regulatory Ca^{2+}-binding site; cardiac troponin-T (cTnT), the TM-binding unit that anchors the Tn complex to actin-TM; and cardiac troponin-I (cTnI), the inhibitory unit that Ca^{2+}-dependently inhibits muscle contraction [3,11,12]. cTn, together with TM and polymerized-actin, constitutes the thin filament, whereas myosin is the main component of the thick filament. The overall stoichometry of the thin filament is seven actin subunits, one TM and one cTn complex. Once $[Ca^{2+}]_i$ increase, Ca^{2+}-binds to the single regulatory site on cTnC initiating a series of cooperative interactions among the thin filament proteins. This allows for the effective interactions between myosin and actin. Detachment of Ca^{2+} from cTnC initiates another set of conformational changes among thin filament proteins and triggers muscle relaxation. In addition to cytosolic $[Ca^{2+}]$, muscle contraction and relaxation are also mediated by myofilament Ca^{2+} sensitivity. Given this, muscle contraction has the ability to be strengthened by increasing $[Ca^{2+}]_i$ or myofilament Ca^{2+} sensitivity.

Numerous models have been proposed over the years to better understand the details of the molecular mechanism for the Ca^{2+}-dependent switch of muscle contraction described above and have been the subject of numerous reviews (16-18). The current perceptions of thin filaments in relaxed and contracted states are depicted in Figure 2. In the relaxed state, there is no Ca^{2+}-binding to the regulatory site of cTnC, and the position of TM impedes force generating cross-bridges from reacting with actin. TM is held in this state by the inhibitory actions of the hyper variable N-terminal tail of cTnT in conjunction with the C-terminal mobile domain of cTnI (19-21). During contraction, Ca^{2+}-binding to cTnC exposes a hydrophobic patch on its surface that attracts the inhibitory C-terminus of cTnI [16]. This critical event releases inhibitory interactions between the mobile domain of cTnI and actin-TM. Release of inhibition allows the

movement of TM over the surface of actin thereby exposing myosin binding sites on actin. Myosin can then bind to actin and use ATP hydrolysis for force generation. TM has an essential role in this regulatory mechanism transmitting the information from the Ca^{2+} receptor to the actin-myosin interaction that generates force.

A relatively new, widely accepted three-state model describing TM's role in the regulation of muscle contraction was developed by McKillop and Geeves (22). This model suggested that thin filaments exist in rapid equilibrium between three states in which TM occupies three distinct positions on actin (Figure 3).When $[Ca^{2+}]_i$ is low, thin filaments are in the "blocked or B" state where all myosin binding to actin is blocked by TM. In this state, muscle is relaxed and the heart is in diastole. When $[Ca^{2+}]_i$ increases and Ca^{2+} binds to cTnC, TM moves ~25° towards the inner groove of actin, thus exposing weak myosin binding sites (23-25). In this "closed or C" state, only the reaction of weakly-bound crossbridges is allowed. Another ~10° shift of TM is promoted only after isomerization of myosin and strong-binding to actin which brings the thin filaments to the fully activated "open or M" state (25). In this fully active state, the heart is in systole and pressure develops as the cardiac muscle produces force. In this model, Ca^{2+} binding to cTnC is the regulator for the equilibrium between "blocked" and "closed" states, while strong crossbridge binding is the regulator for the equilibrium between "closed" and "open" states. It is believed that structural flexibility of TM is one of the main mediators of these regulatory movements of TM on the surface of actin during muscle activation (systole) and relaxation (diastole) processes.

C. Composition, Structure and Flexibility of Tropomyosin

Comprehensive reviews on structural features of TM were published earlier (26-28). Therefore this section focuses on flexibility of TM after providing a brief background on the essential features of TM's amino acid sequence and structure.

TM was first isolated by Bailey in 1946 and described as an asymmetric protein (4). Following an X-ray study by Astbury (29), Crick proposed that TM has an α-helical coiled-coil structure with two helices that associate to form a supercoil (30). In 1975, the amino acid sequence of α-TM was completed (31). It was deduced that TM is a 284 amino acid, negatively charged protein with a molecular weight of ~33,000 Da. (32). The two helices of TM associate in parallel and in register to form a rod-shaped, 40 nm long coiled-coil that spans the length of seven actin subunits. NH2-acetylation facilitates end-to-end polymerization of TM along the actin filaments (33,34). Detailed investigations of the amino acid sequence of TM confirmed an anticipated heptapeptide repeat structure (Figure 4B), where a repeating pattern of hydrophobic residues in the first and fourth positions of succeeding groups of seven residues pack in a "knobs" into "holes" fashion to hold the two chains together. In this so called heptapeptide repeat structure, the positions of residues are labeled as *a-b-c-d-e-f-g* (see Figure 4). Non-polar residues are found at the hydrophobic core of the two helices at positions *a* and *d*, where they provide stability to the protein. On the other hand, *e* and *g* positions favor charged residues and can form salt bridges between two helices to further stabilize the coiled-coil. Residues located at positions *b*, *c* and *f* are often polar or charged and located on the exterior of the coiled-coil. These residues are thought to confer solubility to TM and interact with other thin filament proteins. Further

investigations of the amino acid sequence of TM revealed seven quasi-equivalent actin binding zones (periods) with a periodic distribution of charged and non-polar residues (35,36).

Destabilizing breaks in the heptapeptide repeat structure, which are known as “skips” or “stutters”, are common in proteins with long coiled-coil structures. They alter flexibility of long coiled-coil domains by affecting their coiled-coil stability, as in myosin (37), and thus regulate their function or molecular interactions. However, TM is unique in that it has no discontinuity in its heptapeptide repeats. On the other hand, it is well established that TM has structurally distinct domains that differ in their stability and flexibility. The first evidence for non-uniform stability of TM along the molecule came from elucidation of multiple thermal unfolding domains at different temperatures and different levels of susceptibility to proteolysis (38-40). The X-ray crystal structure of the full length TM is currently available at 7Å resolution (Figure 5). This structure confirmed local perturbations in the coiled-coil structure of TM illustrating a flexible molecule (41,42). More recently, as the structure of a series of TM fragments became available knowledge of TM’s atomic structure has finally emerged at a higher resolution (43-47). These data illuminated the dynamic nature of TM’s structure more clearly. However, it was not yet understood what was responsible for the dynamic properties and structurally distinct domains along the uninterrupted heptapeptide repeat structure of TM. In these higher resolution structures, Brown et al. pointed out that the coiled-coil interface of TM was less well packed around Ala residues or so called “Ala clusters” (Figure 4A), which are spread along the protein and located mainly in the core positions (*a* and *d*) (45). It was postulated that “Ala clusters” function as “skips” or “stutters” in TM structure and they destabilize regions of TM to provide flexibility to the molecule. This was the first high resolution evidence showing that the core

residue sequence of TM was important for its flexibility. Using mutagenesis studies, these destabilizing Ala clusters were later shown to be necessary for binding of TM to actin (48,49).

In addition to poorly packed Ala cluster regions, subsequent studies identified another poorly packed region around the residue Asp137 (Figure 5) (44). This negatively charged residue is unexpectedly located at the *d* position in the heptad repeat sequence (Figure 4A). A non-polar residue is expected instead at a *d* position, because, as described above, it is part of the stabilizing hydrophobic interface or 'core' between the two chains of the TM coiled-coil dimer. A previous database search reported that although exceptional polar and charged residues are found at *a* and *d* positions of many coiled-coil proteins, Asp is alone in being excluded from *d* positions of all parallel coiled-coil proteins identified in the Protein Data Bank (50). Interestingly, Asp137 is conserved across species and isoforms, except those from yeast, suggesting that it is important to TM function. The presence of two negatively charged residues in the hydrophobic core of a parallel coiled-coil structure is expected to increase flexibility by causing destabilization within this region. Earlier studies reported that Asp137 is located at a particularly unstable mid-region of α-TM that is susceptible to trypsin cleavage at a single site between Arg133 and Ala134 (40). Therefore Sumida et al. tested how conversion of Asp137 to a hydrophobic Leu affects tryptic susceptibility of TM (51). It was shown in this previous study that the D137L mutation prolonged tryptic cleavage time of TM. It is known that proteolytic susceptibility is related to the fraction of time that the cleavage site is accessible to protease via local fluctuations (52), thus a decrease in proteolytic susceptibility suggested a decrease in local fluctuations and local flexibility. In other words, this result demonstrated that Asp137 is responsible for local flexibility of TM in that region. In addition to the structural importance of the negatively charged Asp137, this residue was also shown to be important for *in vitro* regulatory functions of TM. Although

actin binding was shown to be preserved, reconstituted filaments regulated by α-TM-D137L indicated a higher myosin subfragment-1 (S1) ATPase activity (51). Despite previous studies on the role of Asp137 in local flexibility and *in vitro* regulatory function of TM, the role of Asp137 in global flexibility of TM, and more importantly, in its cardiac function has not yet been fully explored. In this study we addressed these gaps in the literature by examining the global structural implications of the D137L mutation on TM in the first part, and the physiological implications of D137L mutation on regulation of heart function in the second part.

D. Heart Disease and Tropomyosin

1. Cardiomyopathies

CMs are diseases of the myocardium (muscular tissue of the heart) that cause cardiac dysfunction. There are various causes of CMs, such as genetic and sporadic mutations of sarcomeric proteins as well as hypertension, ischemia and inflammation. This section focuses on CMs resulting from sarcomeric protein mutations. The significance of sarcomeric protein mutations in cardiac disease was first pointed out by Drs. J. and C. Seidman, who demonstrated a linkage between missense mutations in myosin heavy chain (MHC) and inherited HCM (53). After this initial finding, it was also shown that mutations in other sarcomeric proteins, including α-TM, cause HCM (54,55). Other α-TM mutations were later linked to inherited DCM, a phenotypically distinct disease from HCM. Identification of these CM-linked mutations in α-TM gene highlighted the key role of α-TM in human cardiac diseases. Twenty eight CM-linked mutations have been identified in α-TM to date (Figure 5 and Table I). Today we still do not

understand exactly the detailed molecular mechanism of how these disease-causing mutations of sarcomeric proteins deteriorate cardiac function.

a) Hypertrophic cardiomyopathy

Inherited HCM is an autosomal dominant disease that has characteristic features of thickened ventricular walls, myocyte disarray, fibrosis, increased Ca^{2+} sensitivity of myofilaments, systolic hyper contractility, cardiac arrhythmias and diastolic dysfunction. There is a high incidence of sudden cardiac death in athletes and young patients carrying HCM mutations. It is also known that HCM can progress to heart failure. Mutations in many sarcomeric proteins, such as cTnI, α- and β-MHC, cTnT, myosin light chains (MLC), myosin binding protein-C (MyBP-C) and α-TM have been associated with HCM. One should, however keep in mind that symptoms and disease severity are quite heterogeneous in patients and there are not many common functions perturbed due to different HCM-linked sarcomeric mutations. HCM is the most common cardiovascular single gene disorder with the incidence frequency of 1:500 (56). The incidence of α-TM mutations linked to HCM is less than 5% (57). To date, at least fifteen α-TM mutations linked to HCM have been identified (Figure 5 and Table I).

b) Dilated Cardiomyopathy

DCM is characterized by increased left ventricular volume or ventricular dilation, and systolic dysfunction, or impaired ability of heart muscle to contract. In some cases, diastolic abnormalities are present. It causes weakening of the ventricular walls and enlargement

of the heart, which impairs the blood pumping ability of the heart or depresses contractility. DCM can also progress to heart failure. Sudden cardiac death is also associated with DCM. It is a very common CM with an incidence of 36.5 out of 100,000 people (58). There are a number of causes of DCM, such as genetic, acquired, alcoholic/toxic, inflammatory, nutritional and idiopathic. Here we focus on DCM linked to sarcomeric protein mutations, specifically to α-TM mutations. In inherited genetic cases, autosomal-dominant inheritance is the predominant transmission pattern. Missense mutations on MHC, MyBPC, cTnT, actin and TM have been linked to DCM (58). At least twelve α-TM mutations linked to DCM have been identified up until now (Figure 5 and Table I).

c) Tropomyosin mutations linked to hypertrophic and dilated cardiomyopathies

As mentioned above, so far, twenty eight CM-linked mutations have been identified in α-TM (Figure 5 and Table I). Investigations that try to understand how these mutations cause cardiac disorders are inconclusive. There is no consistent pattern for the location of these CM-linked mutations in α-TM sequence: they lie on different periods and/or different position in the heptad repeats. Some lie within cTnT binding regions of α-TM around residues 175-190 and 258-284 (59). Some are located at the extreme C-terminus that is involved in end-to-end interactions of α-TM. Although the majority of these mutations (twenty one out of twenty eight) alter residues involved in stabilizing the coiled-coil structure of α-TM (*a, d, f, e* positions of heptad repeats), mutations are also found in *b,c* and *g* positions. Sixteen of these mutations result from a point mutation that causes a charge change in α-TM. Due to the coiled-coil structure of α-TM, charge change can play an important role both in its structure and its

interactions with other sarcomeric proteins. Functional effects of CM-linked α-TM mutations are studied using both *in vitro* thin filament preps reconstituted from recombinant proteins and transgenic (TG) mouse models are extensively reviewed elsewhere (13,60-62). In these extensive studies, the most consistent characteristic of HCM and DCM linked mutations has been identified as their effects on Ca^{2+} sensitivity of the thin filaments. While HCM mutants have been shown to increase Ca^{2+} sensitivity, DCM mutants showed an opposite effect with decreasing Ca^{2+} sensitivity. However recent studies demonstrated that there are significant exceptions to this characteristic as well, especially for DCM linked mutations (63). It was shown for example, in one study that DCM linked α-TM Asp230Asn mutation increases Ca^{2+} sensitivity (64). In recent years, the changes CM-linked mutations caused in the structural flexibility of α-TM have emerged as a hot topic in the field. From currently available studies on a number of HCM and DCM linked α-TM mutants, increased flexibility of TM appears to be the characteristic of HCM-linked mutations (Glu180Gly, Asp175Asn, Lys70Thr, and Ala63Val) (65-67), while the DCM-linked Glu40Lys and Glu54Lys mutations were reported to decrease TM flexibility (68). In this thesis, we showed that expression of decreased flexibility mutant α-TM-D137L in TG mouse hearts resulted in a phenotype similar to DCM. While it is likely that additional factors contribute to the disease mechanism, our findings support the hypothesis that altered flexibility of α-TM is an essential initial molecular abnormality that leads to disease phenotype.

E. Hypothesis and Objectives

Proteins need to have a balance between flexibility and stiffness in order to function properly. α-TM has poorly packed, destabilizing regions that provide flexibility to the molecule. However the importance of these flexible regions in cardiac function has not yet been adequately examined. Alterations in the flexibility of α-TM have been implicated by a number of CM linked TM mutations, making structural and functional implications of TM flexibility an important characteristic that needs to be fully understood. Our overall hypothesis is that altered flexibility of α-TM is a major initial molecular abnormality that leads to disease phenotype. It has been shown in a previous study that substitution of a conserved Asp137 to Leu decreases flexibility of α-TM at a local, central region and affects the cooperative activation of thin filaments *in vitro.* However, the role of Asp137 in global flexibility of α-TM, and more importantly, in cardiac function of α-TM has yet to be explored. Therefore our specific objectives in this study are as follows: (i) to understand global structural implications of the D137L mutation on α-TM, and (ii) to reveal the effects of the D137L mutation on cardiac function and investigate the underlying mechanism. Our findings from this study support our overall hypothesis and suggest a link between flexibility of TM and cardiac disorders.

FIGURES and TABLES

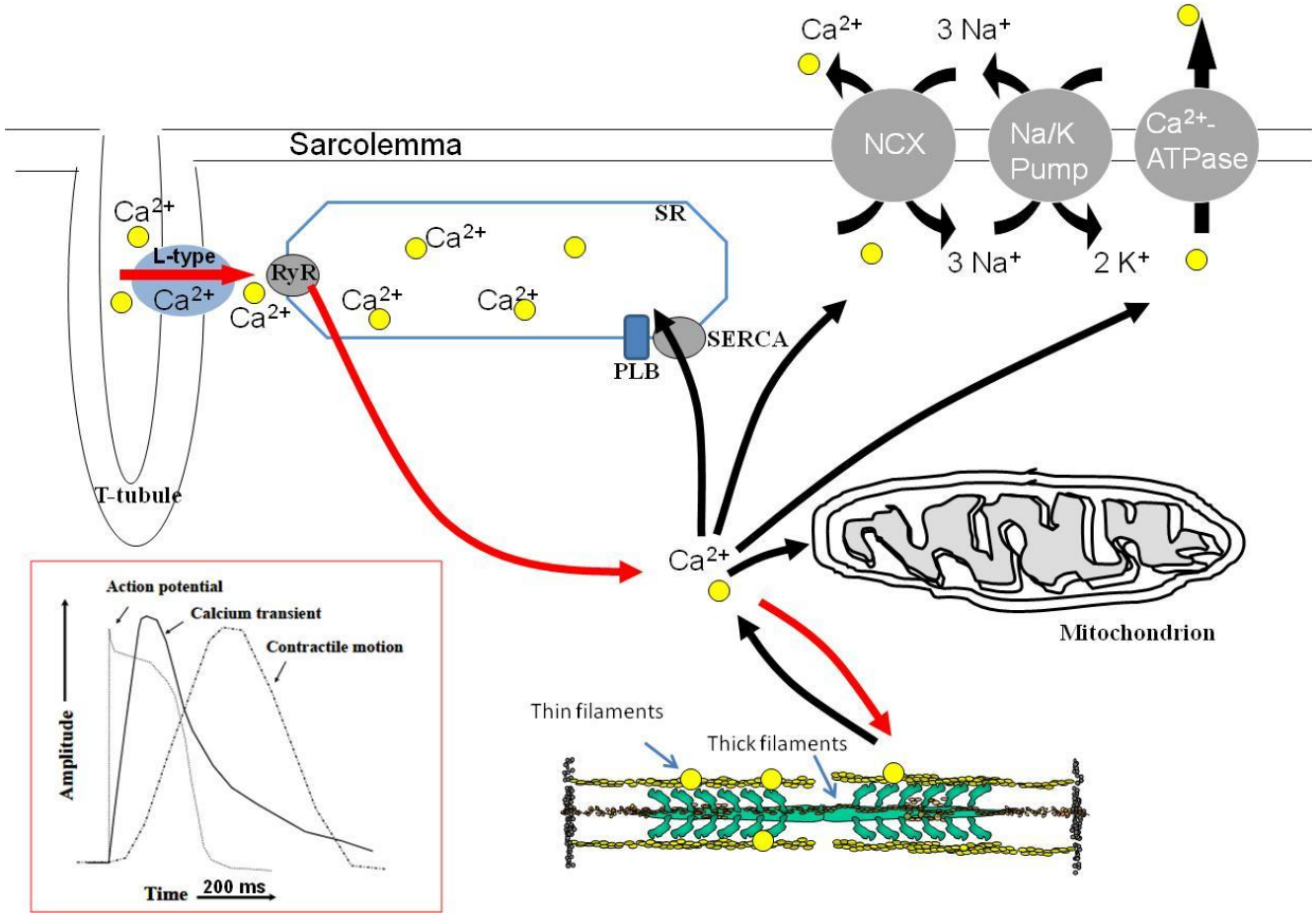

Figure 1. Cardiac excitation-contraction coupling. Depolarization of cell membrane by an action potential leads to Ca^{2+} entry to the cardiomyocyte through L-type Ca^{2+} channels. This "trigger Ca^{2+}" is sensed by ryanodine receptors (RyR) located on SR, which triggers larger amounts of Ca^{2+} release into the cytosol. This process is called "Ca^{2+}-induced-Ca^{2+} release". Binding of intracellular free Ca^{2+} to myofilaments, specifically to cTnC, leads to movement of actin relative to myosin (muscle contraction). During repolarization, Ca^{2+} is removed from the cytosol, leading to muscle relaxation. Inset shows time dependent appearance of action potential, Ca^{2+} release into the cytosol and cardiomyocyte contraction.

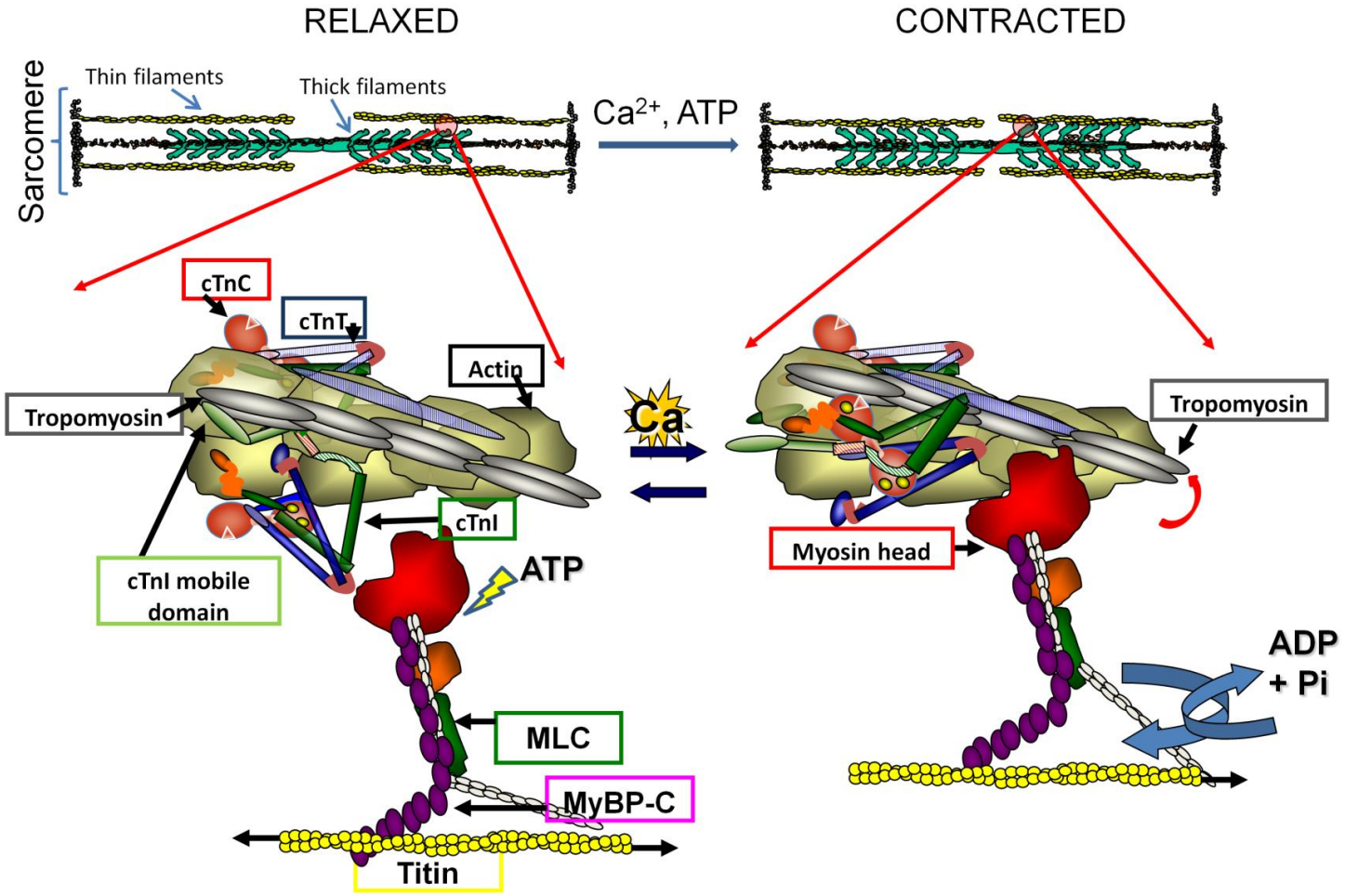

Figure 2. TM functions to regulate muscle contraction. Sarcomere is the smallest functional unit of striated muscle, which is mainly composed of thick and thin filaments. Thin filament is made up of actin, Tn complex and TM, whereas thick filament is mainly composed of myosin. Transition from relaxed to contracted state of muscle occurs when intracellular [Ca^{2+}] increases. When Ca^{2+} binds to TnC, inhibitory actions of Tn on TM is released. This critical event allows movement of TM over the surface of actin, which exposes myosin binding sites on actin. Myosin can then bind to actin and muscle contracts. (See text for more details) (Modified from the original figure courtesy of R. John Solaro)

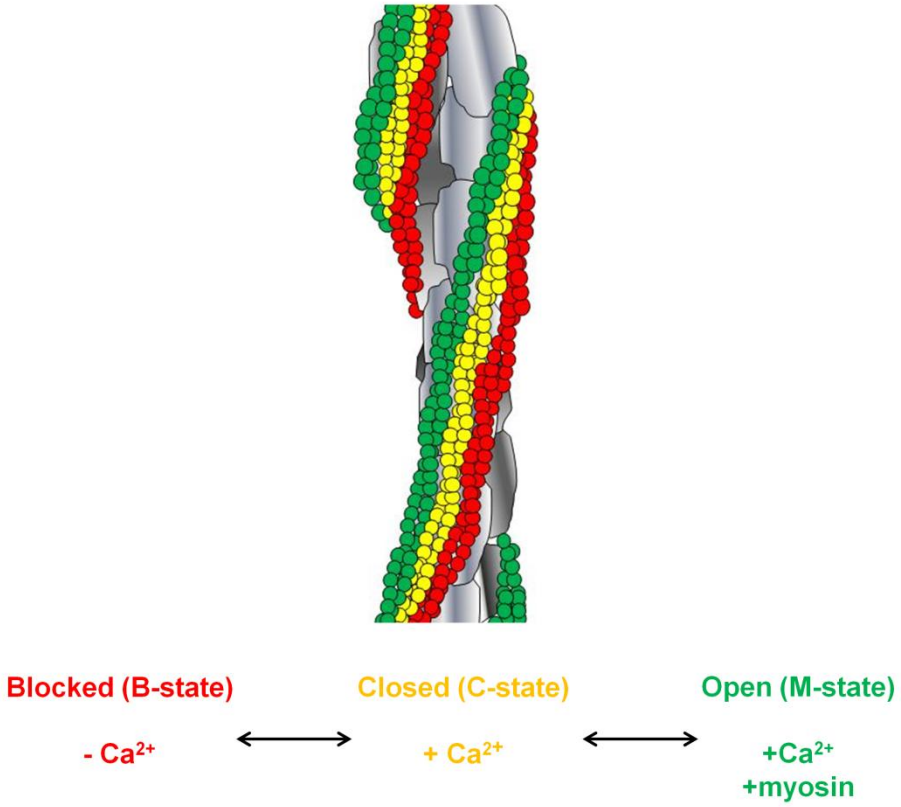

Figure 3. Three state of thin filaments. Three average positions of TM on the surface of actin are shown. When intracellular [Ca^{2+}] is low, TM is in B-state, where it covers weak myosin binding sites on the surface of actin (red). Once intracellular [Ca^{2+}] rises and Ca^{2+} binds to cTnC, moves TM azimuthally towards the inner domain of actin (C-state shown in yellow). At C-state, reaction of weakly-bound crossbridges is allowed. Isomerization of myosin heads from weak-binding to strong-binding shifts TM into M-state (green). M-state is the force-generating state. Actin filaments are depicted in gray. cTn is not shown for simplicity.

A.

	a	*b*	*c*	*d*	*e*	*f*	*g*
1	M	D	A	I	K	K	K
8	M	Q	M	L	K	L	D
15	K	E	N	A	L	D	R
22	A	E	Q	A	E	A	D
29	K	K	A	A	E	D	R
36	S	K	Q	L	E	D	E
43	L	V	S	L	Q	K	K
50	L	K	G	T	E	D	E
57	L	D	K	Y	S	E	A
64	L	K	D	A	Q	E	K
71	L	E	L	A	E	K	K
78	A	T	D	A	E	A	D
85	V	A	S	L	N	R	R
92	I	Q	L	V	E	E	E
99	L	D	R	A	Q	E	R
106	L	A	T	A	L	Q	K
113	L	E	E	A	E	K	A
120	A	D	E	S	E	R	G
127	M	K	V	I	E	S	R
134	A	Q	K	D	E	E	K
141	M	E	I	Q	E	I	Q
148	L	K	E	A	K	H	I
155	A	E	D	A	D	R	K
162	Y	E	E	V	A	R	K
169	L	V	I	I	E	S	D
176	L	E	R	A	E	E	R
183	A	E	L	S	E	G	K
190	C	A	E	L	E	E	E
197	L	K	T	V	T	N	N
204	L	K	S	L	E	A	Q
211	A	E	K	Y	S	Q	K
218	E	D	K	Y	E	E	E
225	I	K	V	L	S	D	K
232	L	K	E	A	E	T	R
239	A	E	F	A	E	R	S
246	V	T	K	L	E	K	S
253	I	D	D	L	E	D	E
260	L	Y	A	Q	K	L	K
267	Y	K	A	I	S	E	E
274	L	D	H	A	L	N	D
281	M	T	S	I			

B.

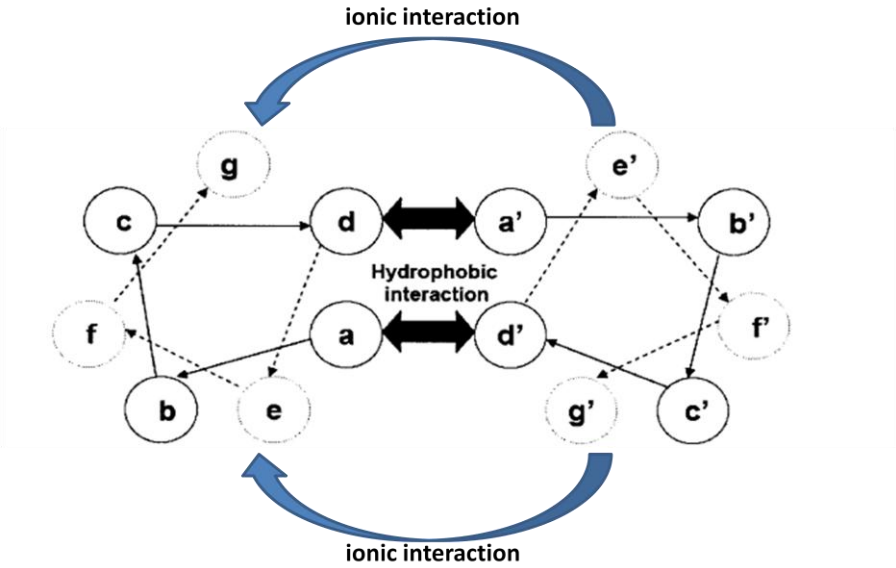

Figure 4. Amino acid sequence and heptad repeats of α-TM. (A) Protein sequence of mouse α-TM (Uniprot entry no: P58771) displays a seven-residue long motif called "heptad repeats". In this heptad structure, residues are located in positions *a-b-c-d-e-f-g.* Ala residues located at *a* and *d* positions are shown in red. Aps137 is shown inside a red box. (See text for more detail). (B) Heptapeptide repeat structure of TM's α-helical coiled-coil structure viewed from the N-terminus down to the axis of TM dimer. Locations of different heptad positions (*a-b-c-d-e-f-g)* are shown.

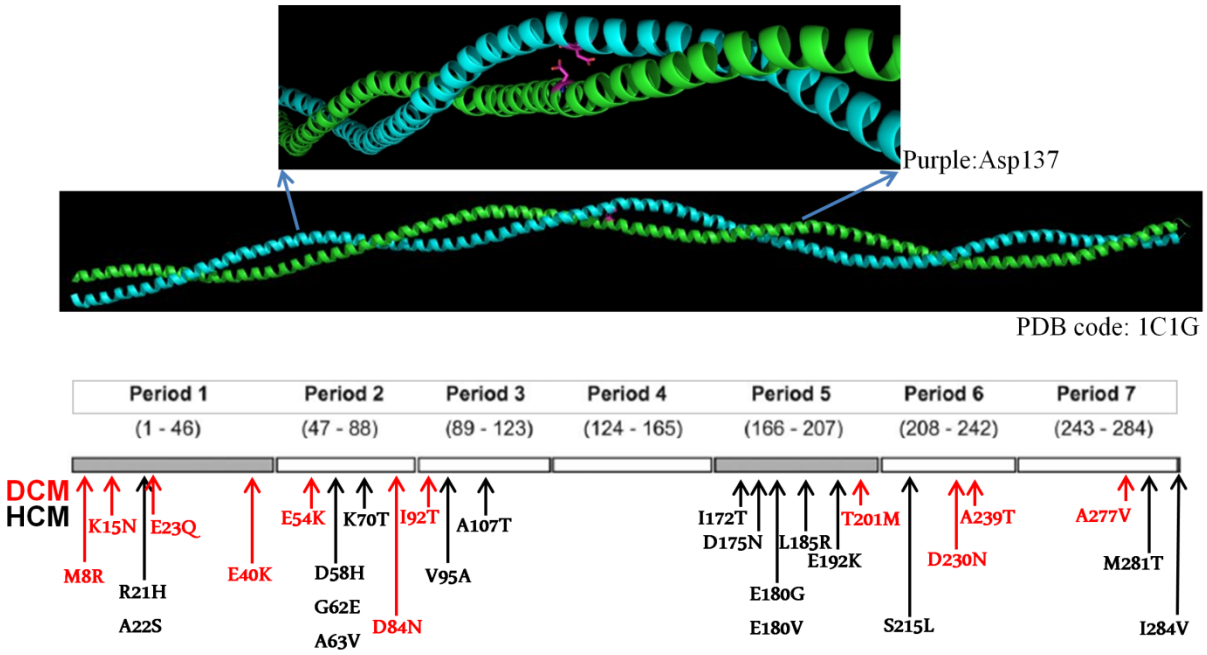

Figure 5. Crystal structure and CM-linked mutations of α-TM. Currently available x-ray crystal structure of the full length α-TM at 7Å resolution (PDB code: 1C1G) (middle panel). Inset shows zoomed in region of α-TM around the period 4, Aps137 is shown in purple. Bottom panel shows distribution of HCM and DCM linked α-TM mutations, which are listed at Table I, along the primary structure of the molecule. DCM-linked mutations are shown in red while HCM-linked mutations are shown in black. Seven quasiequivalant repeats (periods) of α-TM are represented as gray or white boxes.

TABLE I. LIST OF KNOWN HCM- AND DCM-LINKED MUTATIONS MAPPED TO α-TM GENE

Mutation	Disease Phenotype	Position in Heptad repeat	Period	Reference
Met 8 Arg	DCM	*a*	1	(61)
Lys15Asn	DCM	*a*	1	(69)
Arg21His	HCM	*g*	1	(70)
Ala22Ser	HCM	*a*	1	(71)
Glu23Gln	DCM	*b*	1	(69)
Glu40Lys	DCM	*e*	1	(72)
Glu54Lys	DCM	*e*	2	(72)
Asp58His	HCM	*b*	2	(73)
Glu62Gln	HCM	*f*	2	(74)
Ala63Val	HCM	*g*	2	(75)
Lys70Thr	HCM	*g*	2	(76)
Asp84Asn	DCM	*g*	2	(77)
Ile92Thr	DCM	*a*	3	(69)
Val95Ala	HCM	*d*	3	(78)
Ala107Thr	HCM	*b*	3	(71)
Ile172Thr	HCM	*d*	5	(79)
Asp175Asn	HCM	*g*	5	(54)
Glu180Gly	HCM	*e*	5	(54)
Glu180Val	HCM	*e*	5	(80)
Leu185Arg	HCM	*c*	5	(81)
Glu192Lys	HCM	*c*	5	(82)
Thr201Met	DCM	*e*	6	(83)
Ser215Leu	HCM	*e*	6	(84)
Asp230Asn	DCM	*f*	6	(61)
Ala239Thr	DCM	*a*	7	(69)
Ala277Val	DCM	*d*	7	(69)
Met281Thr	HCM	*a*	7	(79)
Ile284Val	HCM	*d*	7	(85)

*Table is modified from (13)

II. EXPERIMENTAL PROCEDURES

A. Expression and Purification of Recombinant Proteins

All recombinant TMs used in this study carry an Ala-Ser N-terminal extension to mimic N-terminal acetylation of the native TM, which is required for stability and functionality of TM and thus regulate muscle contraction (33,34). T7-based pET-3d rat-striated muscle α-TM vector was a gift from Dr. Larry Tobacman (University of Illinois at Chicago). The amino acid sequences of rat and mouse α-TM are identical. This vector was used to express and purify α-TM, and it was also used as a template for preparation of α-TM-D137L plasmid. A QuikChange lightning site-directed mutagenesis kit (Stratagene) was used with primers listed in Table II to produce the α-TM-D137L clone. The coding sequences of both expression plasmids were confirmed by DNA sequencing. For expression of both α-TM and α-TM-D137L, BL21(DE3) *Escherichia coli* cells (Stratagene) were transformed with clones and purified as previously described but with minor changes (33). TM plasmid was transformed into BL21(DE3) cells and a single colony from the agar plate inoculated into 20 mL of LB + 100 mg/L ampicillin and grown over night on a shaker at 220 rpm. In the next morning, two 1 L LB + 100 mg/L ampicillin was inoculated with 10 mL from the overnight culture and grown until A_{600}=0.8. Isopropyl-1-thio-β-D-galactopyranoside was added to a final concentration of 0.7 mM, and incubation was continued for another 3 h at 37 °C on a shaker at 220 rpm. Cells were then spun down with centrifugation at 4500 x g for 15 min at 4 °C. The supernatant fraction was discarded and pellet was resuspended in 70 mL of 50 mM Tris-HCl pH 8.0, 25% (w/v) sucrose, 50% (w/v) lysozyme and 1 mM ethylenediaminetetraacetic acid (EDTA), and incubated on ice for 1 h.

Next, enough 5 M NaCl was added to give final 1 M NaCl concentration. And the resuspended pellet solution was sonicated (Sonic Dismembrator 550, Fisher Scientific) in a small plastic beaker on ice at power level 5 for 5 times with 30 sec on and 1 min off intervals. After sonication, the lysate was cleared (10,000 x g, 1 h, 4 °C), and 3 X volumes of 95 % ethanol was added to the supernatant fraction, which was stirred gently overnight at room temperature. In the morning, the precipitate was collected by centrifugation (10,000 x g, 30 min, 4 °C) and the pellet was resuspended in 80 mL of 95 % ethanol, and dried on large weigh boats. The ethanol powder was extracted with 50 mM Tris-HCl pH 8.0, 1 M NaCl, 0.1 mM dithiothreitol (DTT), 0.01% NaN_3, and 0.1 mM phenylmethylsulfonyl fluoride (PMSF) at 4 °C for 4 h with gentle stirring. After extraction, the preparation was cleared with centrifugation at 10,000 x g for 30 min at 4 °C. The supernatant fraction was saved and its pH was slowly dropped to 4.6 with the addition of 0.1 to 0.3 N HCl drops on ice with gentle stirring. Once pH 4.6 was reached, gentle stirring continued for another 10 min. The precipitate obtained by centrifugation (10,000 x g, 30 min, 4 °C) was resuspended in ~10 mL of 1 M Tris-HCl pH 8.0. The suspension was then dialyzed against 6 M urea, 25 mM NaCl, 0.5 mM EDTA, 50 mM tris-HCl pH 8.0, 0.5 mM DTT and 0.01% NaN_3 overnight. DTT was removed from the last dialysis buffer. α-TM is a negatively charged protein with a slightly acidic isoelectric point (pI) (approximately 4.6), therefore the sample was loaded into anion-exchange diethylaminoethanol-fast flow (DEAE-FF) column, which was equilibrated with the same dialysis buffer without DTT, and eluted with 25 mM – 0.5 M NaCl gradient on Fast protein liquid chromatography (FPLC) (Figure 9). Purity of TM fractions was checked on 12% sodium dodecyl sulfate polyacrylamide gel electrophoresis (SDS-PAGE) (Figure 10). Pure fractions were pooled and dialyzed against 1 mM NH_4HCO_3 before freeze-drying. Freeze-dried samples were kept at -20 °C until use.

For ^{1}H-^{15}N heteronuclear single quantum coherence (HSQC) nuclear magnetic resonance (NMR) measurements, ^{15}N enriched α-TM and α-TM-D137L were prepared using the same TM expression and purification protocol described above except that M9 media contained $^{15}NH_4Cl$ as a sole nitrogen source (Cambridge Isotope Laboratories).

Recombinant mouse cTnC and cTnT were expressed in BL21(DE3) cells using pET vectors and purified according to protocols reported by Kobayashi et al. (86). Recombinant mouse cTnI was expressed and purified as described somewhere else (87).

Actin was prepared from rabbit skeletal muscle acetone powder as described by Spudich and Watt (88) . Myosin S1 was prepared by chymotrypric digestion of rabbit psoas muscle myosin and purified on a SP-Sephadex column as described previously (89).

Purified protein concentrations were determined by absorbance using extinction coefficients calculated according to a model developed by Gill and von Hippel (90). The following extinction coefficients were used to calculate protein concentrations: E_{280nm} = 1.56 x 10^4 $M^{-1}cm^{-1}$ for α-TM and α-TM-D137L, E_{280nm} = 1.522 x 10^4 $M^{-1}cm^{-1}$ for cTnT, E_{280nm} = 1.105 x 10^4 $M^{-1}cm^{-1}$ for cTnI, E_{280nm} = 4.08 x 10^3 $M^{-1}cm^{-1}$ for cTnC, E_{290nm} = 0.63 $(mg/ml)^{-1}$ for actin and E_{280nm} = 0.75 $(mg/ml)^{-1}$ for myosin S1.

B. Reconstitution of Troponin Complex

Recombinant cTn ternary complex was reconstituted as described previously with minor modifications (91). Equimolar amounts of previously purified and lyophilized cTnI, cTnC and cTnT in solubilization buffer containing 6 M urea, 1 M NaCl, 5 mM $MgCl_2$, and 20 mM Tris-HCl pH 8.0. The solution was then subjected to sequential dialysis to decrease salt

concentration slowly (1 M to 0.1 M) against the same solubilization buffer without urea. Finally, the solution was brought into 0.1 M NaCl, 5 mM $MgCl_2$, 20 mM Tris-HCL, pH 8.0 and 0.01% NaN_3. Next, the ternary protein complex was separated from the monomeric cTn components by anion exchange chromatography on a RESOURCE-Q column (Amersham Biosciences) using a linear gradient from 100% buffer with 0.1 M NaCl, 5 mM $MgCl_2$, 20 mM Tris-HCl, pH 8.0 and 0.01% NaN_3 to 100% of the same buffer but with 0.5 M NaCl. Finally, purity of the cTn comlex was checked with 12% SDS-PAGE (Figure 15). Prepared cTn complex was dialyzed against the buffer of interest before use.

C. Differential Scanning Calorimetry

Differential scanning calorimetry (DSC) measures changes in physical and chemical properties of proteins in their native form by measuring the heat change associated with thermal denaturation. In this study, DSC experiments were performed on a VP-DSC (MicroCal) at the Center for Structural Biology, University of Illinois at Chicago. All measurements were carried out using reduced recombinant α-TM and α-TM-D137L (1.8 mg/ml) in 20mM 3-(N-morpholino)propanesulfonic acid (MOPS), pH 7.0, 1 mM EDTA, 0.1 M NaCl and 1 mM β-mercaptoethanol, at a scanning rate of 1 ºC/min. The reversibility of thermal transitions was tested by a second heating of the sample immediately after cooling from the first scan. The calorimetric traces were corrected for instrument background by subtracting a scan with buffer in both cells. The DSC data were analyzed using Origin 7.0 (MicroCal) as described (66). The heat capacity (*Cp*) versus temperature curve was analyzed to determine the transition temperature (*Tm*) and the calorimetric enthalpy of transition (ΔH_{cal}). *Tm* was used to compare thermal

stability of TM species. ΔH_{cal}, which is calculated by integrating the area under the peak, was used to compare the size of the transition for each calorimetric domain.

D. Reductive Methylation

Reductive methylation is used to ^{13}C label ε-amino group of Lys residues and N-terminal primary amine groups of proteins for NMR studies (92). Typically, this labeling is performed by adding formaldehyde to the protein solution in the presence of a reducing agent. At the end, Lys residues are converted to ^{13}C-labeled dimethyl-Lys. A schematic of the reaction is shown in Figure 6.

In this work, reductive methylation of recombinant α-TM and α-TM-D137L was performed as previously described (92) prior to NMR measurements. Briefly, 20 µl of 1M borane-ammonia complex (H_3N-BH_3) (Sigma) and 40 µl of 1 M ^{13}C formaldehyde (Cambridge Isotope Laboratories, Inc) were added to 1 ml of protein and the reaction proceeded for 2 h at 4 °C. The same step was repeated, and the sample was kept at 4 °C for another 2 h. Next, another 10 µl of 1M H_3N-BH_3 was added and the sample was kept at 4 °C overnight. In the morning, the reaction was quenched by adding glycine (200 mM final concentration at pH 7.5), which neutralizes formaldehyde. Finally, unbound products were removed by dialysis against our buffer of interest; 25 mM sodium-phosphate buffer, pH 7.0, 0.1 M NaCl, 1mM EDTA.

E. Nuclear Magnetic Resonance Spectroscopy

^{1}H-^{15}N-edited HSQC experiment provides a highly sensitive two dimensional (2D) NMR experiment. The basic scheme of this experiment involves the magnetization transfer between two bonded heteronuclei; ^{1}H and ^{15}N. In a ^{15}N labeled protein, magnetization transfer occurs between backbone amide protons attached to nitrogens as well as in side chains with nitrogen-bound protons, and produces an observable peak in the HSQC spectrum. The HSQC spectrum of a protein is like a fingerprint because each ^{1}H-^{15}N bond in the backbone of a protein has a unique electromagnetic environment thus producing a unique signal in the HSQC spectrum. By comparing the HSQC spectrum of a wild type (WT) and a mutant protein, changes in the chemical shifts of some peaks may be observed, suggesting a change in the electromagnetic environment of the corresponding nuclei.

In the experiments reported in this thesis, ^{15}N methyl signals of ^{15}N-labeled α-TM and α-TM-D137L were collected using HSQC experiments at 25 ºC with a 900 MHz Bruker spectrometer equipped with a cryogenic probe. Conditions were 10% D_2O, 55mM NaCl, 25 mM sodium phosphate (pH 7.0), 1 mM EDTA and 2 mM DTT. Protein concentration was 200 μM. The data were processed and analyzed using NMRPipe software (93).

HSQC experiment is also applicable to other nuclei, such as ^{13}C. We also conducted ^{1}H-^{13}C HSQC experiments of reductively methylated α-TM and α-TM-D137L at 25 ºC with a 900 MHz Bruker spectrometer equipped with a cryogenic probe. Buffer conditions for reductively methylated α-TM and α-TM-D137L were 10% D_2O, 25 mM sodium-phosphate, pH 7.0, 0.1 M NaCl, 1mM EDTA and 2 mM DTT. The concentration of TMs used in these NMR experiments was 5 μM. The data were processed and analyzed using NMRPipe software (93).

F. *In Vitro* Acto-Myosin S1-ATPase Activity Assay

First, all purified protein samples (cTnC, cTnT, cTnI, α-TM, α-TM-D137L, reductively methylated α-TM, reductively methylated α-TM-D137L, actin and myosin S1 were dialyzed against 70 mM NaCl, 10 mM $MgCl_2$ and 40 mM MOPS, pH 7.0. Next, the thin filaments were reconstituted by mixing actin and α-TM first, and then adding cTn complex. ATPase activity measurements were conducted by the malachite green procedure as described elsewhere (86,94). The final reaction conditions were 0.2 μM myosin S1, 5 μM actin, 1.5 μM TM, 1.5 μM Tn in 35 mM NaCl, 5 mM $MgCl_2$, 20 mM MOPS, pH 7.0, 1 mM ATP and either 0.1 mM $CaCl_2$ or 2 mM ethylene glycol tetraacetic acid (EGTA) at 25 °C.

G. Care and Use of Animals

All animal procedures were carried out according to the National Institutes of Health *Guide* for the Care and Use of Laboratory Animals and approved by the Animal Care and Use Committee (ACC# 11-227 and #11-112) at the University of Illinois at Chicago. All experiments were carried out with 4 and 8 mon old female and male mice.

H. Generation of alpha-Tropomyosin-D137L Transgenic Mice

TG mice (FVB/N background) were generated in Dr. David F. Wieczorek's laboratory at the University of Cincinnati. The mouse α-TM striated muscle specific cDNA (1.1 kb) (accession number: X64831) was cloned into the pBlueScript II SK (+) (pBS +) vector,

which was subjected to site directed mutagenesis. Three nucleotide changes (GAT > CTG) corresponding to an amino acid substitution at codon 137 (Asp137Leu) were carried out using the QuikChange site-directed mutagenesis kit (Stratagene). The sequence was verified by automated DNA sequencing and compared with the published sequence. The α-TM-D137L cDNA was cloned into a vector (95), which contained the cardiac-specific α-MHC promoter and the human growth hormone (HGH) poly (A) signal sequence. The transgene construct was purified to generate TG mice strain as described (96). Founder mice were identified by polymerase chain reaction (PCR) and the mutation in the TG lines was verified by nucleotide sequencing of TG mouse genomic DNA.

I. Genotyping of Transgenic Mice

Genomic DNA samples were extracted from tail clips of 17 day-old mice and PCR was employed for genotyping of generated TG α-TM-D137L strain. Sequences of primers used for genotyping are shown in Table II. An untargeted site of genomic DNA amplification was used as an internal control for the PCR reactions. After PCR, the amplicons were resolved on a 1% agarose gel. The α-MHC forward and α-TM reverse primers produced a PCR product of ~ 200 bp (called α-TM-D137L band) and the glyceraldehyde-3-phosphate dehydrogenase (GAPDH) control primer produce a PCR product of ~ 500 bp. NTG samples produce a single GAPDH band whereas TG samples produce both GAPDH and α-TM-D137L bands in the agarose gel (Figure 7).

K. Transthoracic Echocardiography

Mice were anesthetized with 1% isoflurane in 100% oxygen using a face mask. Animals were maintained in the supine position on a heating plate and body temperature was maintained at 36-37^{o}C. Echocardiography of 4 and 8 mon old animals was then performed using a 30-MHz high-resolution transducer with an integrated rail system (Vevo 770 High-Resolution Imaging Systems, RMVTM 707B scan head, VisualSonics). M-Mode images of the left ventricle outflow tract (LVOT), ascending aorta (AO) and left atrium (LA) were taken from the parasternal long axis view. The parasternal short axis view at the level of the papillary muscles was used to measure the LV internal dimension (LVID), inter-ventricular (IV) septal wall thickness (SWT) and posterior wall thickness (PWT). Pulsed Doppler was performed with the apical four-chamber view. The mitral inflow was recorded with the Doppler sample volume at the tip of the mitral valve leaflets to obtain the peak velocities of flow in the early phase of diastole (E) and after LA contraction (A). Then, in order to measure time intervals, the Doppler sample volume was moved toward the LVOT and both the mitral inflow and LV outflow were obtained simultaneously. Three parameters of the LV diastolic function were evaluated: 1) E/A ratio, 2) E wave deceleration time (DT), which is the time from E to the end of the early diastole; and 3) LV isovolumic relaxation time (IVRT), which is the time measured from the aortic valve closure to the mitral valve opening. Additional information about the diastolic function was obtained with tissue Doppler imaging. Peak myocardial velocities in the early (E_m) and late (A_m) diastole were obtained with the sample volume at the septal side of the mitral annulus in the four chamber view. All measurements and calculations were averaged from three consecutive cycles

and performed according to the American Society of Echocardiography guidelines (97,98). Data analysis was performed with the Vevo 770 Analytic Software.

K. Pressure-Volume Loop Analysis

Male and female mice (4 mon old) were sedated with etomidate (8 µg/g body weight) administered intraperitoneally and then intubated and ventilated (100% O_2 / 1% isofluorane) with a rodent ventilator (stroke volume set at 0.2 to 0.4 mL and a respiration rate of 125 breaths/min). A small incision was made in the lower chest to expose the xiphoid process and a stay suture was placed around the xiphoid to stabilize and lift the chest wall. A mid-line incision was then made along the linea alba and the diaphragm was then cut and retracted to expose the heart and inferior vena cava. A 1.4 French ultra-miniature pressure–volume catheter (SPR-839; Millar Instruments) was inserted into the apex of the heart to measure baseline recordings of heart rate, LV systolic/diastolic pressure and volume, the first derivative of pressure change over time ($\pm dP/dt$), and pressure–volume loops. The mouse was allowed to stabilize before inferior vena cava occlusion. The inferior vena cava was isolated and occluded while simultaneously measuring pressure-volume (PV) loops to determine end-systolic pressure-volume relationship (ESPVR) and contractility of the ventricle independent of loading conditions. A series of 10–20 loops was used to estimate the ESPVR and end-diastolic pressure-volume relationship (EDPVR). All data were analyzed using the PVAN software package (Millar Instruments).

L. Isolation of Mouse Cardiomyocytes

Mouse ventricular myocytes were isolated from TG and non-transgenic (NTG) mice essentially as previously described (99,100). Mice were heparinized (5000 U/kg body weight) and then anesthetized with pentobarbital sodium (50 mg/kg body weight IP) 30 mins later. Animals were first assessed for proper depth of anesthesia using the pedal reflex. Hearts were then quickly excised and cannulated via the ascending aorta, and perfused by the Langendorff method at 37°C for 4 min with a Ca^{2+}-free perfusion buffer of the following composition: 113 mM NaCl, 4.7 mM KCL, 0.6 mM NaH_2PO_4, 1.2 mM $MgSO_4$, 0.032 mM phenol red, 12 mM $NaHCO_3$, 10 mM $KHCO_3$, 30 mM taurine, 10 mM 4-(2-hydroxyethyl)-1-piperazineethanesulfonic acid (HEPES), 5.5 mM glucose and 10 mM 2,3-butanedione monoxime (pH 7.4). Subsequently, the hearts were perfused for 8-12 min with a digestion buffer containing perfusion buffer and 12.5 µM Ca^{2+} together with 0.15 mg/mL Blendzyme 2 (Roche, Germany) and 0.14 mg/mL trypsin (Invitrogen, CA). After the hearts were well-digested, the ventricles were removed and placed into a dish containing digestion buffer and cut in very small pieces and gently triturated. Following this trituration period, the cell suspension was filtered through a mesh collector and placed into centrifuge tubes and the digestion process was stopped with equal volume of perfusion buffer containing 12 µM Ca^{2+} plus 10% bovine calf serum (v/v). The cells were allowed to collect at the bottom of the tubes by gravity for 7 min. The supernatant fraction was removed and the cells were resuspended in fresh control solution of the following composition: 133.5 mM NaCl, 4.0 mM KCL, 1.2 mM $MgSO_4$, 1.2 mM NaH_2PO_4, 1O mM HEPES, with serial increases in Ca^{2+} concentrations; first 200 µM Ca^{2+}, followed by 500 µM and then 1mM Ca^{2+}. The cells were stored at room temperature (22-23°C) until used the same day.

M. Simultaneous Measurements of Cardiomyocyte Cell Shortening and Calcium Transients

Fura-2 fluorescence and shortening of cells were monitored simultaneously as previously described (99). Following cardiomyocyte isolation as described above, an aliquot of cells was transferred to a perfusion chamber mounted on the stage of an inverted Nikon microscope and allowed to settle onto the glass. Background fluorescence recordings were taken daily for noise reduction. Following this recording, another aliquot of myocytes was loaded for 15 min with the Ca^{2+} indicator fura-2 (3 μM, Invitrogen) prepared from a dimethyl sulfoxide (DMSO) stock solution. Following loading, cells were perfused using a dye-free 1.2 mM Ca^{2+} solution to allow for de-esterification of the indicator. Single intact ventricular myocytes were then field stimulated by applying a 4 ms square supra-threshold voltage pulse at 0.5 Hz to the bath through parallel platinum electrodes. For determination of the 340/380 fluorescence ratio of fura-2 as reflection of ($[Ca^{2+}]_i$), myocytes were alternatively excited at wavelengths of 340 and 380 nm and the emitted fluorescence was collected at a wavelength of 505 nm by a photomultiplier tube and stored in the acquisition software (Felix32, Photon Technology International) for later off line analysis. Cell shortening images were collected by the X40 Nikon objective and transmitted to a multi-image module. Unloaded cell shortening assessment was carried out using edge detection where a video-edge detector (Crescent Electronics) was used to monitor cell length. Recordings were stored using an acquisition software program (Felix 32, Photon Technology International) for later analysis. The peak percentage of cell shortening was calculated from 4 individual shortening peaks and expressed as an average of shortening. The shortening and relengthening velocities were calculated as the first derivative of the cell

shortening trace using Felix32, and the maximal velocity peak was determined from the average of 4 individual peaks.

The $[Ca^{2+}]_i$ transient measurements were reported as a function of the ratio emissions from 340/380 (fura-2 ratio) excitation wavelength after background subtraction. The baseline and peak $[Ca^{2+}]_i$ transient was manually determined from the average of 4 individual tracings. The decay time (tau) was assessed by a monoexponential fit to the declining phase of the $[Ca^{2+}]_i$ transient using pClamp 9.0 (Molecular Devices).

N. Preparation of Detergent Skinned Fiber Bundles

Mice were anesthetized with pentobarbital sodium (50 mg/kg) intraperitoneally, and the hearts were rapidly excised and rinsed in ice-cold high relaxing (Hr) solution containing 10 mM EGTA, 41.89 mM K-proprionate, 6.57 mM $MgCl_2$, 100 mM N, N-Bis(2-hydroxyethyl)-2-aminoethanesulfonic Acid (BES), 6.22 mM ATP, 10 mM creatine phosphate sodium salt (Na_2CrP) and 5 mM NaN_3 at pH 7.0. The Hr solution also contained 1 µg/ml leupeptin, 2.5 µg/ml pepstatin-A, and 50 µM PMSF. Papillary muscles were then isolated from left ventricles of 4 and 8 mon old NTG and TG mice and dissected under a dissection microscope at 4 °C into fiber bundles ~200 µm in width and 3-4 mm in length. Next, to detergent extract membranes fiber bundles were skinned in Hr solution with 1% Triton X-100 for 3 h at 4 °C. Then, prepared skinned fibers were used in the experiments described below.

O. Calcium-, Rigor Cross-Bridge- and Length-Dependent Force Measurements of Skinned Fiber Bundles

Detergent-extracted fiber bundles were mounted between a force transducer and a micromanipulator via applying a small amount of cellulose-acetate glue to each tip of the fiber. Fibers were then incubated in Hr solution and measurements were conducted as described below.

For Ca^{2+}-dependent force measurements, skinned fiber bundles, which were incubated in Hr solution, were maximally activated in activating solution at pCa 4.5 (10 mM EGTA, 9.9 mM $CaCl_2$, 22.16 mM K-proprionate, 6.2 mM $MgCl_2$, 100 mM BES, 6.29 mM ATP, 10mM Na_2CrP, 5mM NaN_3 at pH 7.0). This activation was followed by a relaxation in Hr. Then, sarcomere length (SL) was set at 2.2 µm employing a He-Ne laser system to determine the first diffraction pattern. Afterwards, fibers were quickly activated one more time in activating solution and then placed back into Hr solution. Once baseline force was stabilized, fiber bundles were incubated in a series of solutions containing increasing Ca^{2+} concentrations (pCa 8 to 4.5) and generated force was recorded with a chart recorder. Solutions with varying [Ca^{2+}] were prepared by mixing Hr with activating solution at pCa 4.5. A schematic of the experimental setup is shown in Figure 8.

Rigor cross-bridge-dependent force measurements were conducted similar to pCa-force measurements described above, except that skinned fiber bundles were subjected to a sequential decrease in [MgATP] using a procedure modified from that of Brandt et al. (101). The fiber bundles were initially placed in Hr and then subjected to decreases in [MgATP] (10^{-4}-10^{-6} M). Solutions with varying [MgATP] were prepared by mixing pMgATP 3 (10 mM EGTA, 63.45 mM K-proprionate, 2.8 mM $MgCl_2$, 1.07 mM ATP, 12 mM Na_2CrP, 20 mM BES, 5 mM NaN_3 at pH 7.0) solution with pMgATP 8 (10 mM EGTA, 68.98 mM K-proprionate, 1.8 mM $MgCl_2$,

$1x10^{-5}$ mM ATP, 12 mM Na_2CrP, 20 mM BES, 5 mM NaN_3 at pH 7.0) solution. SL was set at 2.2 µm.

Length-dependent force measurements of skinned fibers were performed similarly to pCa-force measurements described above, but this time force measurements were obtained at two different SL; 1.9 µm and 2.3 µm.

In all skinned fiber measurements, solutions contained the following protease inhibitors: pepstatin-A (2.5 µg/ml), leupeptin (1 µg/ml), and PMSF (50 µmol/L). Also, 10 IU/ml creatine phosphokinase was freshly added to all solutions before use. Force measurements were corrected according to the calculated cross sectional area of each fiber. Ionic strength of all solutions (150 mM), and [MgATP] and free [Ca^{2+}] were calculated with the computer program of A. Fabiato (102) using binding constants listed by Godt and Lindley (103). Isometric tension measurements and length-dependent tension measurements were plotted as a function of pCa, whereas rigor cross-bridge dependent tension measurements were plotted as a function of pMgATP. Using nonlinear least-square regression analyses in prism software (GraphPad Ver.5), data were fit to a modified the *Hill* equation (shown below),

$$\mathbf{F=Fmax.*\ [Ca^{2+}]^{n} / ([Ca^{2+}]^{n} + EC_{50}^{n})}$$

where, F is the developed isometric force (mN / mm^2), Fmax is the isometric force at maximal activation, EC_{50} (or pCa_{50}) is the [Ca^{2+}] at 50% maximal force, and n or *Hill* coefficient is the slope of the relationship corresponding to the degree of cooperativity of cross bridge cycling.

P. Myofibrillar Protein Preparation

The hearts of NTG and TG mice were excised as described (104). Myofibrillar proteins were prepared from left ventricular myocardium of NTG and TG mice, in the presence of protease (Sigma-Aldrich) and phosphatase (Calbiochem) inhibitor mixtures, according to methods described previously (105). In brief, myofibrils were purified and solubilized from ventricular homogenates in UTC buffer (8 M Urea, 2 M thiourea, and 4 % (w/v) 3-[(3-cholamidopropyl)dimethylammonio]-1-propanesulfonate (CHAPS)) at a 1:20 w:v ratio using dounce homogenizers. Samples were clarified with centrifugation (18 000 X g for 10 min, 4 ºC) and the supernatant fraction was kept at -80 ºC until use. Myofibrillar protein sample concentrations were determined using RC-DC assay kit (Bio-Rad). Samples used for two-dimensional difference in-gel electrophoresis (2D-DIGE) experiments were treated with 2D clean-up kit from GE Healthcare, and then re-suspended in UTC buffer.

Q. Two-Dimensional Difference In-Gel Electrophoresis

We performed 2D-DIGE essentially as described previously (104-107). Myofibrillar proteins (100 µg) were prepared as described above. Next, samples from NTG and TG mice and an internal standard (mixture of all NTG and TG samples used in the run) were randomly labeled with fluorescent cyanine dyes (Cy) (GE Healthcare) at 100 pmol/50 µg protein ratio as described (105). Isoelectric focusing was performed using the following immobilized pH gradient strips (GE Healthcare) in the 1st dimension: for α-TM and α-TM-D137L; 24cm pH 3.9-5.1 from BioRad, for cTnI; 18 cm pH 7-11, cTnT and MLC 18cm pH 4-7, for MyBP-C 24cm pH

3-11. The 2nd dimension was run on a 12% SDS-PAGE gel (105) using the Criterion gel system (BioRad). Gels were then washed in double distilled water (ddH_2O) for 30 mins and imaged on a Typhoon 9410 imager (GE Healthcare) with Cy3 (532-nm laser), Cy5 (633-nm laser) and Cy2 (488-nm laser). Images were analyzed using PDQuest software (v8.0 advanced, BioRad). The spot density as a percentage of totals was calculated by dividing the density of a particular spot by the total of all spot densities for that protein.

R. Analysis of Myosin Heavy Chain Isoform Expression

Assessment of MHC isoform content in NTG and TG mouse hearts was done employing electrophoretic separation between α and β isoforms of MHC on a special SDS-PAGE system described previously (108). Myofibrillar samples from ventricles of 1 day old neonatal mice were used as control expressing both α and β isoforms. Quantification of band densities was done using ImageLab software (v.3.0, BioRad).

S. Statistical Analysis

Measurements from experiments with isolated cardiomyocytes, tension-pCa, tension-pMgATP, SL-dependent tension generation, heart-weight to tibia-length ratio, 2D-DIGE, PV loop and *in vitro* ATPase activity were analyzed employing an unpaired Student's *t*-test. In addition, echocardiography data from 4 and 8 mon old mice were compared among and between groups using ANOVA followed by Bonferroni post hoc analysis. $P \leq 0.05$ was considered statistically significant. Data are expressed as ± SEM.

FIGURES and TABLES

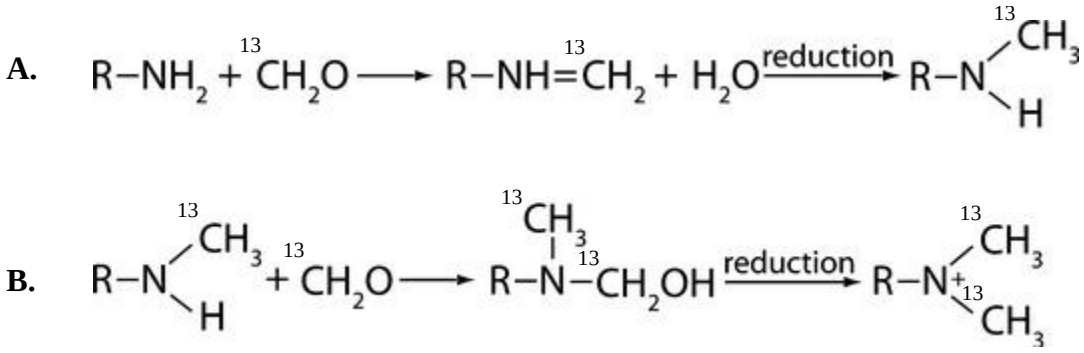

Figure 6. Reductive methylation reaction. (A) In the presence of ^{13}C formaldehyde**,** a ^{13}C methyl group is added to ε-amino group of a Lys residue or N-terminal primary amine group through formation of a Schiff base intermediate. **(B)** In the presence of sufficient ^{13}C formaldehyde and reducing agent, reaction rapidly proceeds to give ^{13}C labeled, di-methylated product.

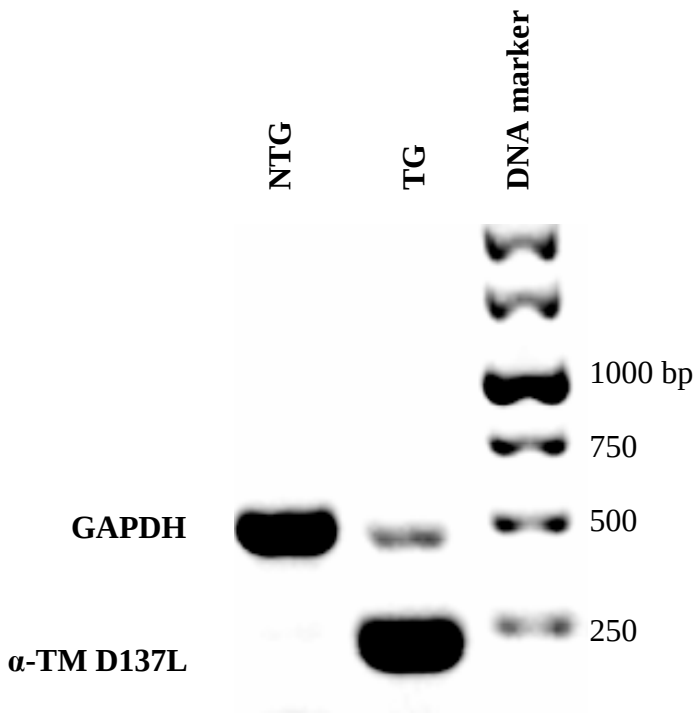

Figure 7. Genotyping NTG and TG mice. A representative 1% agarose gel image of PCR products of NTG and TG genomic DNA samples is shown. (see text for more detail)

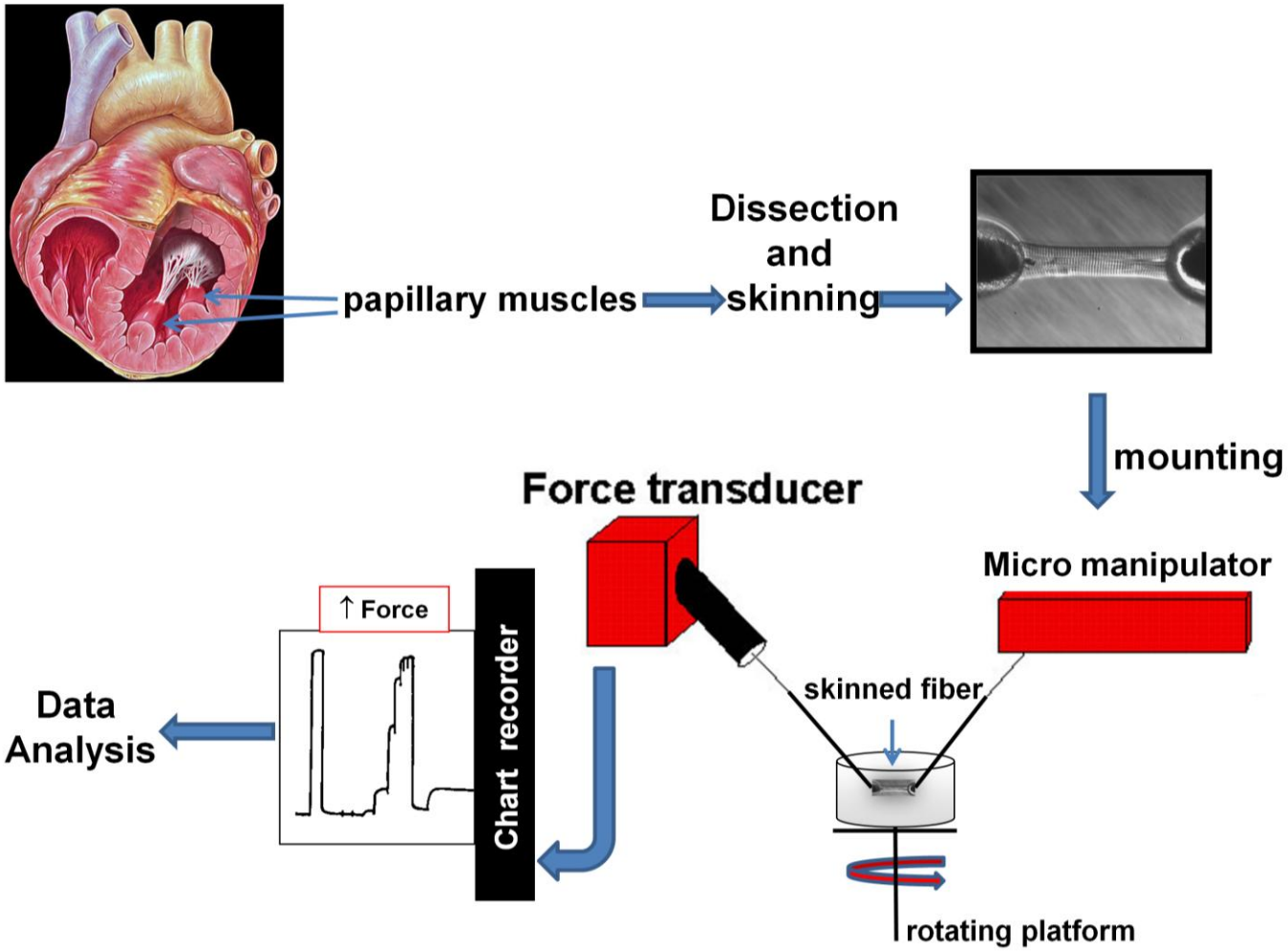

Figure 8. **Schematic representation of skinned fiber experimental set up.** First fiber bundles are dissected from left ventricular papillary muscles of mouse hearts. Next, fibers were skinned and mounted between a force transducer and a micro manipulator. Fiber was then bathed in experimental solutions while force is simultaneously measured and recorded on a chart recorder.

Table II. PRIMERS UTILIZED TO GENERATE RECOMBINANT α-TM-D137L PLASMID

Primer Name	Primer Sequence
α-TM-D137L Forward	5`-CAT TGA AAG CCG AGC CCA AAA ACT TGA AGA AAA GAT GGA GAT TCA G-3`
α-TM-D137L Reverse	5`-CTG AAT CTC CAT CTT TTC TTC AAG TTT TTG GGC TCG GCT TTC AAT G-3`

Table III. PRIMERS UTILIZED FOR GENOTYPING

Primer Name	Primer Sequence
α-MHC Forward	5'- GCC CAC ACC AGA AAT GAC AGA - 3'
α-TM Reverse	5'- TCC AGT TCA TCT TCA GTG CCC - 3'
GAPDH Control Forward	5'- AGC GAG CTC AGG ACA TTC TGG - 3'
GAPDH Control Reverse	5'- CTC CTA ACC ACG CTC CTA GCA- 3'

III. RESULTS

A. Structural Implications of D137L Mutation on alpha-Tropomyosin

1. Recombinant alpha-tropomyosin-D137L exhibited increased thermal stability compared to alpha-tropomyosin

In order to assess the effects of the D137L mutation on structural features of TM, we employed DSC and compared thermal stability of α-TM-D137L with α-TM. Recombinant proteins, α-TM and α-TM-D137L were expressed and purified as described in the methods section (Figure 9 and Figure 10). It was previously reported that disulfide bridges decrease flexibility of proteins and correspondingly increase their thermostability (109). The amino acid sequence of α-TM contains a cysteine residue at position 190 that can cross-link the two chains of the coiled-coil and affect DSC measurements. Also, it was previously demonstrated by Lehrer et al. that TM in rodent cardiac tissue exists in a reduced non-crosslinked state (110). Therefore we conducted DSC measurements under reducing conditions. All TM samples used in DSC measurements were in fully reduced state as shown in Figure 11.

The excess heat capacity curves for reduced recombinant α-TM-D137L and α-TM are presented in Figure 12 A and B. The thermal unfolding character of α-TM-D137L was noticeably different from α-TM. This was reflected in pronounced increases in the thermal stability indicator, *Tm* value of the two calorimetric domains of α-TM-D137L (Table IV). Calorimetric domains of the α-TM were seen at maxima 43.35 ºC (domain-1) and 49.99 ºC (domain-2). Calorimetric enthalpy values for these domains were 91.13 kcal/mol (70.5% of total)

and 38.07 kcal/mol (38.0% of total) respectively. In the case of the α-TM-D137L, the same two calorimetric domains were observed but thermal transitions were at higher maxima 45.68 ºC (domain-1) and 52.19 ºC (domain-2) with ΔH_{cal} values of 94.58 kcal/mol (36.5% of total) and 168 kcal/mol(63.0% of total) respectively. The reversibility of thermal transitions was confirmed by a second heating of the sample immediately after cooling from the first scan (data not shown). Previous studies revealed that the least thermostable domain-1 corresponds to the thermal unfolding of the unstable middle region (residues 130-190) and the C-terminal half whereas the domain-2 corresponds to the N-terminal unfolding of striated α-TM (66,111-113). Thus our results suggested that the D137L mutation increases thermal stability of both the N- and C-terminus of TM with almost equal increases in *Tm* values of domain-1 and -2. However, a prominent increase in calorimetric enthalpy of N-terminal calorimetric domain compared to C-terminal domain indicated a higher stabilization effect of Leu substitution at position 137 on the N-terminal domain.

Observations on correlation between protein thermostability and protein flexibility were previously reported (114-116). Accordingly, the detected increase in coiled-coil stability of α-TM-D137L compared to α-TM suggested a decrease in the structural flexibility of the protein due to the D137L mutation.

2. Long-range rearrangements were observed in alpha-tropomyosin-D137L structure

The research undertaken further studied structural implications of the D137L mutation on TM by employing NMR spectroscopy. We first acquired ^{1}H-^{15}N edited HSQC

spectra of ^{15}N labeled α-TM and α-TM-D137L**.** The ^{1}H-^{15}N HSQC spectrum is a good structural fingerprint of a protein because each ^{1}H-^{15}N bond in the backbone of a protein has a unique electromagnetic environment producing a unique signal in the spectrum. By comparing the ^{1}H-^{15}N HSQC spectra of α-TM and α-TM-D137L, we anticipated to analyze possible chemical shift changes of peaks due to the D137L mutation. An overlay of NMR spectra of α-TM (red) and α-TM-D137L (black) (Figure 13) demonstrated significant signal overlap, which was expected due to the high molecular weight of α-TM homodimers (~65 kDa). Additionally, low chemical shift dispersion was observed in their spectra. However we do not anticipate that this is due to a folding problem, as activity of both α-TM and α-TM-D137L was confirmed in an *in vitro* acto-myosin S1 ATPase activity assay (see next section). One explanation for low chemical shift dispersion could be the repeated alpha-helical structure of TM in which residues repeatedly face similar environments. Due to significant signal overlap and low chemical shift dispersion, the assignment of resonances in the spectra was not possible. However, comparison of acquired α-TM and α-TM-D137L spectra showed that D137L mutation caused a higher degree of line broadening, which may indicate a decrease in structural flexibility of α-TM-D137L.

In order to increase the sensitivity of NMR signals and overcome the molecular weight limitation in our initial NMR measurements, reductive methylation approach was used. Another advantage of reductive methylation is that non-specific protein aggregation is considered to be minimal due to the low concentrations of protein usage. In reductive methylation, ε-amino groups of Lys residues and N-terminal primary amine groups of proteins are ^{13}C labeled (Figure 6). α-TM has 39 Lys residues in its amino acid sequence and they are spread along the protein, therefore the reductive methylation approach allowed observation of effects of D137L mutation on TM's long-range structural features. An overlay of ^{1}H-^{13}C-edited HSQC spectra of

reductively methylated α-TM (blue) and α-TM-D137L (red) is shown in Figure 14. Significant signal overlap was again observed in the spectra of α-TM and α-TM-D137L. However, 26 out of 39 signals were still detectable in either spectrum. Comparison of α-TM and α-TM-D137L spectra showed methyl chemical shift perturbations in all resonances. This result indicated that the structural rearrangements that are observed throughout the α-TM-D137L molecule were a consequence of long-range effects from the D137L mutation.

3. *In vitro* acto-myosin S1 ATPase activity of reductively methylated alpha-tropomyosin-D137L and alpha-tropomyosin

In previous studies, it has been shown that reductive methylation does not perturb protein structure (117-119), and reductively methylated side chains retain their positively charged nature at neutral pH and are, therefore still able to participate in intra- and inter-molecular binding events (117). However, some proteins may be inactivated due to reductive methylation (120). We thus tested the effects of reductive methylation on the regulatory function of TM in thin filament dynamics using the *in vitro* acto-myosin S1-ATPase activity assay. Purified cTn complex (Figure 15) was combined with actin and α-TM-WT, α-TM-D137L, reductively methylated α-TM or reductively methylated α-TM-D137L to reconstitute thin filaments. ATPase rates of thin filament-myosin S1 preparations were then measured. ATPase rate in relaxing conditions (+EGTA) was not affected by the presence of modified α-TM or α-TM-D137L. Ca^{2+} switched on the ATPase rate in α-TM ($0.26 \pm 0.02\ s^{-1}$) and α-TM-D137L ($0.36 \pm 0.02\ s^{-1}$) as well as in reductively methylated α-TM ($0.72 \pm 0.03\ s^{-1}$) and α-TM-D137L ($0.81 \pm 0.04\ s^{-1}$). Although the maximum ATPase rate was higher in the reductively methylated TM

variants, the difference in ATPase rates at maximum Ca^{2+} between α-TM and α-TM-D137L (0.1 ± 0.01 s^{-1}) was same as that for reductively methylated α-TM and α-TM-D137L (0.09 ± 0.03 s^{-1}).

FIGURES and TABLES

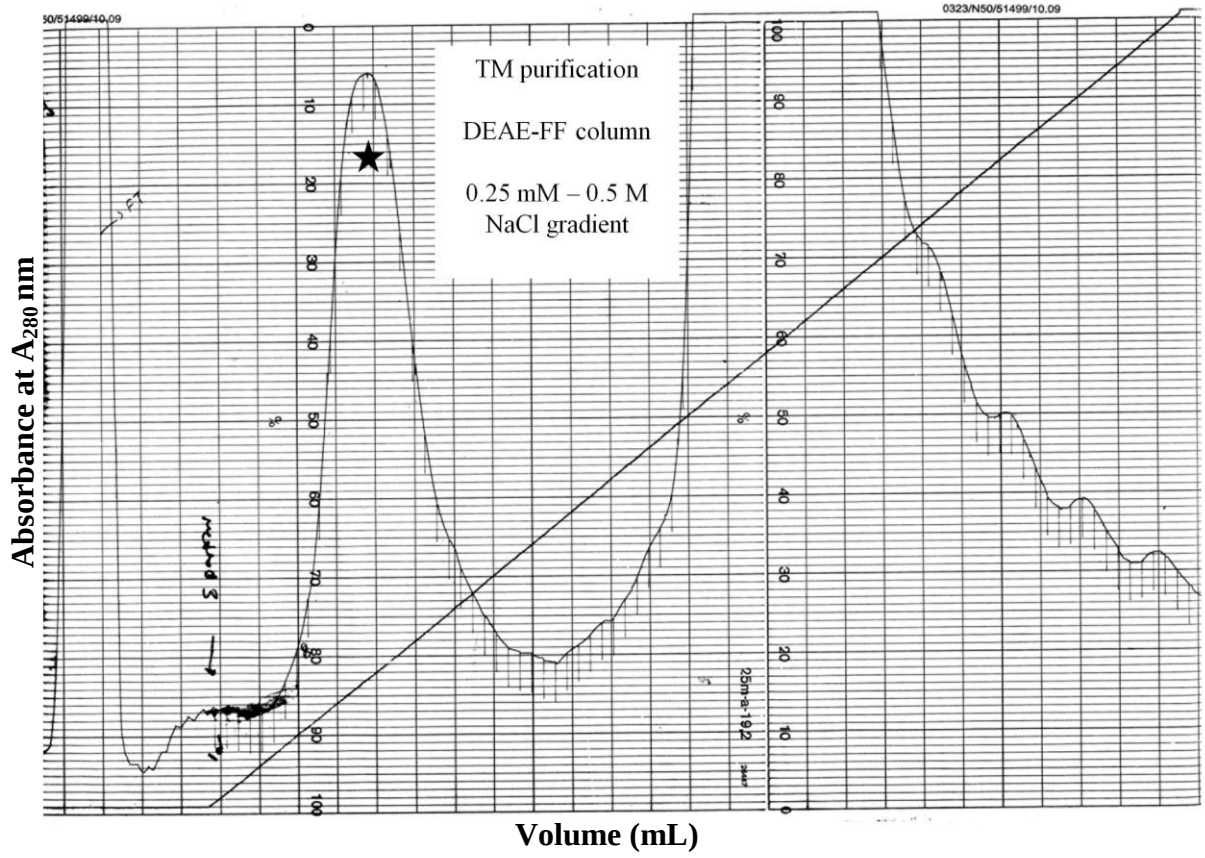

Figure 9. Representative anion-exchange FPLC purification-chromatogram of α-TM using DEAE-FF column. FPLC was performed at 1 mL/min. Elution profile was obtained by the absorbance at 280 nm of the collected fractions, after elution by linear NaCl gradient (0.25 mM-0.5 M, diagonal line) in 6 M urea, 0.5 mM EDTA, 50 mM tris-HCl pH 8.0, and 0.01% NaN_3.The *star* shows the peak corresponding to those fractions containing purified TM. Representative SDS-PAGE of purified fractions is shown in Figure 10.

A.

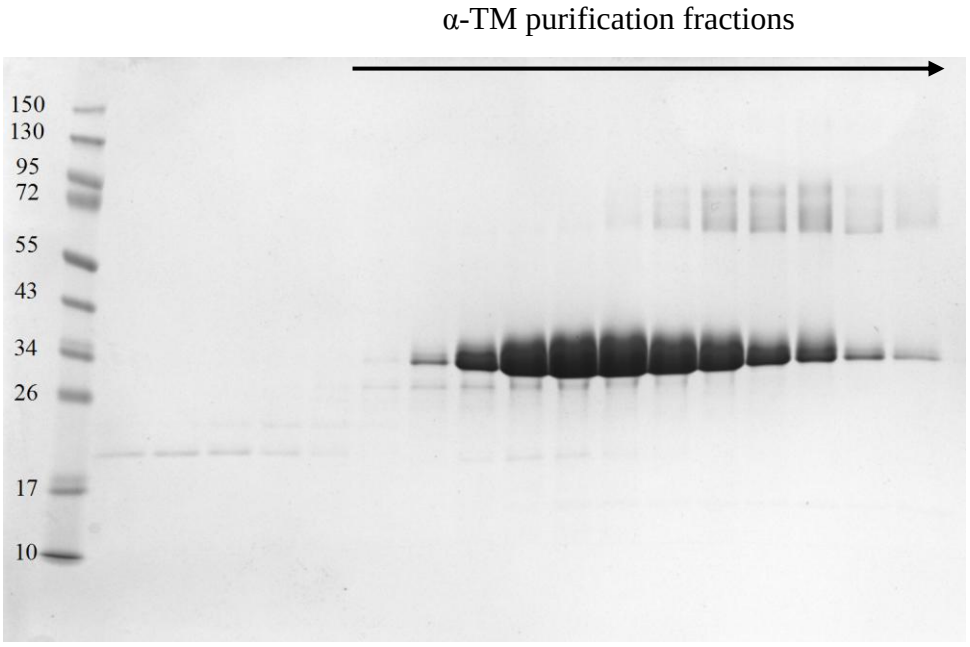

B.

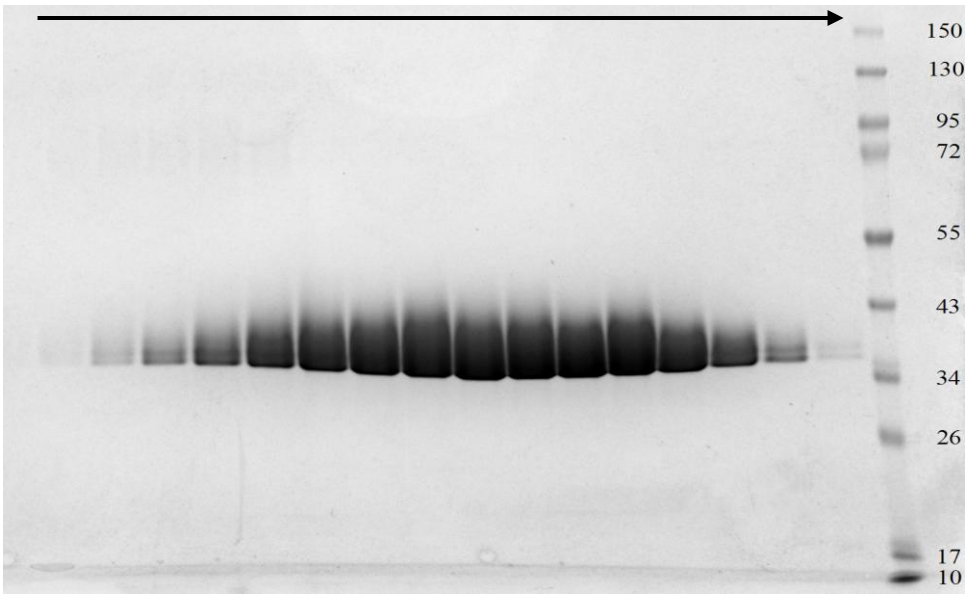

Figure 10. Protein content of eluted fractions from the anion-exchange purification of α-TM and α-TM-D137L. Representative 12% SDS-PAGE images of eluted fractions from **(A)** α-TM and (**B)** α-TM-D137L purification are shown. In both cases, 7.5 µl 2X laemmli loading buffer with 35mM DTT was mixed with 7.5 µl of a purification fraction, and 13 µl of this mixture was loaded into the gel.

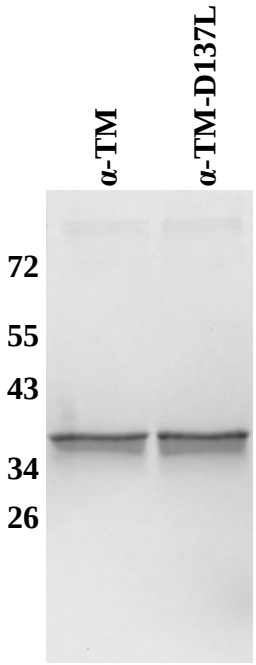

Figure 11. SDS-PAGE gel of reduced recombinant α-TM and α-TM-D137L samples that were used in DSC measurements. In both lanes, 15 µl of 2.7 µM protein sample was mixed with 15 µl 2X laemmli loading buffer in the presence of 1 mM β-mercaptoethanol and 20 µl of this mixture was loaded into 12% SDS-PAGE gel.

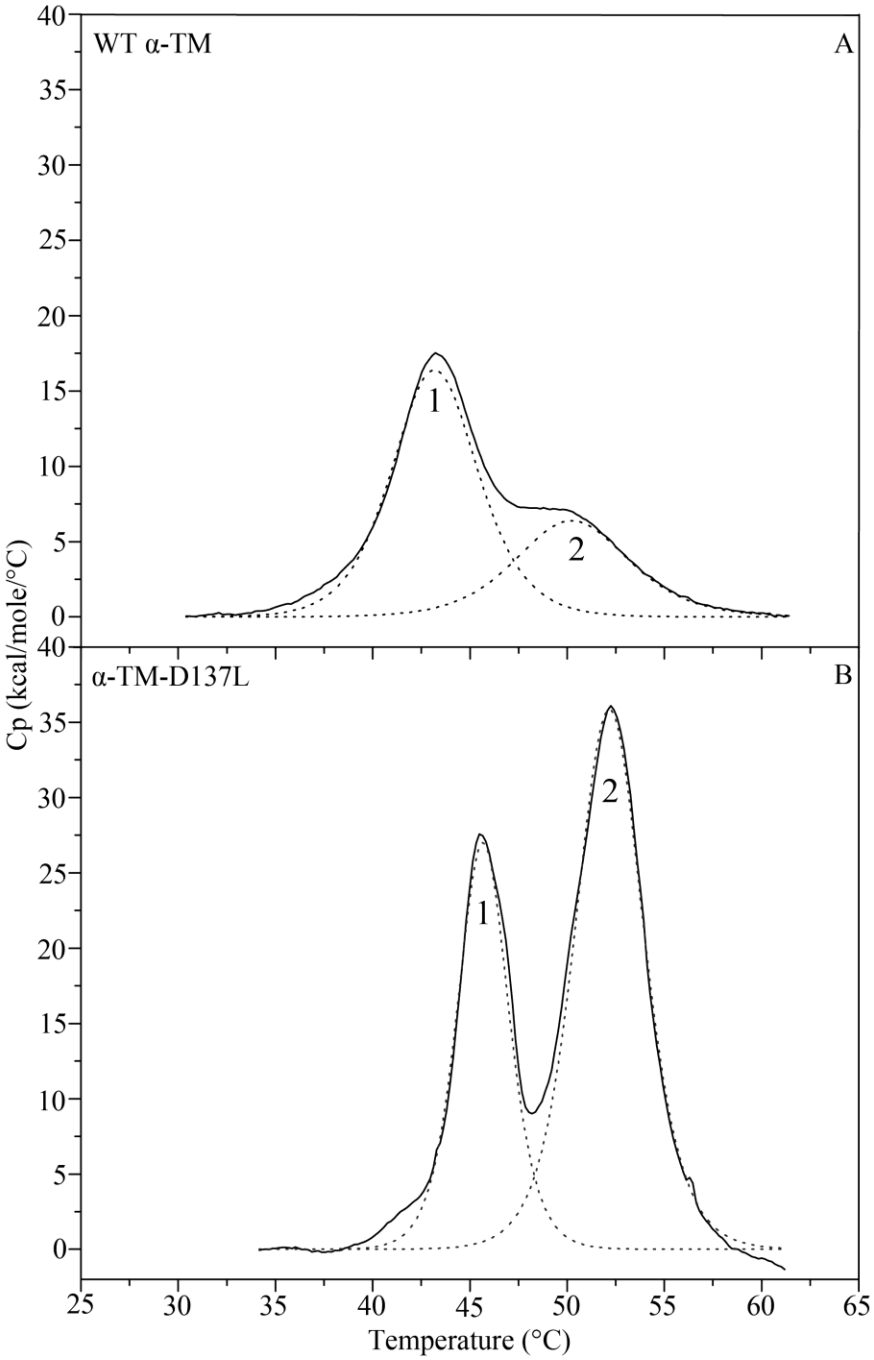

FIGURE 12. Deconvolution analysis of the excess heat capacity (C_p) function of reduced (A) WT α-TM and (B) α-TM-D137L. Solid lines represent experimental curves after subtraction of chemical and instrumental base lines. Dotted lines show individual thermal transitions (domains) obtained from fitting the data to the non-two-state model. The heating rate was 1 ºC/min. Concentration of reduced protein samples were 1.8 mg/ml. Buffer conditions were 20 mM MOPS, pH 7.0, 1 mM EDTA, 0.1 M NaCl and 1 mM β-mercaptoethanol. Samples were heated up to 90°C but only a temperature region below 65°C, where thermal transitions occurred, is depicted. (See Table IV for parameters)

TABLE IV. CALORIMETRIC PARAMETERS OBTAINED FROM DSC MEASUREMENTS OF RECOMBINANTLY EXPRESSED WT α-TM AND α-TM-D137L

	Domain-1(C-terminal region)		**Domain-2 (N-terminal region)**	
	*Tm** (°C)	ΔH_{cal} ♯ (kcal/mole) (% of total)	*Tm** (°C)	ΔH_{cal} ♯ (kcal/mole) (% of total)
α-TM	43.35	91.13 (70.5%)	49.99	38.07(29.5%)
α-TM-D137L	45.68	94.58 (36.5%)	52.19	168 (63%)

* The error of the given values of *Tm* (transition temperature) did not exceed ±0.2 °C.

♯ The relative error of the given values of Δ*H*cal (calorimetric enthalpy) did not exceed ±10%.

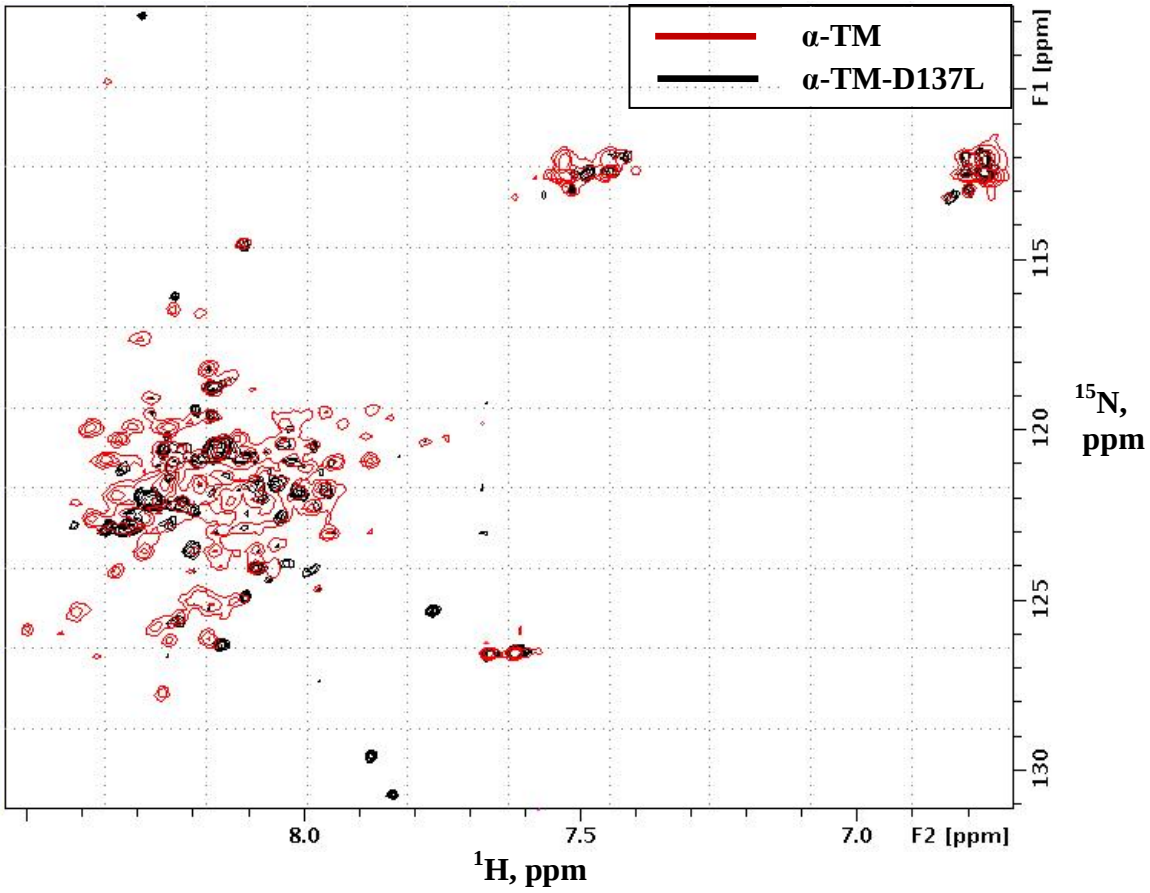

Figure 13. An overlay of 2D ^{1}H-^{15}N edited HSQC spectra of N^{15} labeled α-TM (red) and α-TM-D137L (black). The spectra of 200 μM dimers were obtained at 25 °C on a 900 MHz Bruker NMR spectrometer. Conditions were 55mM NaCl, 25 mM sodium phosphate (pH 7.0), 1 mM EDTA and 2 mM DTT.

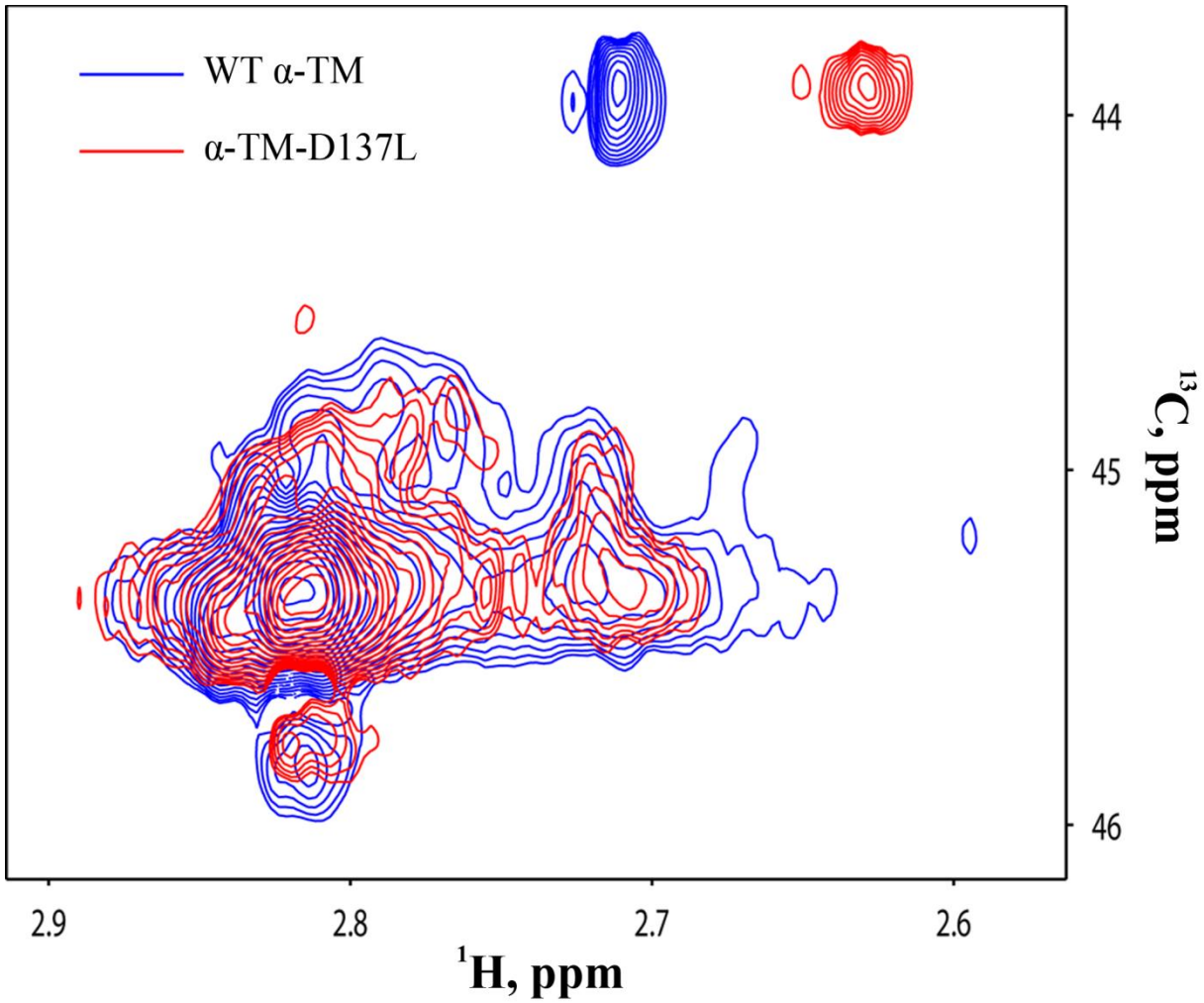

FIGURE 14. An overlay of ^{1}H-^{13}C edited HSQC spectra of reductively methylated WT α-TM (blue) and α-TM-D137L (red). The spectra of 5 µM proteins were obtained at 25 °C on a 900 MHz Bruker NMR spectrometer. Conditions were 25 mM sodium-phosphate buffer, pH 7.0, 0.1 M NaCl, 1mM EDTA and 2 mM DTT.

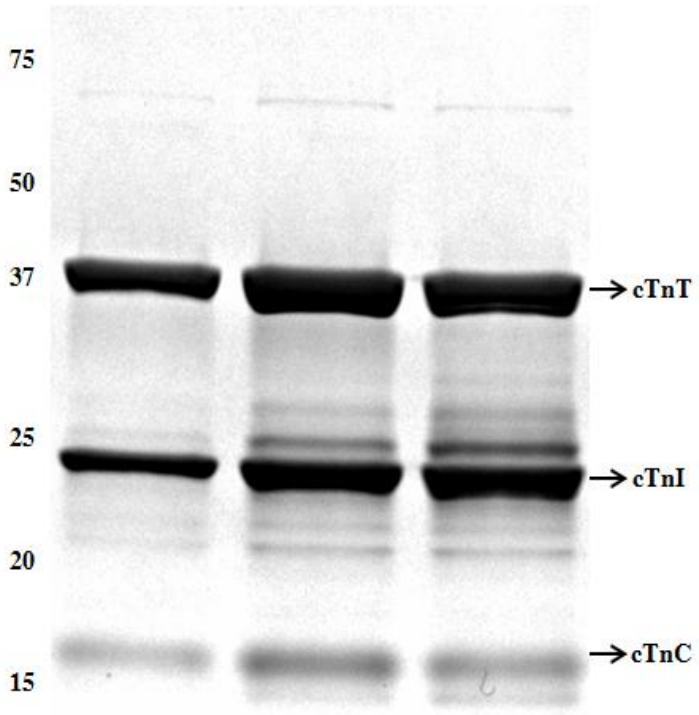

Figure 15. SDS-PAGE gel of cTn complex purification fractions that were used in *in vitro* acto-myosin S1 in ATPase activity assay. Fractions were eluted from a resource Q column. Fractions were run on a 12 % Tris-Glycine precast SDS-PAGE gel (BIORAD). 5 µl 3X laemmli loading buffer with 30 mM DTT were mixed with 10 µl of a purification fraction, and 15 µl of this mixture were loaded into the gel.

B. Effects of Decreased Structural Flexibility of alpha-Tropomyosin on Cardiac Regulation in a Novel Transgenic Mouse Model

1. Generation of alpha-tropomyosin-D137L transgenic mice

In order to examine the physiological importance of the residue Asp137 and the decreased TM flexibility in ejecting hearts, we generated α-TM-D137L TG mice as described under the methods section. The transgene construct utilized to generate the α-TM-D137L TG mice is shown in Figure 16A. The α-MHC promoter drives cardiac specific expression of the α-TM-D137L cDNA.

a) Expression of alpha-tropomyosin-D137L in transgenic mouse hearts

Multiple TG mice lines expressing various percentages of the α-TM-D137L protein were initially generated. However, all studies in this thesis were conducted using the TG mice line with the highest α-TM-D137L expression level. This decision was made after initial echocardiographic assessment of multiple TG lines. We found that line 168 displayed the greatest cardiac dysfunction parallel to its highest α-TM-D137L expression level (81.3 ± 1.5 %).

We were not able to separate endogenous α-TM and α-TM-D137L protein bands using traditional SDS-PAGE approach given only a 2 Dalton difference between Leu and Asp. Instead, α-TM-D137L expression level in TG mouse hearts was analyzed using 2D-DIGE. Differentially labeled myofibrillar protein preparations from hearts of age matched NTG and TG mice were run on 2D gels. Results from NTG samples displayed one unphosphorylated and one phosphorylated (P-) TM spot (Figure 16 B, channel 1) that have been well characterized previously in our

laboratory (105). As anticipated, we detected four TM spots from TG samples (Figure 16 B, channel 2). Overlay of the differentially labeled NTG and TG channels allowed us to clearly identify these four spots (Figure 16 B, channel 3). Conversion of a negatively charged Asp residue to a neutral Leu resulted in a rightward shift (towards the minus end of the pH strip) in TM spots due to loss of charge in the protein. Quantification of 2D-DIGE gels showed an 81.3 ± 1.5% replacement (total α-TM-D137L / total α-TM) of WT TM with the variant TM in TG mouse hearts. There was a concomitant decrease in NTG TM levels, maintaining 100% total TM levels. Myofibrillar protein preparations from NTG and TG mice hearts were run on an SDS-PAGE gel as a control, which demonstrated that all other major cardiac myofilament proteins were expressed at a similar stoichiometric ratio in TG mouse hearts compared to NTG ones (data not shown).

b) Phosphorylation of tropomyosin in transgenic mouse hearts

Post translational modification (PTM) is one of the most important ways to modulate function and interactions of sarcomeric proteins in the heart. It has been recently reported in both *in vitro* and *in vivo* studies that TM phosphorylation plays a role in sarcomeric function and thin filament activation (121,122). Thus, we tested whether α-TM-D137L expression in TG mouse hearts alters phosphorylation level of TM.

Percent total TM phosphorylation (total P-TM / total TM) % in myofibrillar protein samples from 4 mon old NTG and TG mouse hearts was determined using the same 2D-DIGE approach which was used for quantification of α-TM-D137L expression in mouse hearts (Figure 16 B). No statistically significant difference between total P-TM levels in 4 mon old TG (~27%)

and NTG (~25%) mouse hearts was detected (Table IX). Further analysis of TM phosphorylation in 8 mon old NTG (~33%) and TG (~37%) mice again showed no statistically significant difference between the two (Table X).

2. *In situ* cardiac function

a) ***Echocardiography measurements and pressure-volume loop analysis of transgenic mouse hearts suggested a phenotype similar to dilated cardiomyopathy***

Echocardiography followed by PV loop measurements was conducted to detect whether expression of α-TM-D137L with reduced structural flexibility has an effect on *in vivo* cardiac function.

Echocardiography results from 4 and 8 mon old α-TM-D137L TG and NTG mice are shown in Figure 17 and Table V. Data suggested that 4 mon old TG mice had systolic dysfunction as indicated by a significant depression in velocity of circumferential shortening (Vcf), fractional shortening (FS), ejection fraction (EF) and mitral annulus systolic velocity (Sm). These defects in systolic function observed in 4 mon old TG mice were maintained at 8 mon old TG animals without any statistically significant, age dependent worsening compared to 4 mon old animals. This was also confirmed with measurements of Ca^{2+}-dependent active tension development of skinned fiber preparations from 4 and 8 mon old TG mouse hearts and NTG controls (see next section). Thus, the rest of our studies, including PV loop analysis, were conducted on 4 mon old animals only.

An indication of diastolic dysfunction although mild, was also observed in 4 mon old TG mouse hearts as demonstrated by prolongation of IVRT and an increase in the ratio of early LV filling and early mitral annular velocity (E/Em). The statistical significance in E/Em ratio was lost in echocardiography measurements taken in 8 mon old TG mice, however IVRT remained significantly prolonged.

A mild left ventricular dilation was also present in 4 mon old TG mice with a significant increase in left ventricular internal dimension in systole (LVIDs). This dilated phenotype became more prominent in 8 mon old TG mouse hearts which demonstrated significant increases in both LVIDs and left ventricular internal dimension in diastole (LVIDd).

Stroke volume (SV) and cardiac output (CO) were maintained. There was no change in heart rate (HR) of TG mice compared to NTG controls.

In agreement with morphology data obtained from echocardiography, heart-weight to tibia-length ratio, which is an independent measure of hypertrophy, was not significantly different between 4 and 8 mon old NTG and TG mouse hearts (Figure 19 A). Additionally, survival analyses suggested no significant difference between the viability of TG and NTG mice over the course of 8 mon. (Figure 19 B).

In echocardiography measurements, we identified significantly depressed contractile function coupled to mild but significant dilation in left ventricles of TG mouse hearts, both in 4 and 8 mon of age. This phenotype is highly comparable to DCM. Since investigations of the PV relation are acknowledged as the most appropriate and thorough means of indexing ventricular contractility independent from loading conditions (123,124) we further characterized the cardiac cycle of TG mice by employing PV loop analysis.

Marked changes were observed in the left ventricular hemodynamics of 4 mon old TG mice. In agreement with findings from echocardiography measurements, pump function was significantly depressed in TG mouse hearts as shown in representative baseline PV loops during an inferior vena cava (IVC) occlusion (Figure 18 and Table VI). There was a downward and rightward shift in the position of the PV loops obtained from TG mouse hearts compared to NTG controls. This decrease in the slope of ESPVR, which is a load-independent index of cardiac contractility that defines chamber end-systolic stiffness, indicates a loss of intrinsic inotropy. This led to an increase in end-systolic volume (ESV) and end-diastolic volume (EDV). There was also a decrease in end-systolic pressure (ESP). However, the decrease in SV was not significant. Even so, due to slight decrease in SV and significant increase in EDV, the decrease in EF was significant.

Systolic dysfunction was additionally apparent by the significant decreases in d*P*/d*t* max (peak rate of pressure rise), d*P*/d*t*-EDV (a load independent index of contractility as preload dependence of d*P*/d*t* max is effectively reduced by using this regression) and preload recruitable stroke work (PRSW) (a preload independent index that is the slope of SW-EDV relation and is less sensitive to minor measurement errors compared to the slope of ESPVR).

The decrease in the slope of EDPVR suggests an increase in ventricular compliance. This increase in compliance is likely associated with dilation of the ventricles. Altogether, in agreement with echocardiography results, the apparent depression of contractility, the increase in ESV and EDV, and the rightward shift of ESPVR and EDPVR lines demonstrate a phenotype similar to DCM.

3. Cardiomyocytes

a) Contractile mechanics of cardiomyocytes isolated from transgenic mouse hearts were diminished without any changes in intracellular calcium transients

In order to study underlying cellular mechanisms of systolic dysfunction in TG mouse hearts, which was detected by echocardiography and PV loop measurements, we measured cardiomyocyte contractile function and intracellular Ca^{2+} transients.

The regulation of cardiac contractility is dependent upon the changes in the functional state of the myofilaments in addition to the characteristics of the intracellular Ca^{2+} transients. Therefore we examined cell shortening and the Ca^{2+} transient relations in ventricular cardiomyocytes from 4 mon old NTG and TG mice using video edge detection and fura-2 fluorescence. The representative recordings of cell shortening (Figure 20 A), the kinetics of contraction and relaxation (Figure 20 B), and intracellular Ca^{2+} transients expressed as fura-2 fluorescence ratio (Figure 20 C) are demonstrated. Cardiomyocytes isolated from TG mice exhibited a statistically significant 30% reduction in the extent of unloaded cell shortening (NTG= 8.5% ± 0.34 vs. TG= 6.0 ± 0.30%). The peak rate of contraction (NTG= 131.4 ± 5.3 vs. TG 87.2 ± 3.0 μm/s) and the peak rate of relaxation (NTG= 92.9 ± 5.1 vs. TG= 61.8 ± 2.7 μm/s) were also diminished in cells expressing α-TM-D137L (Figure 20 D). The observed changes in contractility were independent of any alteration in Ca^{2+} transient (Table VII). There was also no significant difference in the average size of cardiomyocytes isolated from NTG and TG mouse hearts (data not shown). In summary, results demonstrated an inherent defect in myocyte

contractility due to α-TM-D137L expression in cardiomyocytes isolated from α-TM-D137L TG mouse hearts with no change in intracellular Ca^{2+} transients.

4. Mechanical properties of myofilaments

In addition to abnormalities in contractile properties of cardiomyocytes, alterations in cardiac myofilament mechanics can contribute to reduced pump function in TM-D137L TG mouse hearts. Hence, we compared mechanical properties of myofilaments from NTG and TG mouse hearts.

a) Myofilaments from transgenic mouse hearts showed decreased calcium sensitivity

In order to further elucidate the mechanisms responsible for the systolic dysfunction observed in the hearts of TG mice, we compared Ca^{2+}-dependent active tension development of cardiac skinned fiber preparations from α-TM-D137L TG mice and NTG controls. Ca^{2+}-dependent tension generation in myofilaments from 4 and 8 mon old NTG and TG mouse hearts was measured. In both instances, there was no significant change in the maximum developed tension of myofilaments from NTG and TG mice (Table VIII). However, the pCa_{50} (–log [Ca^{2+}] at 50%) was decreased in myofilaments from TG mouse hearts at both ages (Table VIII). This decrease in Ca^{2+} sensitivity or pCa_{50} was reflected by a rightward shift in the [Ca^{2+}]-tension curves of TG mice as shown in Figure 21.

The relationship between the [Ca^{2+}] and tension generation is sigmoidal and there is a relatively steep slope region within the middle of this curve reflecting the cooperative nature of the interaction. The maximal slope of this relationship is referred to as *Hill* coefficient (*n*H). Therefore, changes in cooperative activity of myofilaments are reflected by a change in the *Hill* coefficient. In our [Ca^{2+}]-tension measurements, a significant increase in *Hill* coefficient of TG myofilaments at both ages was demonstrated (Table VIII).

b) Expression of alpha-tropomyosin-D137L did not alter rigor cross-bridge dependent activation of myofilaments from transgenic mice

To probe whether the presence of α-TM-D137L in the cardiac myofilaments affects cooperative activation of the thin filaments induced by strongly bound cross-bridges, we varied the population of rigor cross-bridges in the myofilaments by varying the [MgATP] at pCa 9 and measured thin filament activation from the generated force.

Results showed no significant difference between the ability of strong cross-bridges to activate thin filaments from 4 mon old NTG and TG mouse hearts (Figure 22). The similarity in $pMgATP_{50}$ (pMgATP needed to induce half-maximal rigor force generation) of NTG and TG myofilaments suggested that the sensitivity of rigor force to ATP was unaffected due to α-TM-D137L expression. There was also no significant difference in the *Hill* coefficient and maximum force (Fmax) generation between two groups. This demonstrates that in contrast to altered Ca^{2+}-dependent cooperative activation of thin filaments from TG mice, α-TM-D137L expression did not affect cooperative activation of myofilaments by strongly bound cross-bridges.

c) Alpha-tropomyosin-D137L expression impaired length-dependent activation of myofilaments from transgenic mouse hearts

There is considerable evidence that Starling's Law of the Heart involves a dependence of myofilament Ca^{2+} sensitivity on SL (125). At relatively long SL, myofilament response to Ca^{2+} is higher at relatively short SL. This dependence of force on length at sub-maximal levels of activating Ca^{2+} is a determinant of the shape of the ESPVR and contractility (126). In order to study whether the presence of α-TM-D137L in the cardiac myofilaments affects length-dependent activation of thin filaments and helps define a mechanism for the depressed contractile function of TG mouse hearts, Ca^{2+}-dependent tension generation of myofilaments from 4 mon old NTG and TG mouse hearts at SL 1.9 μm and 2.3 μm was measured (Figure 23). pCa_{50} values for myofilaments from NTG mice at SL 1.9 μm, NTG mice at SL 2.3 μm, TG mice at SL 1.9 μm and TG mice at SL 2.3 μm were 5.88 ± 0.02, 5.97 ± 0.01, 5.83 ± 0.02 and 5.88 ± 0.04 respectively. *Hill* coefficients for myofilaments from NTG mice at SL 1.9 μm, NTG mice at SL 2.3 μm, TG mice at SL 1.9 μm and TG mice at SL 2.3 μm were 3.66 ± 0.13, 2.92 ± 0.15, 4.57 ± 0.56 and 3.42 ± 0.27 respectively. Hearts expressing α-TM-D137L demonstrated that length-dependent activation was altered with a reduced delta pCa_{50} (ΔpCa_{50}; the difference between the pCa_{50} obtained at SL 2.3 μm and 1.9 μm). This result suggested that compared to NTG controls, length dependent increase in Ca^{2+} sensitivity was blunted in TG mouse hearts.

5. Myofibrillar proteins

a) Expression of alpha-tropomyosin-D137L did not change expression levels and post-translational modification status of major myofilament proteins from transgenic mouse hearts

PTM of the sarcomeric proteins is one means by which the heart can respond to ever-changing hemodynamic demands to maintain cardiac output in health and disease. Therefore alteration in the PTM state of the major myofilament proteins is another possible mechanism underlying the systolic impairment observed in TG mouse hearts. To elucidate whether α-TM-D137L expression alters the modification status of other myofilament proteins in TG mouse hearts, we again employed the 2D-DIGE approach. Results indicated no significant difference between the modification levels of major myofibrillar proteins (cTnI, cTnT, MLC and MyBP-C) from 4 mon old NTG and TG mice (Figure 24 and Table IX). Likewise the modification state of myofilament proteins remained unchanged in samples from 8 mon old NTG and TG mouse hearts (Table X).

b) Slightly increased beta-myosin heavy chain expression was detected in transgenic mouse hearts

In addition to PTMs, variable expression of myofibrillar protein isoforms also regulates heart function. One important protein that is known to undergo isoform switching with cardiac stress is MHC (127). A differential expression of MHC isoforms is known to alter

contraction and myofilament Ca^{2+} sensitivity. There are two cardiac MHC isoforms; α- and β-MHC. Adult mouse and human hearts predominantly express α-MHC in ventricles. We measured relative levels of α- and β-MHC expression in ventricular tissue from 4 and 8 mon old NTG and TG mice. Results demonstrated that β-MHC expression was slightly higher in myofibrillar preparations from 4 mon old TG mice compared to controls (Figure 25A) and this elevated level of β-MHC expression did not increase further with age (Figure 25 B).

FIGURES and TABLES

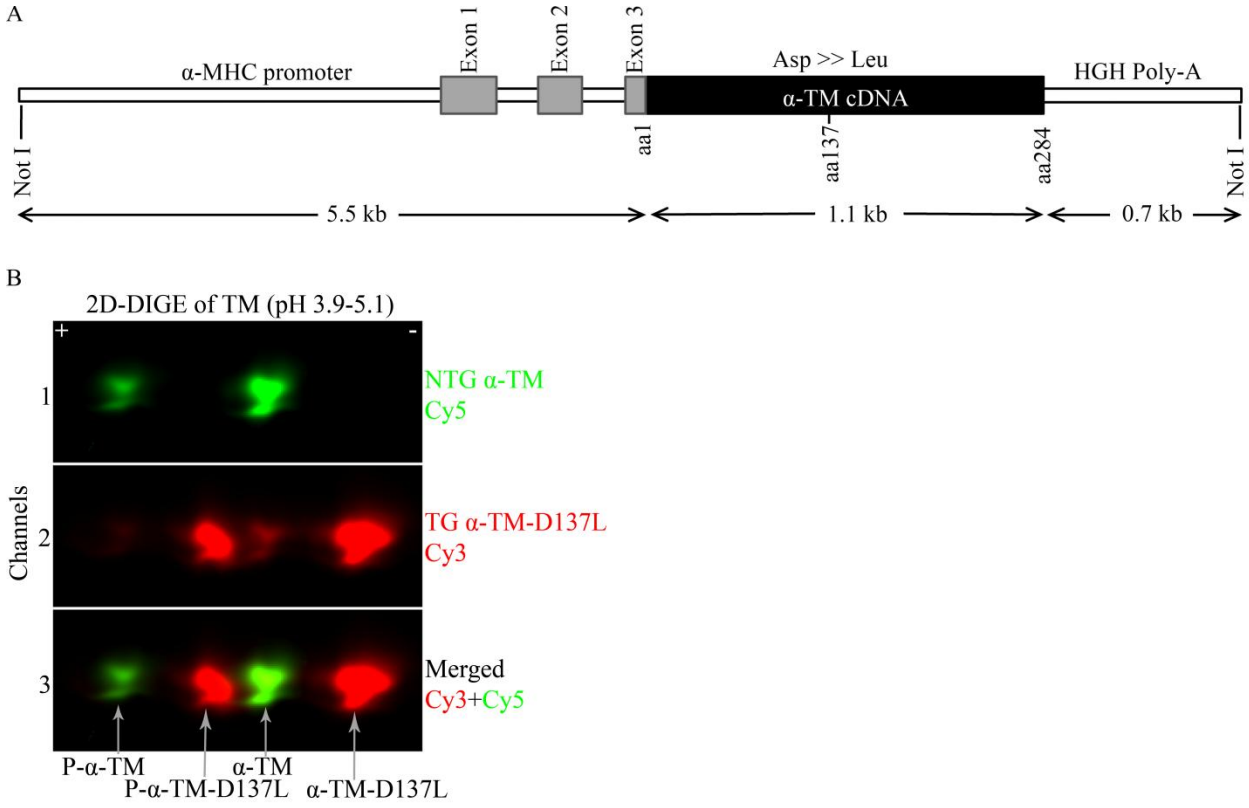

FIGURE 16. Generation of α-TM-D137L TG mouse. (A) The α-TM-D137L construct used to generate the TG mice. The α-MHC promoter drives cardiac specific expression of the striated muscle α-TM with encoded substitution at amino acid 137 (D137L). **(B)** TM region from a representative 2D-DIGE gel of myofibrillar proteins from 4 mon old NTG and TG mouse hearts is demonstrated. Myofibrillar fractions were labeled separately and mixed equally. Channel 1 shows Cy5 labeled α-TM (green), channel 2 shows Cy3 labeled α-TM-D137L (red) and channel 3 shows the merged image of channels 1 and 2. 81.3 ± 1.5% replacement (total α-TM-D137L / total α-TM) in TG mouse hearts was detected (n=11). P indicates phosphorylated protein.

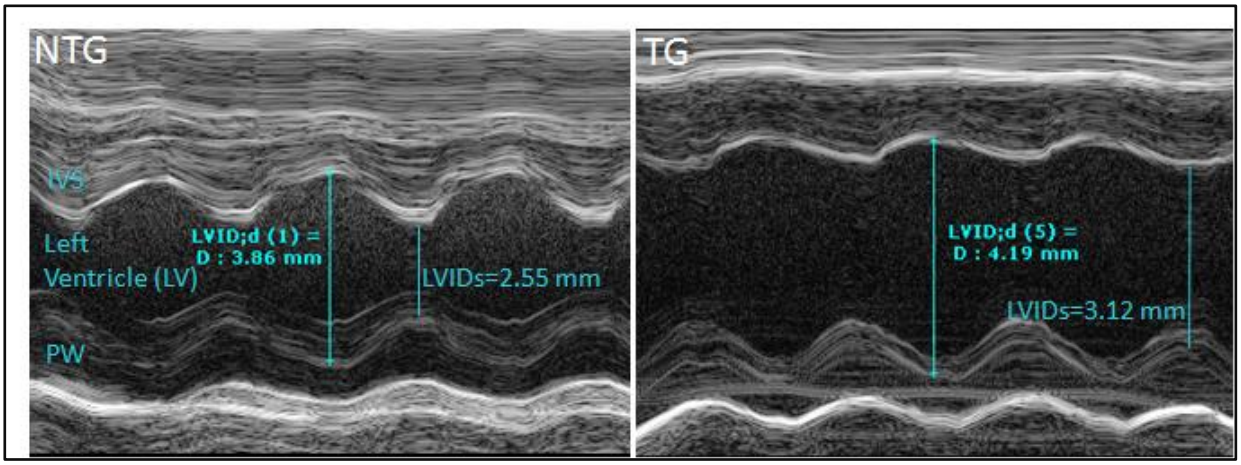

Figure 17. Representative M-mode echocardiography image of 8 mon old NTG and TG mouse heart ventricles. (IVS: interventricular septum, PW: posterior wall)

TABLE V. CARDIAC FUNCTION OF NTG AND α-TM-D137L TG MICE AT 4 AND 8 MON OF AGE ASSESSED BY ECHOCARDIOGRAPHY

Parameters	NTG 4 mon (n=11)	TG 4 mon (n=12)	NTG 8 mon (n=7)	TG 8 mon (n=9)
Systolic				
FS %	34.91 ± 0.91	30.34 ± 1.16*	37.83 ± 1.31	26.85 ±1.40 ≠
EF %	64.72 ± 1.26	57.93 ± 1.76*	68.31 ± 1.72	52.33 ± 2.10≠
V_{cf} (circ/sec)	6.45 ± 0.23	5.42 ± 0.29*	7.93 ± 0.26	5.17 ± 0.26≠
Sm (mm/sec)	22.33 ± 0.58	16.25 ± 0.80*	23.02 ± 1.17	15.56 ± 1.03≠
CO (mL/min)	19.52 ± 1.48	20.88 ± 0.96	26.73 ± 2.67	22.17 ± 1.30
HR (beats/min)	439.04 ± 9.33	462.56 ± 10.88	484.38 ± 10.89	473.93 ± 10.69
SV (μl)	44.77 ± 2.30	42.63 ± 2.23	47.01 ± 3.94	45.21 ± 2.14
Diastolic				
E/A Ratio	1.86 ± 0.11	1.82 ± 0.19	1.63 ± 0.10	1.52 ± 0.15
E/Em Ratio	31.03 ± 1.47	43.33 ± 3.95*	32.10 ± 0.73	39.21 ± 3.54
IVRT (ms)	13.02 ± 0.42	18.51 ± 1.01*	13.44 ± 0.66	18.52 ± 1.42≠
E wave DT (ms)	22.74 ± 1.19	22.25 ± 1.07	21.71 ± 1.68	21.45 ± 1.82
Morphology				
LA (mm)	2.04 ± 0.04	2.06 ± 0.08	2.13 ± 0.12	1.82 ± 0.07
LVIDs (mm)	2.63 ± 0.09	3.14 ± 0.10*	2.62 ± 0.10	3.21 ± 0.08≠
LVIDd (mm)	3.92 ± 0.10	4.22 ± 0.08	3.94 ± 0.16	4.41± 0.08≠
LV mass (mg)	74.91 ± 3.43	88.24 ± 5.00	104.46 ± 8.75	105.62 ± 3.84
RWT (mm)	0.32 ± 0.02	0.31 ± 0.01	0.41 ± 0.02	0.40 ± 0.01

E/A ratio, ratio of maximal velocity of E (early LV filling and A (atrial contraction) waves; E wave DT, E wave deceleration time; RWT, relative wall thickness. See methods section for the rest of the abbreviations.

* indicated $P< 0.05$ vs NTG at 4 mon old.

≠ indicated $P< 0.05$ vs NTG at 8 mon old

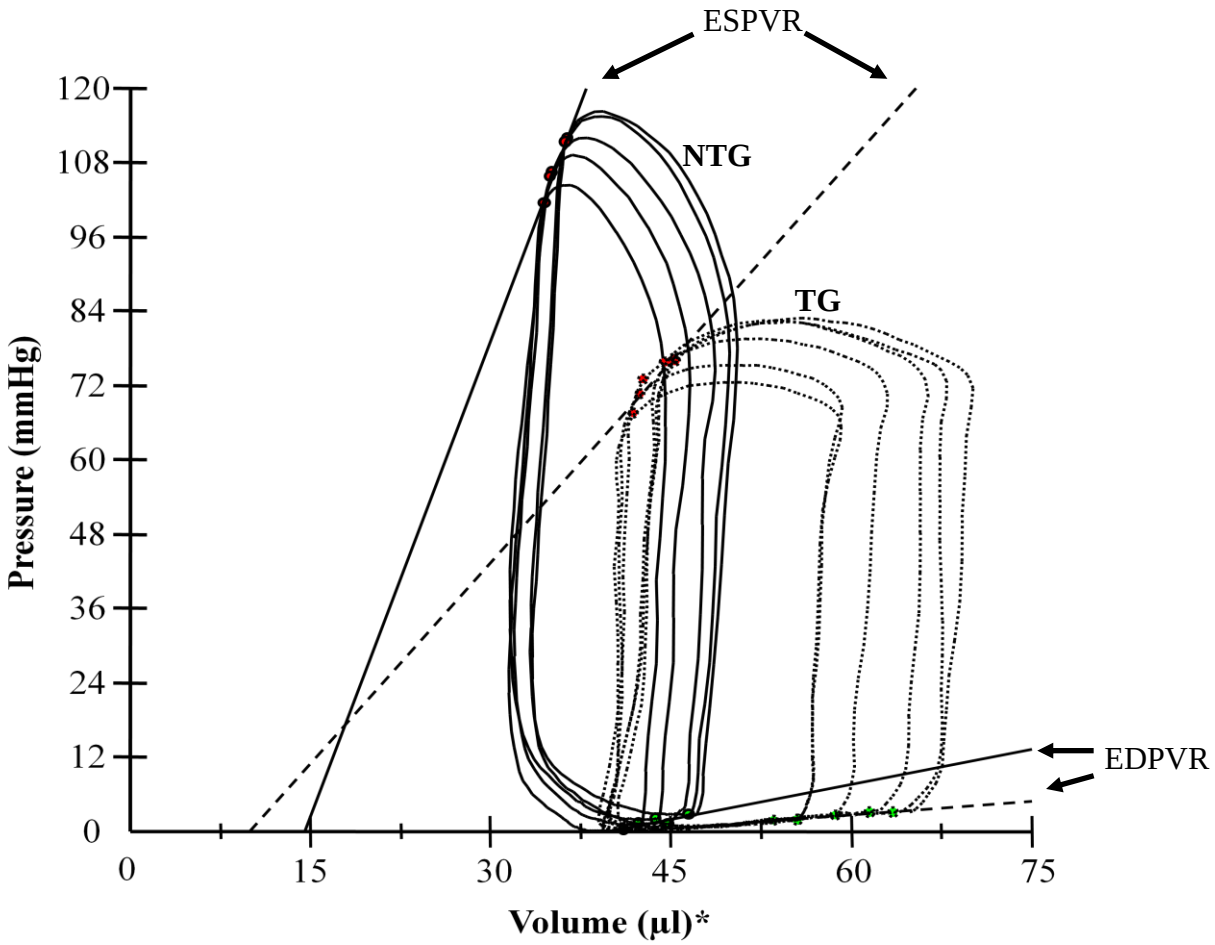

*Volume is uncorrected for parallel conductance

Figure 18. Representative left ventricular PV loops under baseline conditions, following an inferior vena caval occlusion. The black solid loops and solid slope are indicative of the ESPVR in the NTG group. The dotted black loops and dotted slope represent the depressed ESPVR in the TG group. See table VI for absolute values for all hemodynamic parameter.

TABLE VI. STEADY STATE AND HEMODYNAMIC PARAMETERS FROM PV LOOP MEASUREMENTS OF 4 MON OLD NTG AND TG MOUSE HEARTS

Parameters	**NTG 4 mon (n=10)**	**TG 4 mon (n=8)**
ESP (mmHg)	109.01 ± 6.15	87.94 ± 5.31*
EDP (mmHg)	4.12 ± 0.54	4.53 ± 0.89
ESV (µL)	29.84 ± 3.28	52.15 ± 6.06*
EDV(µL)	49.93 ± 4.78	70.17 ± 6.69*
SV(µL)	28.22 ± 3.19	26.15 ± 2.71
Systolic Indices		
EF (%)	49.75 ± 2.77	33.32 ± 3.67*
d*P*/d*t* max (mmHg/sec)	10950 ± 785.10	6968 ± 726.4*
SW (mmHg* µL)	2306 ± 293.51	1855 ± 185.72
ESPVR (mmHg/ µL)	9.13 ± 1.0	4.44 ± 0.70*
d*P*/d*t* /EDV (mmHg/sec/ µL)	286.34 ± 24.73	185.61 ± 25.34*
PRSW (mmHg)	111.01 ± 10.34	74.25 ± 10.61*
Diastolic Indices		
d*P*/d*t* min (mmHg/sec)	-8596 ± 969.51	-6583 ± 1032.31
EDPVR (mmHg/ µL)	0.23 ± 0.03	0.11 ± 0.03*
Tau_g (msec)	12.12 ± 1.29	15.93 ± 2.26

See text for abbreviations.

* indicated $P < 0.05$ vs NTG at 4 mon old.

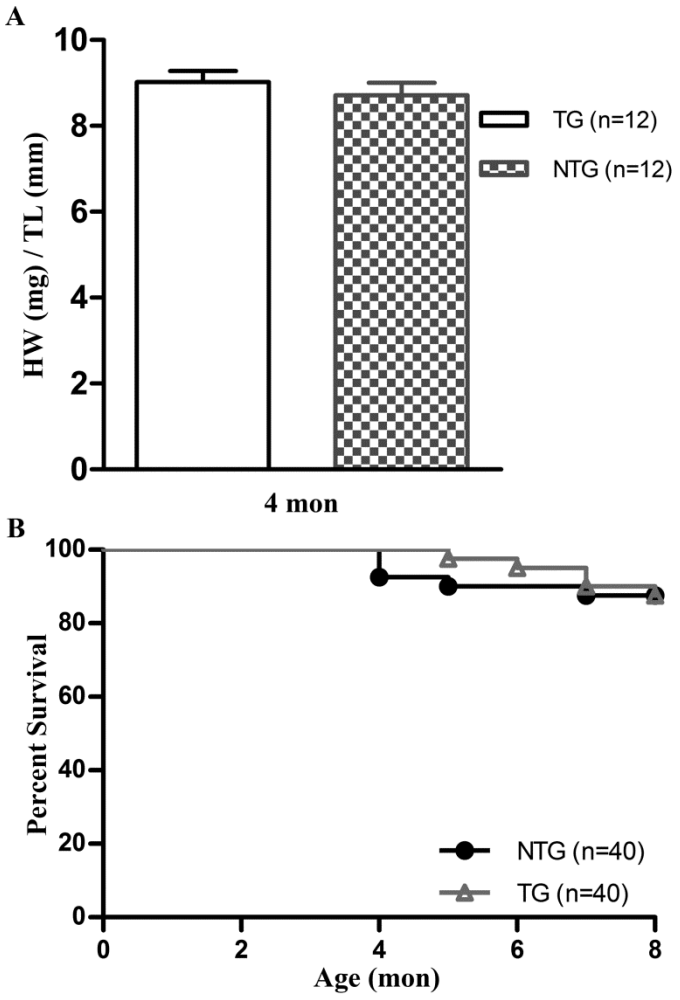

FIGURE 19. (A) Ratio of heart weight (HW) to tibia-length (TL) of 4 mon old NTG and TG mice. **(B)** Survival curve of NTG and TG mice over the course of 8 mon period.

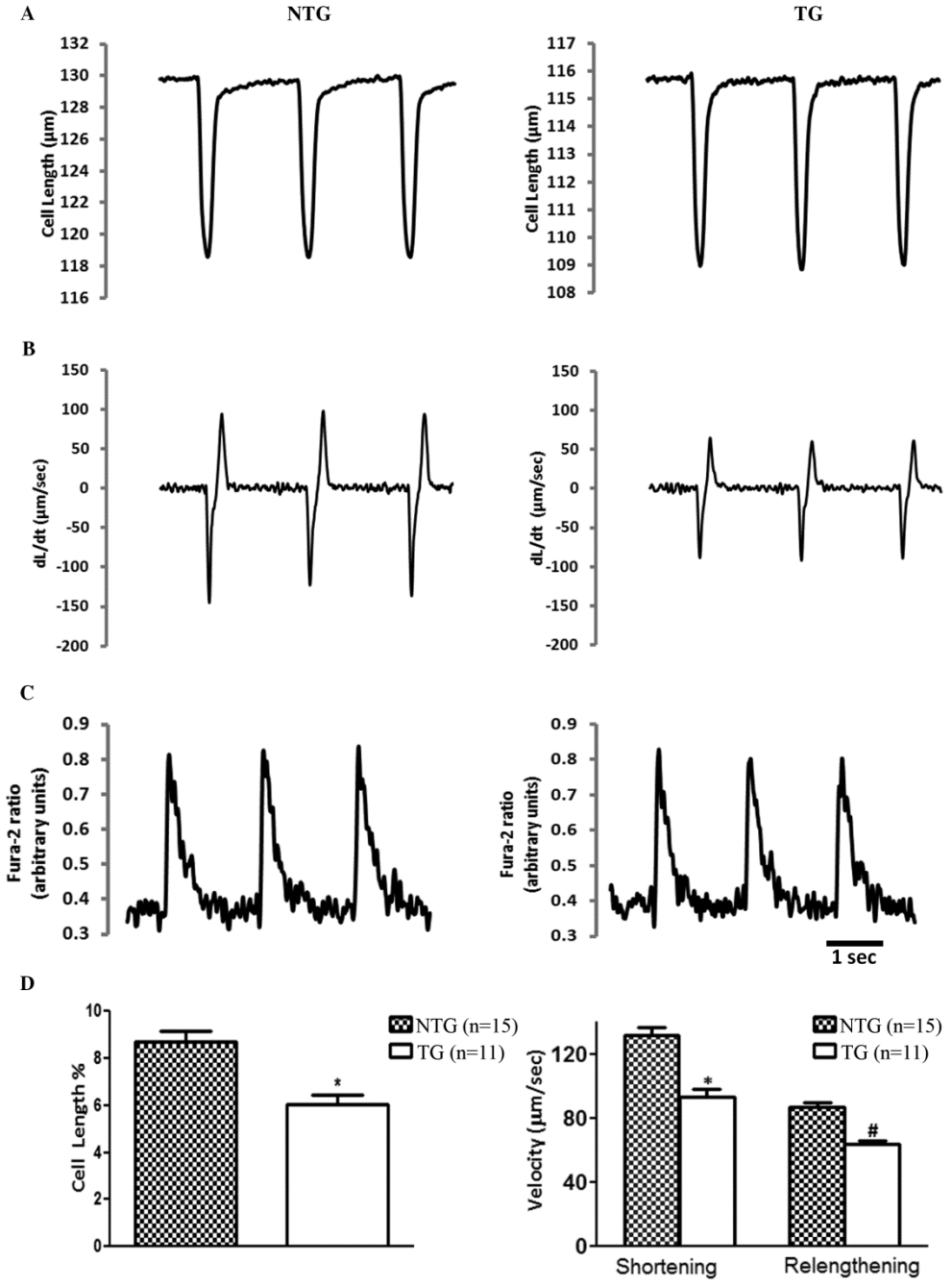

FIGURE 20. **Analysis of contractile mechanics and Ca^{2+} transients of mouse ventricular cardiomyocytes.** Representative recordings of **(A)** unloaded cell shortening, **(B)** kinetics of twitch contraction and relaxation and **(C)** intracellular Ca^{2+} transients (see Table VII. for parameters) of single isolated cardiomyocytes from 4 mon old NTG and TG animals. **(D)** Quantification of the contractile parameters (percent of shortening and maximal rates of contraction and relaxation). Five NTG animals (15 cells) and four TG (11 cells) mouse hearts were studied.*, # $p<0.05$ vs NTG.

TABLE VII. Ca^{2+} TRANSIENTS OF CARDIOMYOCYTES ISOLATED FROM 4 MON OLD NTG AND α-TM-D137L TG MOUSE HEARTS

	NTG 4 mon (n=15)	**TG 4 mon (n=11)**
Baseline	0.37 ± 0.01	0.36 ± 0.01
Amplitude (ratio units)	0.49 ± 0.01	0.44 ± 0.02
Tau (ms)	257.61 ± 9.52	255.44 ± 8.54

n indicated number of cells from 5 NTG and 4 TG mice hearts.

Representative recordings are shown in Figure 20.

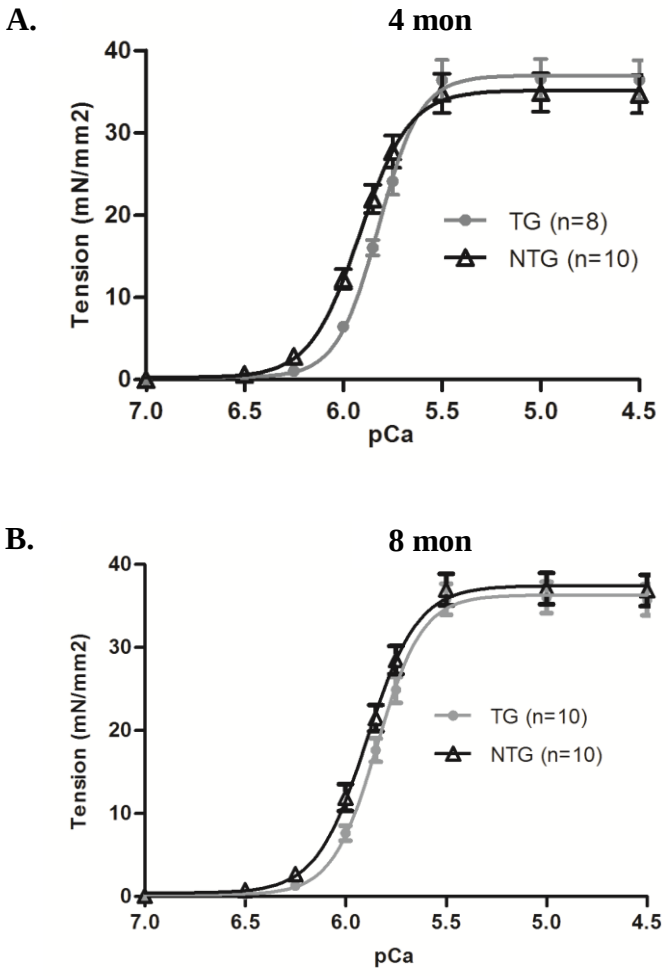

FIGURE 21. pCa-tension relation of skinned fiber bundles. Fibers from (A) 4 mon and (B) 8 mon old NTG (black) and TG (gray) mouse hearts. Measurements were carried out at SL= 2.2 μm, at 25°C. (see Table VIII for parameters)

TABLE VIII. PARAMETERS DESCRIBING Ca^{2+} DEPENDENT TENSION GENERATION IN SKINNED FIBER BUNDLES FROM 4 AND 8 MON OLD NTG AND TG MOUSE HEARTS

	NTG 4 mon (n=10)	**TG 4 mon (n=8)**	**NTG 8 mon (n=10)**	**TG 8 mon (n=10)**
pCa_{50}	5.92 ± 0.01	5.82 ± 0.02*	5.90 ± 0.01	5.84 ± 0.01$^{\sharp}$
n_H	3.51 ± 0.08	4.12 ± 0.06*	3.56 ± 0.10	4.01 ± 0.10$^{\sharp}$
Max. Force (mN/mm^2)	35.12 ± 2.34	36.91 ± 2.45	37.40 ± 1.89	36.30 ± 1.91

n_H indicates Hill coefficient.

n indicated number of fibers from 5 NTG and 4 TG mice hearts.

*****indicated $P< 0.05$ vs NTG at 4 mon of age.

$^{\sharp}$indicated $P< 0.05$ vs NTG at 8 mon of age.

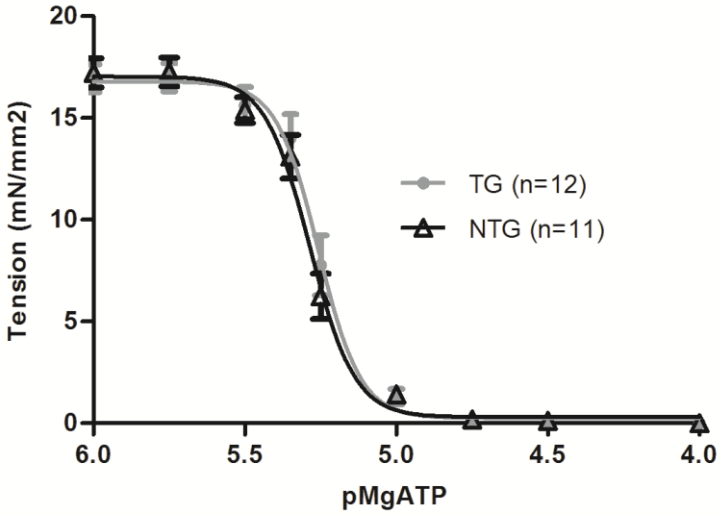

FIGURE 22. pMgATP-tension relation of skinned fiber bundles from 4 mon old NTG (black) and TG (dark gray) mouse hearts. SL = 2.2μm, at 25°C. NTG $[MgATP]_{50}$ = 5.28±0.01, TG $[MgATP]_{50}$ =5.26±0.01, NTG n_H=5.11±0.5, TG n_H=5.42±0.28, NTG Fmax= 16.51±0.81 mN/mm^2, TG Fmax=17.03±0.69 mN/mm^2.

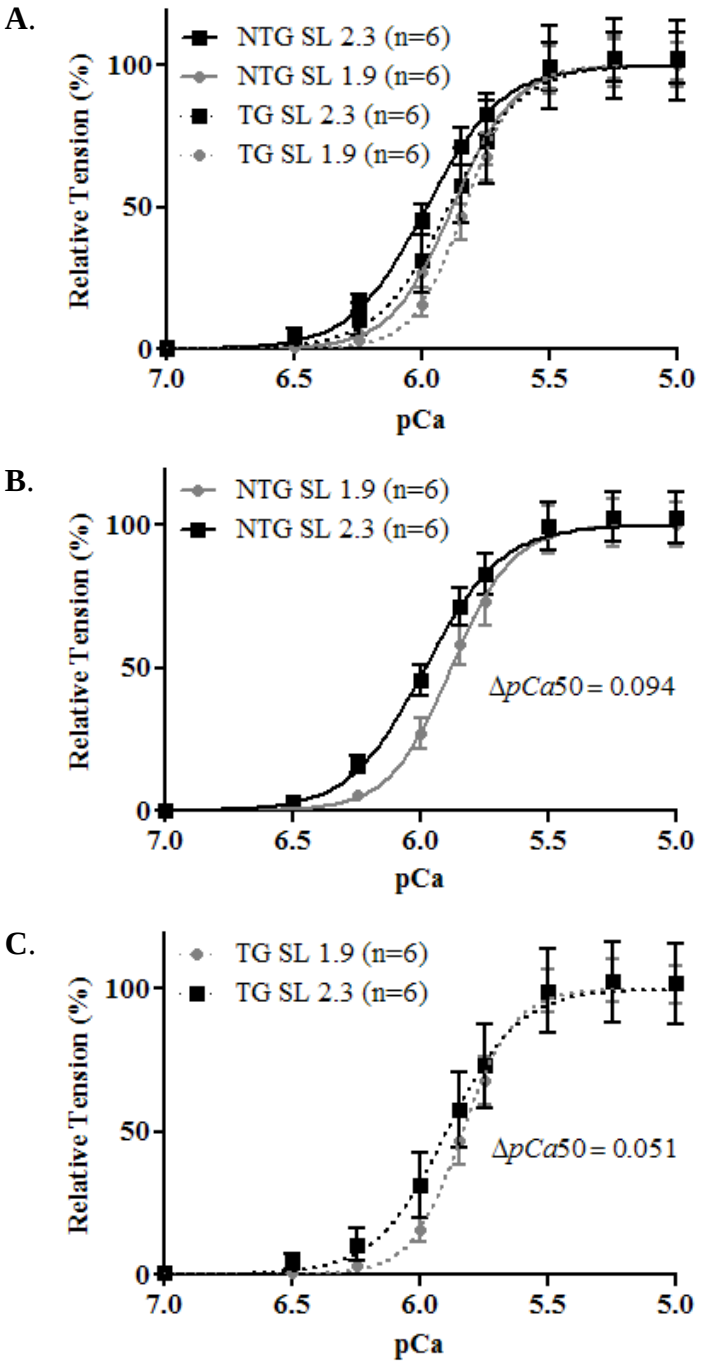

Figure 23. Length-dependent tension generation of skinned fibers from 4 mon old NTG and TG mouse hearts. (A) Isometric tension generation of fibers from NTG and TG mouse hearts at SL 1.9 μm and 2.3 μm. **(B)** Isometric tension generation of fibers from NTG mouse hearts at SL 1.9 μm and 2.3 μm. **(C)** Isometric tension generation of fibers from TG mouse hearts at SL 1.9 μm and 2.3 μm.

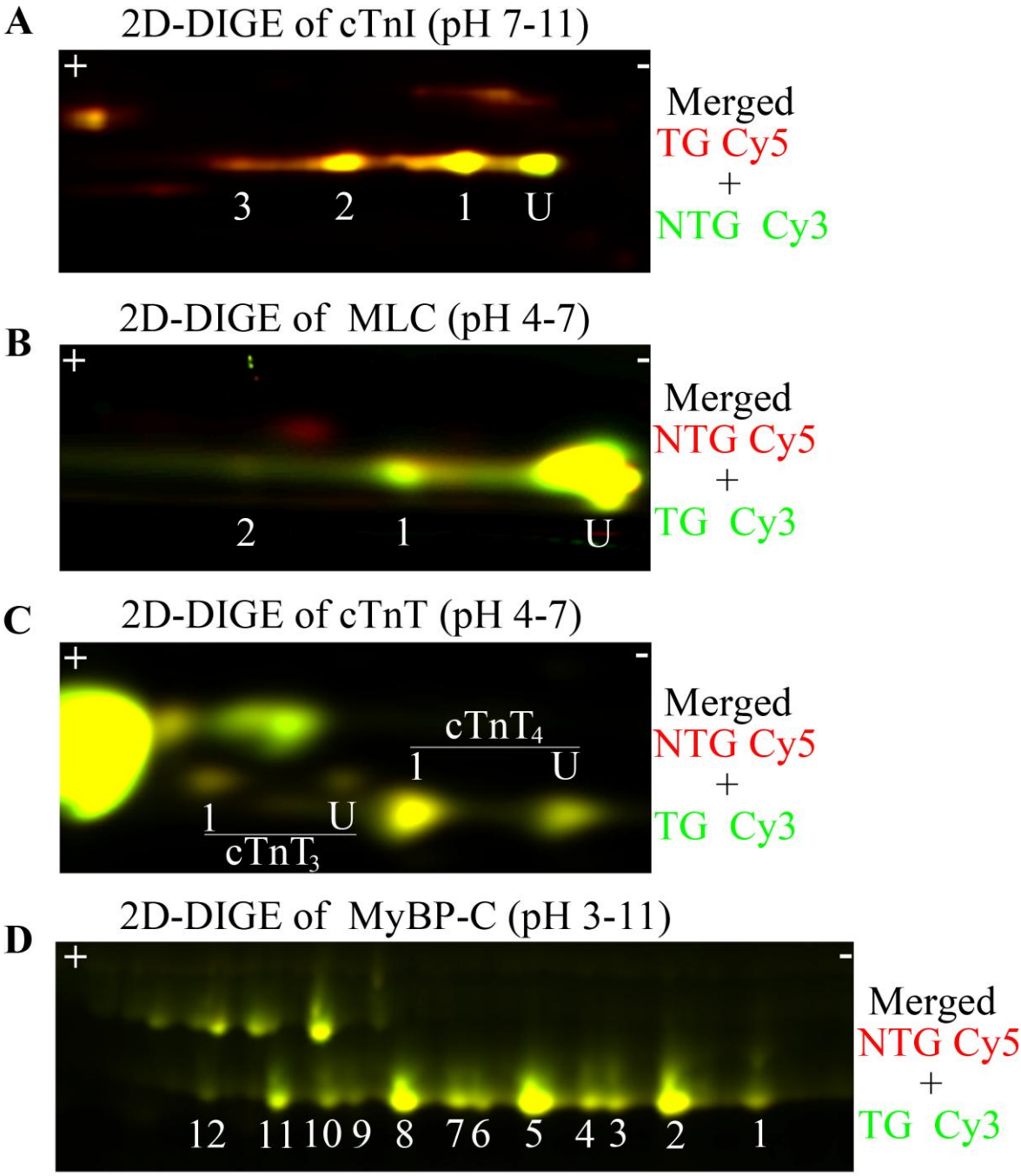

Figure 24. Comparison of PTM status and expression profile of myofibrillar proteins from 4 mon old NTG and TG mouse hearts by 2D-DIGE. Representative 2D-DIGE gel images (merged) showing region of **(A)** cTnI, **(B)** MLC, **(C)** cTnT and **(D)** MyBP-C. In *A* through *C*, U indicates unmodified. pH values indicate the pH range of the strip used for the first dimension. Samples were labeled with different Cy dyes and equally mixed to run in the same 2D gel. Quantification of protein spots are shown in Table IX.

TABLE IX. QUANTIFICATION OF 2D-DIGE GELS OF MYOFILAMENT PROTEINS FROM 4 MON OLD NTG AND TG MOUSE HEARTS

% total P-TM		% of total cTnI					% of total MLC				% of total $cTnT_{3+4}$		
		Spots	**U**	**1**	**2**	**3**	**Spots**	**U**	**1**	**2**	**Spots**	**U**	**1**
NTG	25.11	**NTG**	24.69	27.37	19.91	14.44	**NTG**	80.53	15.09	4.55	**NTG**	35.03	65.04
(n=4)	±1.51	**(n=5)**	±3.04	±0.66	±0.68	±4.08	**(n=4)**	±1.19	±0.98	±0.25	**(n=4)**	±1.3	±0.34
TG	27.13	**TG**	20.02	27.52	16.55	22.52	**TG**	80.50	14.95	4.68	**TG**	37.91	62.11
(n=4)	±1.31	**(n=3)**	±1.0	±1.5	±1.0	±1.0	**(n=4)**	±0.42	±0.45	±0.08	**(n=4)**	±1.3	±1.33

% of total MyBP-C												
Spots	**1**	**2**	**3**	**4**	**5**	**6**	**7**	**8**	**9**	**10**	**11**	**12**
NTG	2.54	3.32	4.01	3.77	10.63	4.32	11.45	19.58	8.21	12.14	14.11	5.95
(n=5)	±0.98	±1.38	±0.93	±0.93	±3.03	±0.2	±0.87	±1.24	±0.84	±1.09	±3.42	±1.19
TG	1.41	4.63	2.96	9.75	11.25	6.21	12.86	19.63	7.73	9.93	13.14	4.82
(n=3)	±0.17	±1.26	±0.89	±4.28	±1.03	±1.71	±0.79	±1.41	±0.88	±0.03	±0.78	±0.48

Representative 2D-DIGE gel images are shown in Figure 24.

TABLE X. QUANTIFICATION OF 2D-DIGE GELS OF MYOFILAMENT PROTEINS FROM 8 MON OLD NTG AND TG MOUSE HEARTS

% total P-TM		% of total cTnI					% of total MLC				% of total $cTnT_{3+4}$		
		Spots	**U**	**1**	**2**	**3**	**Spots**	**U**	**1**	**2**	**Spots**	**U**	**1**
NTG	33.41	**NTG**	24.94	30.41	23.82	14.74	**NTG**	81.61	15.33	3.11	**NTG**	34.81	65.20
(n=4)	±1.95	**(n=4)**	±2.04	±3.32	±2.64	±0.64	**(n=4)**	±1.74	±1.73	±0.32	**(n=4)**	±1.21	±1.2
TG	37.65	**TG**	20.72	28.91	26.96	16.88	**TG**	81.50	15.47	3.04	**TG**	34.94	65.11
(n=4)	±3.25	**(n=4)**	±2.09	±2.51	±0.76	±1.53	**(n=4)**	±1.9	±1.86	±0.52	**(n=4)**	±0.63	±0.63

% of total MyBP-C											
Spots	**1**	**2**	**3**	**4**	**5**	**6**	**7**	**8**	**9**	**10**	**11**	**12**
NTG	4.38	11.03	6.95	5.82	15.42	10.95	5.33	14.71	7.42	3.56	7.41	3.32
(n=4)	±0.43	±0.83	±0.29	±0.37	±1.34	±2.68	±1.29	±1.23	±2.21	±1.4	±0.4	±0.24
TG	4.45	10.31	6.86	6.31	16.50	7.77	8.12	16.94	5.03	4.69	7.70	3.73
(n=4)	±0.33	±1.22	±1.25	±0.93	±0.74	±1.96	±1.44	±1.08	±0.29	±1.6	±0.82	±0.51

Representative 2D-DIGE gel images are shown in Figure 24.

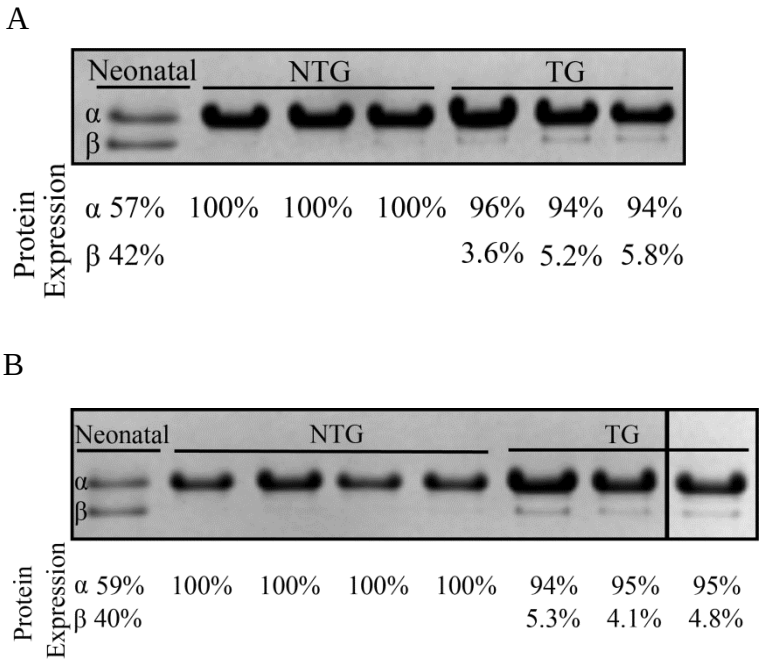

Figure 25. MHC isoform switch. SDS–PAGE gel analysis of myofibrillar proteins from **(A)** 4 mon old and **(B)** 8 mon old NTG and TG mouse hearts. Only the MHC area is shown. First lane in *(A)* and *(B)* are myofibrillar protein sample prepared from 1 day old neonatal mouse heart (2.5 µg/µl). NTG and TG mice samples were loaded at 9 µg/µl concentration. A percent relative quantification for α- and β-MHC bands in each lane is shown below the gel.

IV. DISCUSSION AND CONCLUSIONS

A. Summary of Results

Our initial studies on the structural implications of D137L mutation on recombinant α-TM demonstrated that the thermal unfolding character of α-TM-D137L was significantly different from α-TM. We detected a distinct increase in the thermal stability of both N- and C-terminal domains of α-TM-D137L compared to α-TM. This finding suggested a decrease in the global structural flexibility of α-TM-D137L. Using NMR measurements, we confirmed long-range rearrangements in TM structure due to D137L mutation.

In the second part of this thesis, we studied the physiological implications of decreased structural flexibility of TM in a novel α-TM-D137L TG mouse model. Measurements of ejecting hearts by echocardiography and PV loop analysis showed systolic dysfunction in α-TM-D137L TG mouse hearts with mild ventricular dilation. Overall, the observed phenotype in TG mouse hearts was similar to DCM. Studies with single cardiomyocytes isolated from TG mouse hearts showed a reduction in cell shortening and kinetics of shortening in the absence of any changes in Ca^{2+} transients. Ca^{2+}-dependent active tension generation measurements suggested a decrease in Ca^{2+} sensitivity of chemically skinned fiber bundles from TG mouse hearts, and increase in *Hill* coefficient of thin filament activation. Although cooperative activation of myofilaments by strongly bound cross-bridges was not affected due to α-TM-D137L expression in TG mouse hearts, ability of TG mouse hearts to increase force upon an increase in SL was impaired. Finally, investigations on myofilament proteins isolated from TG mouse hearts exhibited no significant alteration in PTM status of proteins due to α-TM-D137L

expression. There was also no functionally significant increase in β-MHC expression in TG mouse hearts. A schematic summary of the results is shown in Figure 26.

B. Discussion

1. Structural implications of D137L mutation in alpha-tropomyosin

Our principal findings in the first part of this thesis demonstrated that Leu substitution of Asp137 decreased structural flexibility of α-TM and this effect was spread along the protein.

The conserved, non-canonical Asp137 residue of α-TM is located at a particularly unstable mid-region of α-TM that is susceptible to cleavage by trypsin at a single site between Arg 133 and Ala134 (40). The general target site for trypsin is the peptide bond C-terminal to Lys and Arg residues. Although there are 53 possible target sites for trypsin cleavage across α-TM sequence, the initial tryptic digestion of α-TM only occurs at a single site, between Arg 133 and Ala134. This suggested an unstable region in the middle of α-TM because it is known that folded proteins are protected from protease digestion unless they have unstructured or unstable regions (128-130). In order to be digested, parts of the protein must become accessible to the substrate through local fluctuations. Local fluctuations are thought to occur through localized breathing motion within protein structures (52). Sumida et al. previously reported that substitution of Asp137 with a canonical Leu reduced tryptic susceptibility of α-TM, which was associated with reduced flexibility of the mutant (51). In order to reduce tryptic cleavage, the D137L mutation must have decreased local fluctuations in the middle part of α-TM. However, as

previously shown, these local fluctuations do not provide information about global stability of the molecule (131). In our DSC measurements, we extended earlier findings and demonstrated that an increase in the thermal stability of α-TM-D137L compared to control α-TM was a global effect. The stabilizing effect of the D137L mutation was observed at both the N- and C-terminal thermal transition domains of the mutant α-TM. Compared to the C-terminal calorimetric domain, the stabilizing effect of the D137L mutation was stronger on the N-terminal domain. This is consistent with previous work which indicated that the N-terminus of TM is more stable (132). Protein thermostability is correlated with protein flexibility (114-116). Accordingly, an increase in the global coiled-coil stability of α-TM-D137L suggested a decrease in its structural flexibility.

Further structural implications of D137L mutation on TM were investigated employing NMR spectroscopy. ^{1}H-^{13}C-edited HSQC measurements of reductive methylated TM samples confirmed long-range structural rearrangements in the α-TM-D137L structure. Previously, other TM mutations such as HCM-linked E180G and D175N, have also been shown to cause long-range structural rearrangements in TM (133). However, we have not understood exactly how a single point mutation can alter long-range dynamic properties of a rod-shaped molecule, where there is no interaction between non-adjacent regions. One possibility is that local information is transmitted through thermal fluctuations across α-TM and changes in regions of stability/instability or flexibility via single point mutations alter this information transmission, resulting in global structural effects and functional defects.

Flexibility of TM is known to play an important role in its *in vitro* function (48,49,51,134,135); however, the molecular mechanism and the role of TM's structural flexibility on *in vivo* cardiac function are unknown. Structural flexibility of TM is proposed to

regulate the equilibria within the three regulatory positions (blocked, closed and open) of TM on the actin surface. There is no doubt that perturbations in this molecular switch mechanism can eventually alter physiological functioning of TM, resulting in a disease phenotype. Therefore it is crucial to understand the implications of TM flexibility on *in vivo* cardiac function, upon which we focused in the second part of this study.

2. Effects of altered structural flexibility of alpha-tropomyosin on cardiac regulation in a novel transgenic mouse model

We significantly extended *in vitro* studies from the first part of this thesis by employing transgenesis to study a naturally incorporated α-TM-D137L variant in the whole heart, single cardiomyocytes and cardiac myofilaments. Findings from this highly integrative approach allowed us to propose a link between altered structural flexibility of α-TM and cardiac disorders. To our knowledge, this is the first demonstration that marked decrease in TM's flexibility due to substitution of Asp 137 with Leu affects systolic parameters of cardiac contraction, ultimately leading to a phenotype similar to DCM in α-TM-D137L TG mouse hearts.

Systolic dysfunction in TG mouse hearts was initially detected using echocardiography. Although echocardiography allowed us to perform age-dependent measurements on animals, due to the load-dependent nature of some of its major contractility parameters such as EF (136), better assessment of contractile function was acquired using PV loop measurements. PV loop measurements on TG mouse hearts helped us to investigate effects of loss of inotropy on ESPVR and EDPVR. The slope of ESPVR, which provides a load-independent index of contractility

(137,138), became flatter and shifted to the right as inotropy decreased in TG mouse hearts. Because of this change, at any given ventricular volume, less pressure was generated during systole and therefore less volume was ejected from TG mouse hearts. This led to an increase in ESV, which was coupled to a compensatory increase in preload as observed with increased EDV. A harmful consequence of systolic dysfunction is the rise in EDP; however, the increase of EDP in TG mouse hearts was not significant, due likely to the compensatory response to systolic dysfunction via dilation of ventricles as detected by significant increases in LVIDs and LVIDd, and compliance. Collectively, cardiac specific expression of α-TM-D137L in TG mouse hearts led to a phenotype picture of DCM (prominent depression of systolic contractility and mild dilation of ventricles) but no transition to heart failure was observed as animals got older. Also, TG mouse hearts appeared to be in a compensatory phase in which SV, CO and HR were maintained.

The underlying mechanisms for depressed cardiac function due to α-TM-D137L expression in TG mouse hearts could be numerous. In this study we assessed (i) contractile properties and Ca^{2+} transients of single cardiomyocytes, (ii) mechanics of myofilaments, (iii) PTM of major myofilament proteins, and (iv) myosin isoform switching in TG mouse hearts.

Direct demonstration of abnormal cardiomyocyte function in α-TM-D137L TG mouse hearts was achieved using isolated cardiomyocytes where Ca^{2+} transients and sarcomere shortening were measured in unloaded cells. Depressed cell shortening amplitude and velocity of single cardiomyocytes would be projected to depress cardiac function in TG mouse hearts. At the same time one must recognize that contractile properties of the heart cannot be dissociated from cellular Ca^{2+} homeostasis. It is the cystolic Ca^{2+} transients that trigger cross-bridge dynamics which is the fundamental step for cell shortening. However, in the case of single cardiomyocytes

isolated from TG mouse hearts, depressed contractile function occurred in the absence of any changes in Ca^{2+} transients, which indicated a mechanism intrinsic to the myofilaments. Contractile proteins themselves are by far the largest Ca^{2+} buffer in the cardiomyocytes and changes in the Ca^{2+} sensitivity of myofilaments unavoidably affect contractile properties of cardiomyocytes and this can be reflected in impaired performance of the heart. The depressed contractility of TG mouse hearts can thus be partially attributed to decreased Ca^{2+} sensitivity of myofilaments, which is substantiated by our skinned fiber data. Decrease in Ca^{2+} sensitivity is a common phenotype in DCM (61,139-141), thus this result further supports the induction of a DCM phenotype in TG mouse hearts.

Cooperative interactions among regulatory thin and thick filament proteins comprise yet another variable that regulates contractility of myocardium, and TM is a critical contributor of this process (18). Our skinned fiber measurements showed that expression of α-TM-D137L in TG mouse hearts increased cooperativity of thin filament activation by Ca^{2+}. On the other hand, cooperative activation of the thin filaments induced by strongly bound cross-bridges was not altered in skinned fibers from TG mouse hearts. These findings suggested that the excess stability (or decreased flexibility) likely altered cooperative changes in TM's position on actin surface, such that more stable TM decreased or decelerated the access of myosin to the weak binding sites on the surface of actin (**b**locked to **c**losed state transition of TM), but had little or no effect on accessibility of myosin to the strong binding sites on actin (**c**losed to **o**pen state transition of TM).

Dependence of myofilament Ca^{2+}sensitivity on SL is well established (125,142) and this dependence of force on length at sub-maximal levels of activating Ca^{2+} is a determinant of the shape of the ESPVR and contractility (126). Thus, changes in length-dependent activation needs

to be considered in interpreting altered inotropic function of TG mouse hearts. In a previous study, it was suggested that SL influences the transition of thin filaments from the blocked to closed state (143). Therefore, blunted length-dependent activation of myofilaments from TG mouse hearts supports our hypothesis that expression of a more stable TM variant decreases or decelerates the blocked to closed state transition of the thin filaments, and offers a mechanism which underlies systolic dysfunction in our TG mouse hearts.

PTMs of sarcomeric proteins are also critical regulator of cardiac performance under physiological or pathological conditions. Alterations in PTM profiles of major myofilament proteins, TM, cTnI, cTnT, MLC and MyBP-C, are often observed under pathological conditions (121,122,144-147). Our investigations for possible alterations in the PTM profile of major myofilament proteins (TM, cTnI, cTnT, MLC and MyBP-C) from TG mouse hearts showed no difference compared to NTG controls. These findings demonstrated that the level of functional changes in TG mouse hearts and reduced Ca^{2+} sensitivity of myofilaments did not provoke activation of compensatory signal transduction mechanisms or alter major myofilament proteins as substrates for kinases or phosphatases.

Switch in MHC isoform population is another potentially important contributor to contractile dysfunction. In mammalian cardiac muscle α- and β- isoforms of MHC are present (148). α-MHC shows faster actin-activated ATPase activity, shortening velocity, time to peak systole and cross-bridge cycling kinetics compared to β-isoform (149-152). Normal adult mouse hearts express almost entirely the α-isoform of MHC (153), while an economic switch towards β-MHC is observed with increasing workload on the heart. Although a slight increase in β-MHC expression in α-TM-D137L TG mouse hearts was detected, the lack of a hypertrophic phenotype suggested that this slight increase may not be functionally important. Although it remains

possible that increased β-MHC expression might have contributed to reduced contractile function detected in TG mouse hearts (154), studies comparing relative expression of β-MHC with loaded shortening velocity and power demonstrated no significant effects of the presence of up to 10% β-MHC (155).

C. General Discussion and Conclusions

Regulation of cardiac muscle contraction and relaxation requires complex interactions among Ca^{2+}, thin filament proteins and myosin cross-bridges. TM molecules undergo regulatory relocations over the surface of actin filaments in response to Ca^{2+} binding to Tn and myosin binding to actin. According to current models of thin filament regulation of the actin-myosin interaction, Ca^{2+} triggers contraction from a blocked thin filament state to a weak cross-bridge binding or closed state and full activation requires an open state induced by strong cross-bridge binding (22,25,156). Due to a small value for the equilibrium constant between blocked and open states of thin filaments (157), relatively small changes in the thermal fluctuations of TM could easily alter its rapid regulatory movements on the surface of actin. We believe that TM's structural flexibility is one of the key elements for these regulatory relocations of TM on actin and information transmission along the molecule. Therefore, perturbation in the structural flexibility of TM could affect the equilibria between three regulatory positions of TM (blocked-closed-open). Disruptions in this molecular switch mechanism eventually would alter physiological functioning of TM and result in a disease phenotype. Our results demonstrated that expression of a decreased flexibility mutant, α-TM-D137L in TG mouse hearts affected Ca^{2+} dependent activation of thin filaments with no change in the strongly bound cross-bridge

activation in skinned fiber preparations. The decrease in TM's flexibility must have impeded Ca^{2+} dependent relocation of TM between blocked and closed states, resulting in a delay in time sensitive contraction and relaxation processes inside a cardiomyocyte. This proposed delay could eventually cause cardiac dysfunction, as was observed in TG mouse hearts. The excess stability (or decreased flexibility) of TM is likely to exert its effect on Ca^{2+} dependent relocations of TM via increasing stability of blocked state of thin filaments. At the cardiomyocyte level, the release and sequestration of Ca^{2+} by the SR are time sensitive events. Once Ca^{2+} is released to the cytosol, myofilaments have a finite amount of time for contraction. A delay in the thin filament activation process would result in a delay in contraction and premature relaxation of a cardiomyocytes which could explain the depressed cardiac function observed in TG mice hearts. The answer for why we did not observe any change in Ca^{2+} dependent maximum tension generation of myofilaments from TG mouse hearts would be simply the fact that accessibility of myofilaments to Ca^{2+} is not a time dependent phenomenon in skinned fiber experiments.

From a clinical point of the view, different single point mutations in the α-TM gene are known to cause inherited cardiac diseases, either HCM or DCM. Various biochemical and physiological approaches have been used to investigate the effects of these mutations on structure, and contractile functions of α-TM. Although there is no consistent pattern for specific alterations in TM structure and function due to these CM-linked mutations (13), as part of the complex mechanisms, our findings offer a possible association between TM flexibility and cardiac disorders. Previously, the DCM-linked Glu54Lys mutation was reported to increase temperature stability of α-TM (139). In contrast, increased flexibility appears to be a characteristic of HCM-linked TM mutations (Glu180Gly, Asp175Asn, Lys70Thr, and Ala63Val) (65-67). While the α-TM-D137L mutation is not associated with inherited cardiac diseases, our

findings provide a unique insight to our understanding of how TM point mutations can significantly alter dynamic properties of TM, hence affect regulatory functions of TM in the heart.

To conclude, overall objectives in this thesis were (i) to contribute to the understanding of the link between structural flexibility of TM and cardiac function, and (ii) to investigate the functional role of destabilizing, conserved Asp137 in cardiac function. The work presented here addressed two specific aims: (i) to understand global structural implications of the D137L mutation on α-TM, and (ii) to reveal whether the D137L mutation affects cardiac function and if yes, what the mechanism is. In order to address these specific aims we performed a highly integrative study from recombinantly expressed proteins to ejecting heart of a novel TG mouse model. Our findings advance our understanding of the functional importance of a poorly packed, destabilizing central region of TM around conserved residue Asp 137. We demonstrated that structural flexibility of TM provided by Asp137 is essential for its regulatory functions in ejecting mouse hearts. To the best of our knowledge, the results from our study are the first to demonstrate that a marked decrease in TM's structural flexibility due to substitution of Asp 137 with Leu affects systolic parameters of cardiac contraction, ultimately leading to a phenotype similar to DCM in α-TM-D137L TG mouse hearts. While it is likely that additional factors contribute to the disease mechanism, our investigations support our overall hypothesis that altered flexibility of α-TM is a major initial molecular abnormality that leads to disease phenotype. We think these findings will be highly relevant to the interpretation of *in vitro* data as well as adding perspective to the clinical and physiological significance of TM flexibility.

One never notices what has been done; one can only see what remains to be done.
Marie Curie

FIGURES and TABLES

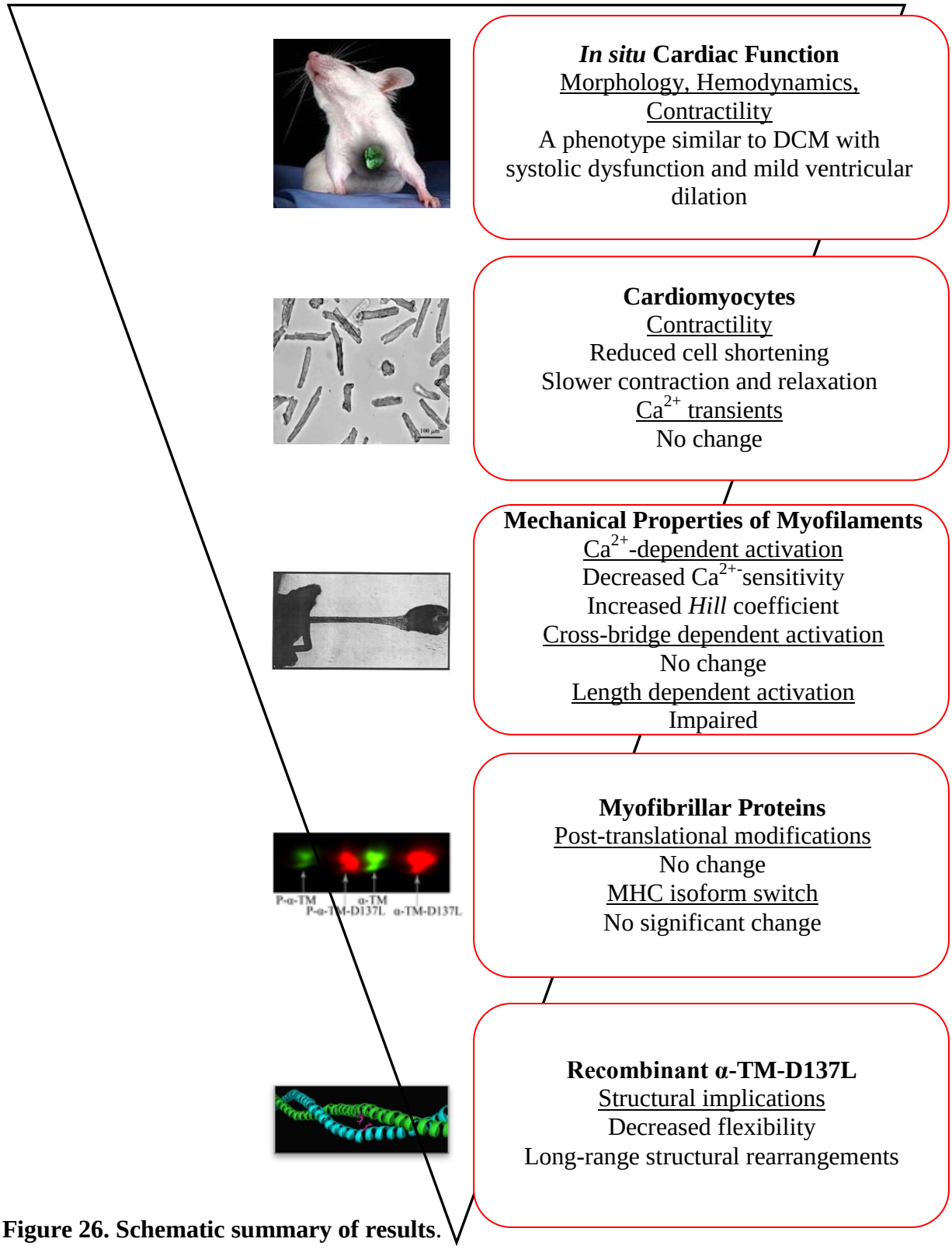

Figure 26. Schematic summary of results.

REFERENCES

1. Gunning, P., O'Neill, G., and Hardeman, E. (2008) Tropomyosin-based regulation of the actin cytoskeleton in time and space. *Physiol Rev* **88**, 1-35

2. Wang, C. L., and Coluccio, L. M. (2010) New insights into the regulation of the actin cytoskeleton by tropomyosin. *Int Rev Cell Mol Biol* **281**, 91-128

3. Bailey, K. (1948) Tropomyosin: a new asymmetric protein component of the muscle fibril. *Biochem J* **43**, 271-279

4. Bailey, K. (1946) Tropomyosin: a new asymmetric protein component of muscle. *Nature* **157**, 368

5. Gooding, C., and Smith, C. W. (2008) Tropomyosin exons as models for alternative splicing. *Adv Exp Med Biol* **644**, 27-42

6. Schevzov, G., and O'Neill, G. (2008) Tropomyosin gene expression in vivo and in vitro. *Adv Exp Med Biol* **644**, 43-59

7. Vrhovski, B., Theze, N., and Thiebaud, P. (2008) Structure and evolution of tropomyosin genes. *Adv Exp Med Biol* **644**, 6-26

8. Purcell, I. F., Bing, W., and Marston, S. B. (1999) Functional analysis of human cardiac troponin by the in vitro motility assay: comparison of adult, foetal and failing hearts. *Cardiovasc Res* **43**, 884-891

9. Karam, C. N., Warren, C. M., Rajan, S., de Tombe, P. P., Wieczorek, D. F., and Solaro, R. J. (2011) Expression of tropomyosin-kappa induces dilated cardiomyopathy and depresses cardiac myofilament tension by mechanisms involving cross-bridge dependent activation and altered tropomyosin phosphorylation. *J Muscle Res Cell Motil* **31**, 315-322

10. Rajan, S., Jagatheesan, G., Karam, C. N., Alves, M. L., Bodi, I., Schwartz, A., Bulcao, C. F., D'Souza, K. M., Akhter, S. A., Boivin, G. P., Dube, D. K., Petrashevskaya, N., Herr, A. B., Hullin, R., Liggett, S. B., Wolska, B. M., Solaro, R. J., and Wieczorek, D. F. (2010) Molecular and functional characterization of a novel cardiac-specific human tropomyosin isoform. *Circulation* **121**, 410-418

11. Blanchard, E. M., Iizuka, K., Christe, M., Conner, D. A., Geisterfer-Lowrance, A., Schoen, F. J., Maughan, D. W., Seidman, C. E., and Seidman, J. G. (1997) Targeted ablation of the murine alpha-tropomyosin gene. *Circ Res* **81**, 1005-1010

12. Rethinasamy, P., Muthuchamy, M., Hewett, T., Boivin, G., Wolska, B. M., Evans, C., Solaro, R. J., and Wieczorek, D. F. (1998) Molecular and physiological effects of alpha-tropomyosin ablation in the mouse. *Circ Res* **82**, 116-123

13. Redwood, C., and Robinson, P. (2013) Alpha-tropomyosin mutations in inherited cardiomyopathies. *J Muscle Res Cell Motil*

14. Eisenberg, B., and Eisenberg, R. S. (1968) Transverse tubular system in glycerol-treated skeletal muscle. *Science* **160**, 1243-1244

15. Fabiato, A. (1983) Calcium-induced release of calcium from the cardiac sarcoplasmic reticulum. *Am J Physiol* **245**, C1-14

16. Leavis, P. C., and Gergely, J. (1984) Thin filament proteins and thin filament-linked regulation of vertebrate muscle contraction. *CRC Crit Rev Biochem* **16**, 235-305

17. Farah, C. S., and Reinach, F. C. (1995) The troponin complex and regulation of muscle contraction. *FASEB J* **9**, 755-767

18. Tobacman, L. S. (1996) Thin filament-mediated regulation of cardiac contraction. *Annu Rev Physiol* **58**, 447-481

19. Tobacman, L. S., Nihli, M., Butters, C., Heller, M., Hatch, V., Craig, R., Lehman, W., and Homsher, E. (2002) The troponin tail domain promotes a conformational state of the thin filament that suppresses myosin activity. *J Biol Chem* **277**, 27636-27642

20. Galinska-Rakoczy, A., Engel, P., Xu, C., Jung, H., Craig, R., Tobacman, L. S., and Lehman, W. (2008) Structural basis for the regulation of muscle contraction by troponin and tropomyosin. *J Mol Biol* **379**, 929-935

21. Pirani, A., Xu, C., Hatch, V., Craig, R., Tobacman, L. S., and Lehman, W. (2005) Single particle analysis of relaxed and activated muscle thin filaments. *J Mol Biol* **346**, 761-772

22. Mckillop, D. F. A., and Geeves, M. A. (1993) Regulation of the Interaction between Actin and Myosin Subfragment-1 - Evidence for 3 States of the Thin Filament. *Biophysical Journal* **65**, 693-701

23. Lehman, W., Craig, R., and Vibert, P. (1994) Ca(2+)-induced tropomyosin movement in Limulus thin filaments revealed by three-dimensional reconstruction. *Nature* **368**, 65-67

24. Xu, C., Craig, R., Tobacman, L., Horowitz, R., and Lehman, W. (1999) Tropomyosin positions in regulated thin filaments revealed by cryoelectron microscopy. *Biophys J* **77**, 985-992

25. Vibert, P., Craig, R., and Lehman, W. (1997) Steric-model for activation of muscle thin filaments. *J Mol Biol* **266**, 8-14

26. Hitchcock-DeGregori, S. E. (2008) Tropomyosin: function follows structure. *Adv Exp Med Biol* **644**, 60-72

27. Brown, J. H., and Cohen, C. (2005) Regulation of muscle contraction by tropomyosin and troponin: how structure illuminates function. *Adv Protein Chem* **71**, 121-159

28. Nevzorov, I. A., and Levitsky, D. I. (2011) Tropomyosin: double helix from the protein world. *Biochemistry (Mosc)* **76**, 1507-1527

29. Astbury, W. T., Reed, R., and Spark, L. C. (1948) An X-ray and electron microscope study of tropomyosin. *Biochem J* **43**, 282-287

30. Crick, F. (1953) The packing of alpha-helices. Simple coiled-coils. *Acta Crystallographica* **6**, 689-697

31. Hodges, R. S., Sodek J, Smillie LB (1972) Tropomyosin: Amino acid sequence and coiled-coil structure. *Cold Spring Harbor Symp. Quant Biol* **37**, 299-310

32. Lehrer, S. S. (1975) Intramolecular crosslinking of tropomyosin via disulfide bond formation: evidence for chain register. *Proc Natl Acad Sci U S A* **72**, 3377-3381

33. Monteiro, P. B., Lataro, R. C., Ferro, J. A., and Reinach Fde, C. (1994) Functional alpha-tropomyosin produced in Escherichia coli. A dipeptide extension can substitute the amino-terminal acetyl group. *J Biol Chem* **269**, 10461-10466

34. Greenfield, N. J., Stafford, W. F., and Hitchcockdegregori, S. E. (1994) The Effect of N-Terminal Acetylation on the Structure of an N-Terminal Tropomyosin Peptide and Alpha-Alpha-Tropomyosin. *Protein Sci* **3**, 402-410

35. Stewart, M., and McLachlan, A. D. (1975) Fourteen actin-binding sites on tropomyosin? *Nature* **257**, 331-333

36. McLachlan, A. D., and Stewart, M. (1976) The 14-fold periodicity in alpha-tropomyosin and the interaction with actin. *J Mol Biol* **103**, 271-298

37. Brown, J. H., Cohen, C., and Parry, D. A. (1996) Heptad breaks in alpha-helical coiled coils: stutters and stammers. *Proteins* **26**, 134-145

38. Ueno, H. (1984) Local structural changes in tropomyosin detected by a trypsin-probe method. *Biochemistry* **23**, 4791-4798

39. Ishii, Y., Hitchcock-DeGregori, S., Mabuchi, K., and Lehrer, S. S. (1992) Unfolding domains of recombinant fusion alpha alpha-tropomyosin. *Protein Sci* **1**, 1319-1325

40. Pato, M. D., Mak, A. S., and Smillie, L. B. (1981) Fragments of rabbit striated muscle alpha-tropomyosin. II. Binding to troponin-T. *J Biol Chem* **256**, 602-607

41. Whitby, F. G., and Phillips, G. N., Jr. (2000) Crystal structure of tropomyosin at 7 Angstroms resolution. *Proteins* **38**, 49-59

42. Phillips, G. N., Jr., Fillers, J. P., and Cohen, C. (1986) Tropomyosin crystal structure and muscle regulation. *J Mol Biol* **192**, 111-131

43. Li, Y., Mui, S., Brown, J. H., Strand, J., Reshetnikova, L., Tobacman, L. S., and Cohen, C. (2002) The crystal structure of the C-terminal fragment of striated-muscle alpha-tropomyosin reveals a key troponin T recognition site. *Proc Natl Acad Sci U S A* **99**, 7378-7383

44. Brown, J. H., Zhou, Z., Reshetnikova, L., Robinson, H., Yammani, R. D., Tobacman, L. S., and Cohen, C. (2005) Structure of the mid-region of tropomyosin: bending and binding sites for actin. *Proc Natl Acad Sci U S A* **102**, 18878-18883

45. Brown, J. H., Kim, K. H., Jun, G., Greenfield, N. J., Dominguez, R., Volkmann, N., Hitchcock-DeGregori, S. E., and Cohen, C. (2001) Deciphering the design of the tropomyosin molecule. *Proc Natl Acad Sci U S A* **98**, 8496-8501

46. Greenfield, N. J., Huang, Y. J., Swapna, G. V., Bhattacharya, A., Rapp, B., Singh, A., Montelione, G. T., and Hitchcock-DeGregori, S. E. (2006) Solution NMR structure of the junction between tropomyosin molecules: implications for actin binding and regulation. *J Mol Biol* **364**, 80-96

47. Minakata, S., Maeda, K., Oda, N., Wakabayashi, K., Nitanai, Y., and Maeda, Y. (2008) Two-crystal structures of tropomyosin C-terminal fragment 176-273: exposure of the hydrophobic core to the solvent destabilizes the tropomyosin molecule. *Biophys J* **95**, 710-719

48. Singh, A., and Hitchcock-DeGregori, S. E. (2006) Dual requirement for flexibility and specificity for binding of the coiled-coil tropomyosin to its target, actin. *Structure* **14**, 43-50

49. Singh, A., and Hitchcock-DeGregori, S. E. (2003) Local destabilization of the tropomyosin coiled coil gives the molecular flexibility required for actin binding. *Biochemistry* **42**, 14114-14121

50. Straussman, R., Ben-Ya'acov, A., Woolfson, D. N., and Ravid, S. (2007) Kinking the coiled coil--negatively charged residues at the coiled-coil interface. *J Mol Biol* **366**, 1232-1242

51. Sumida, J. P., Wu, E., and Lehrer, S. S. (2008) Conserved Asp-137 imparts flexibility to tropomyosin and affects function. *J Biol Chem* **283**, 6728-6734

52. Maity, H., Lim, W. K., Rumbley, J. N., and Englander, S. W. (2003) Protein hydrogen exchange mechanism: Local fluctuations. *Protein Sci* **12**, 153-160

53. Geisterfer-Lowrance, A. A., Kass, S., Tanigawa, G., Vosberg, H. P., McKenna, W., Seidman, C. E., and Seidman, J. G. (1990) A molecular basis for familial hypertrophic

cardiomyopathy: a beta cardiac myosin heavy chain gene missense mutation. *Cell* **62**, 999-1006

54. Thierfelder, L., Watkins, H., MacRae, C., Lamas, R., McKenna, W., Vosberg, H. P., Seidman, J. G., and Seidman, C. E. (1994) Alpha-tropomyosin and cardiac troponin T mutations cause familial hypertrophic cardiomyopathy: a disease of the sarcomere. *Cell* **77**, 701-712

55. Watkins, H., MacRae, C., Thierfelder, L., Chou, Y. H., Frenneaux, M., McKenna, W., Seidman, J. G., and Seidman, C. E. (1993) A disease locus for familial hypertrophic cardiomyopathy maps to chromosome 1q3. *Nat Genet* **3**, 333-337

56. Maron, B. J. (2002) Hypertrophic cardiomyopathy: a systematic review. *JAMA* **287**, 1308-1320

57. Tardiff, J. C. (2005) Sarcomeric proteins and familial hypertrophic cardiomyopathy: linking mutations in structural proteins to complex cardiovascular phenotypes. *Heart Fail Rev* **10**, 237-248

58. Chang, A. N., and Potter, J. D. (2005) Sarcomeric protein mutations in dilated cardiomyopathy. *Heart Fail Rev* **10**, 225-235

59. Jagatheesan, G., Rajan, S., Petrashevskaya, N., Schwartz, A., Boivin, G., Arteaga, G., de Tombe, P. P., Solaro, R. J., and Wieczorek, D. F. (2004) Physiological significance of troponin T binding domains in striated muscle tropomyosin. *Am J Physiol Heart Circ Physiol* **287**, H1484-1494

60. Wieczorek, D. F., Jagatheesan, G., and Rajan, S. (2008) The role of tropomyosin in heart disease. *Adv Exp Med Biol* **644**, 132-142

61. Lakdawala, N. K., Dellefave, L., Redwood, C. S., Sparks, E., Cirino, A. L., Depalma, S., Colan, S. D., Funke, B., Zimmerman, R. S., Robinson, P., Watkins, H., Seidman, C. E., Seidman, J. G., McNally, E. M., and Ho, C. Y. (2010) Familial dilated cardiomyopathy caused by an alpha-tropomyosin mutation: the distinctive natural history of sarcomeric dilated cardiomyopathy. *J Am Coll Cardiol* **55**, 320-329

62. McNally, E. M., Golbus, J. R., and Puckelwartz, M. J. (2013) Genetic mutations and mechanisms in dilated cardiomyopathy. *J Clin Invest* **123**, 19-26

63. Marston, S. B. (2011) How do mutations in contractile proteins cause the primary familial cardiomyopathies? *J Cardiovasc Transl Res* **4**, 245-255

64. Memo, M., Leung, M. C., Ward, D. G., dos Remedios, C., Morimoto, S., Zhang, L., Ravenscroft, G., McNamara, E., Nowak, K. J., Marston, S. B., and Messer, A. E. (2013) Familial dilated cardiomyopathy mutations uncouple troponin I phosphorylation from changes in myofibrillar Ca(2)(+) sensitivity. *Cardiovasc Res* **99**, 65-73

65. Loong, C. K., Zhou, H. X., and Chase, P. B. (2012) Familial hypertrophic cardiomyopathy related E180G mutation increases flexibility of human cardiac alpha-tropomyosin. *FEBS Lett* **586**, 3503-3507

66. Kremneva, E., Boussouf, S., Nikolaeva, O., Maytum, R., Geeves, M. A., and Levitsky, D. I. (2004) Effects of two familial hypertrophic cardiomyopathy mutations in alpha-tropomyosin, Asp175Asn and Glu180Gly, on the thermal unfolding of actin-bound tropomyosin. *Biophys J* **87**, 3922-3933

67. Heller, M. J., Nili, M., Homsher, E., and Tobacman, L. S. (2003) Cardiomyopathic tropomyosin mutations that increase thin filament Ca2+ sensitivity and tropomyosin N-domain flexibility. *Journal of Biological Chemistry* **278**, 41742-41748

68. Mirza, M., Robinson, P., Kremneva, E., Copeland, O., Nikolaeva, O., Watkins, H., Levitsky, D., Redwood, C., El-Mezgueldi, M., and Marston, S. (2007) The effect of mutations in alpha-tropomyosin (E40K and E54K) that cause familial dilated cardiomyopathy on the regulatory mechanism of cardiac muscle thin filaments. *J Biol Chem* **282**, 13487-13497

69. Hershberger, R. E., Norton, N., Morales, A., Li, D., Siegfried, J. D., and Gonzalez-Quintana, J. (2010) Coding sequence rare variants identified in MYBPC3, MYH6, TPM1, TNNC1, and TNNI3 from 312 patients with familial or idiopathic dilated cardiomyopathy. *Circ Cardiovasc Genet* **3**, 155-161

70. Fokstuen, S., Munoz, A., Melacini, P., Iliceto, S., Perrot, A., Ozcelik, C., Jeanrenaud, X., Rieubland, C., Farr, M., Faber, L., Sigwart, U., Mach, F., Lerch, R., Antonarakis, S. E., and Blouin, J. L. (2011) Rapid detection of genetic variants in hypertrophic cardiomyopathy by custom DNA resequencing array in clinical practice. *J Med Genet* **48**, 572-576

71. Otsuka, H., Arimura, T., Abe, T., Kawai, H., Aizawa, Y., Kubo, T., Kitaoka, H., Nakamura, H., Nakamura, K., Okamoto, H., Ichida, F., Ayusawa, M., Nunoda, S., Isobe, M., Matsuzaki, M., Doi, Y. L., Fukuda, K., Sasaoka, T., Izumi, T., Ashizawa, N., and Kimura, A. (2012) Prevalence and distribution of sarcomeric gene mutations in Japanese patients with familial hypertrophic cardiomyopathy. *Circ J* **76**, 453-461

72. Olson, T. M., Kishimoto, N. Y., Whitby, F. G., and Michels, V. V. (2001) Mutations that alter the surface charge of alpha-tropomyosin are associated with dilated cardiomyopathy. *J Mol Cell Cardiol* **33**, 723-732

73. Frisso, G., Limongelli, G., Pacileo, G., Del Giudice, A., Forgione, L., Calabro, P., Iacomino, M., Detta, N., Di Fonzo, L. M., Maddaloni, V., Calabro, R., and Salvatore, F. (2009) A child cohort study from southern Italy enlarges the genetic spectrum of hypertrophic cardiomyopathy. *Clin Genet* **76**, 91-101

74. Jongbloed, R. J., Marcelis, C. L., Doevendans, P. A., Schmeitz-Mulkens, J. M., Van Dockum, W. G., Geraedts, J. P., and Smeets, H. J. (2003) Variable clinical manifestation of a novel missense mutation in the alpha-tropomyosin (TPM1) gene in familial hypertrophic cardiomyopathy. *J Am Coll Cardiol* **41**, 981-986

75. Nakajima-Taniguchi, C., Matsui, H., Nagata, S., Kishimoto, T., and Yamauchi-Takihara, K. (1995) Novel missense mutation in alpha-tropomyosin gene found in Japanese patients with hypertrophic cardiomyopathy. *J Mol Cell Cardiol* **27**, 2053-2058

76. Yamauchi-Takihara, K., Nakajima-Taniguchi, C., Matsui, H., Fujio, Y., Kunisada, K., Nagata, S., and Kishimoto, T. (1996) Clinical implications of hypertrophic cardiomyopathy associated with mutations in the alpha-tropomyosin gene. *Heart* **76**, 63-65

77. van de Meerakker, J. B., Christiaans, I., Barnett, P., Lekanne Deprez, R. H., Ilgun, A., Mook, O. R., Mannens, M. M., Lam, J., Wilde, A. A., Moorman, A. F., and Postma, A. V. (2013) A novel alpha-tropomyosin mutation associates with dilated and non-compaction cardiomyopathy and diminishes actin binding. *Biochim Biophys Acta* **1833**, 833-839

78. Karibe, A., Tobacman, L. S., Strand, J., Butters, C., Back, N., Bachinski, L. L., Arai, A. E., Ortiz, A., Roberts, R., Homsher, E., and Fananapazir, L. (2001) Hypertrophic cardiomyopathy caused by a novel alpha-tropomyosin mutation (V95A) is associated with mild cardiac phenotype, abnormal calcium binding to troponin, abnormal myosin cycling, and poor prognosis. *Circulation* **103**, 65-71

79. Van Driest, S. L., Ellsworth, E. G., Ommen, S. R., Tajik, A. J., Gersh, B. J., and Ackerman, M. J. (2003) Prevalence and spectrum of thin filament mutations in an outpatient referral population with hypertrophic cardiomyopathy. *Circulation* **108**, 445-451

80. Regitz-Zagrosek, V., Erdmann, J., Wellnhofer, E., Raible, J., and Fleck, E. (2000) Novel mutation in the alpha-tropomyosin gene and transition from hypertrophic to hypocontractile dilated cardiomyopathy. *Circulation* **102**, E112-116

81. Van Driest, S. L., Ackerman, M. J., Ommen, S. R., Shakur, R., Will, M. L., Nishimura, R. A., Tajik, A. J., and Gersh, B. J. (2002) Prevalence and severity of "benign" mutations in the beta-myosin heavy chain, cardiac troponin T, and alpha-tropomyosin genes in hypertrophic cardiomyopathy. *Circulation* **106**, 3085-3090

82. Probst, S., Oechslin, E., Schuler, P., Greutmann, M., Boye, P., Knirsch, W., Berger, F., Thierfelder, L., Jenni, R., and Klaassen, S. (2011) Sarcomere gene mutations in isolated left ventricular noncompaction cardiomyopathy do not predict clinical phenotype. *Circ Cardiovasc Genet* **4**, 367-374

83. van Spaendonck-Zwarts, K. Y., van Rijsingen, I. A., van den Berg, M. P., Lekanne Deprez, R. H., Post, J. G., van Mil, A. M., Asselbergs, F. W., Christiaans, I., van Langen, I. M., Wilde, A. A., de Boer, R. A., Jongbloed, J. D., Pinto, Y. M., and van Tintelen, J. P. (2013) Genetic analysis in 418 index patients with idiopathic dilated cardiomyopathy: overview of 10 years' experience. *Eur J Heart Fail* **15**, 628-636

84. Morita, H., Rehm, H. L., Menesses, A., McDonough, B., Roberts, A. E., Kucherlapati, R., Towbin, J. A., Seidman, J. G., and Seidman, C. E. (2008) Shared genetic causes of cardiac hypertrophy in children and adults. *N Engl J Med* **358**, 1899-1908

85. Olivotto, I., Girolami, F., Ackerman, M. J., Nistri, S., Bos, J. M., Zachara, E., Ommen, S. R., Theis, J. L., Vaubel, R. A., Re, F., Armentano, C., Poggesi, C., Torricelli, F., and Cecchi, F. (2008) Myofilament protein gene mutation screening and outcome of patients with hypertrophic cardiomyopathy. *Mayo Clin Proc* **83**, 630-638

86. Kobayashi, T., Patrick, S. E., and Kobayashi, M. (2009) Ala Scanning of the Inhibitory Region of Cardiac Troponin I. *Journal of Biological Chemistry* **284**, 20052-20060

87. Kobayashi, T., Yang, X., Walker, L. A., Van Breemen, R. B., and Solaro, R. J. (2005) A non-equilibrium isoelectric focusing method to determine states of phosphorylation of cardiac troponin I: identification of Ser-23 and Ser-24 as significant sites of phosphorylation by protein kinase C. *J Mol Cell Cardiol* **38**, 213-218

88. Spudich, J. A., and Watt, S. (1971) The regulation of rabbit skeletal muscle contraction. I. Biochemical studies of the interaction of the tropomyosin-troponin complex with actin and the proteolytic fragments of myosin. *J Biol Chem* **246**, 4866-4871

89. Swartz, D. R., and Moss, R. L. (1992) Influence of a strong-binding myosin analogue on calcium-sensitive mechanical properties of skinned skeletal muscle fibers. *J Biol Chem* **267**, 20497-20506

90. Gill, S. C., and von Hippel, P. H. (1989) Calculation of protein extinction coefficients from amino acid sequence data. *Anal Biochem* **182**, 319-326

91. Kobayashi, T., Patrick, S. E., and Kobayashi, M. (2009) Ala scanning of the inhibitory region of cardiac troponin I. *J Biol Chem* **284**, 20052-20060

92. Means, G. E., and Feeney, R. E. (1968) Reductive alkylation of amino groups in proteins. *Biochemistry* **7**, 2192-2201

93. Delaglio, F., Grzesiek, S., Vuister, G. W., Zhu, G., Pfeifer, J., and Bax, A. (1995) NMRPipe: a multidimensional spectral processing system based on UNIX pipes. *J Biomol NMR* **6**, 277-293

94. Kobayashi, M., Debold, E. P., Turner, M. A., and Kobayashi, T. (2013) Cardiac Muscle Activation Blunted by a Mutation to the Regulatory Component, Troponin T. *J Biol Chem*

95. Subramaniam, A., Jones, W. K., Gulick, J., Wert, S., Neumann, J., and Robbins, J. (1991) Tissue-specific regulation of the alpha-myosin heavy chain gene promoter in transgenic mice. *J Biol Chem* **266**, 24613-24620

96. Muthuchamy, M., Grupp, I. L., Grupp, G., O'Toole, B. A., Kier, A. B., Boivin, G. P., Neumann, J., and Wieczorek, D. F. (1995) Molecular and physiological effects of overexpressing striated muscle beta-tropomyosin in the adult murine heart. *J Biol Chem* **270**, 30593-30603

97. Lang, R. M., Bierig, M., Devereux, R. B., Flachskampf, F. A., Foster, E., Pellikka, P. A., Picard, M. H., Roman, M. J., Seward, J., Shanewise, J. S., Solomon, S. D., Spencer, K. T., Sutton, M. S., and Stewart, W. J. (2005) Recommendations for chamber quantification: a report from the American Society of Echocardiography's Guidelines and Standards Committee and the Chamber Quantification Writing Group, developed in conjunction with the European Association of Echocardiography, a branch of the European Society of Cardiology. *Journal of the American Society of Echocardiography : official publication of the American Society of Echocardiography* **18**, 1440-1463

98. Nagueh, S. F., Appleton, C. P., Gillebert, T. C., Marino, P. N., Oh, J. K., Smiseth, O. A., Waggoner, A. D., Flachskampf, F. A., Pellikka, P. A., and Evangelisa, A. (2009) Recommendations for the evaluation of left ventricular diastolic function by echocardiography. *European journal of echocardiography : the journal of the Working Group on Echocardiography of the European Society of Cardiology* **10**, 165-193

99. Wolska, B. M., and Solaro, R. J. (1996) Method for isolation of adult mouse cardiac myocytes for studies of contraction and microfluorimetry. *Am J Physiol* **271**, H1250-1255

100. Louch, W. E., Sheehan, K. A., and Wolska, B. M. (2011) Methods in cardiomyocyte isolation, culture, and gene transfer. *J Mol Cell Cardiol* **51**, 288-298

101. Brandt, P. W., Roemer, D., and Schachat, F. H. (1990) Co-operative activation of skeletal muscle thin filaments by rigor crossbridges. The effect of troponin C extraction. *J Mol Biol* **212**, 473-480

102. Fabiato, A. (1988) Computer-Programs for Calculating Total from Specified Free or Free from Specified Total Ionic Concentrations in Aqueous-Solutions Containing Multiple Metals and Ligands. *Method Enzymol* **157**, 378-417

103. Godt, R. E., and Lindley, B. D. (1982) Influence of Temperature Upon Contractile Activation and Isometric Force Production in Mechanically Skinned Muscle-Fibers of the Frog. *J Gen Physiol* **80**, 279-297

104. Scruggs, S. B., Hinken, A. C., Thawornkaiwong, A., Robbins, J., Walker, L. A., de Tombe, P. P., Geenen, D. L., Buttrick, P. M., and Solaro, R. J. (2009) Ablation of ventricular myosin regulatory light chain phosphorylation in mice causes cardiac dysfunction in situ and affects neighboring myofilament protein phosphorylation. *J Biol Chem* **284**, 5097-5106

105. Warren, C. M., Arteaga, G. M., Rajan, S., Ahmed, R. P., Wieczorek, D. F., and Solaro, R. J. (2008) Use of 2-D DIGE analysis reveals altered phosphorylation in a tropomyosin mutant (Glu54Lys) linked to dilated cardiomyopathy. *Proteomics* **8**, 100-105

106. Yuan, C., Sheng, Q., Tang, H., Li, Y., Zeng, R., and Solaro, R. J. (2008) Quantitative comparison of sarcomeric phosphoproteomes of neonatal and adult rat hearts. *American Journal of Physiology - Heart and Circulatory Physiology* **295**, H647-H656

107. Kirk, J. A., MacGowan, G. A., Evans, C., Smith, S. H., Warren, C. M., Mamidi, R., Chandra, M., Stewart, A. F., Solaro, R. J., and Shroff, S. G. (2009) Left ventricular and myocardial function in mice expressing constitutively pseudophosphorylated cardiac troponin I. *Circ Res* **105**, 1232-1239

108. Warren, C. M., and Greaser, M. L. (2003) Method for cardiac myosin heavy chain separation by sodium dodecyl sulfate gel electrophoresis. *Anal Biochem* **320**, 149-151

109. Sauer, R. T., Hehir, K., Stearman, R. S., Weiss, M. A., Jeitlernilsson, A., Suchanek, E. G., and Pabo, C. O. (1986) An Engineered Intersubunit Disulfide Enhances the Stability and DNA-Binding of the N-Terminal Domain of Lambda-Repressor. *Biochemistry* **25**, 5992-5998

110. Lehrer, S. S., Ly, S., and Fuchs, F. (2011) Tropomyosin is in a reduced state in rat cardiac muscle. *J Muscle Res Cell M* **32**, 63-64

111. Potekhin, S. A., and Privalov, P. L. (1982) Co-operative blocks in tropomyosin. *J Mol Biol* **159**, 519-535

112. Sturtevant, J. M., Holtzer, M. E., and Holtzer, A. (1991) A scanning calorimetric study of the thermally induced unfolding of various forms of tropomyosin. *Biopolymers* **31**, 489-495

113. Williams, D. L., Jr., and Swenson, C. A. (1981) Tropomyosin stability: assignment of thermally induced conformational transitions to separate regions of the molecule. *Biochemistry* **20**, 3856-3864

114. Vihinen, M. (1987) Relationship of Protein Flexibility to Thermostability. *Protein Eng* **1**, 477-480

115. Palfey, B. A., Basu, R., Frederick, K. K., Entsch, B., and Ballou, D. P. (2002) Role of protein flexibility in the catalytic cycle of p-hydroxybenzoate hydroxylase elucidated by the Pro293Ser mutant. *Biochemistry* **41**, 8438-8446

116. Celej, M. S., Montich, C. G., and Fidelio, G. D. (2003) Protein stability induced by ligand binding correlates with changes in protein flexibility. *Protein Sci* **12**, 1496-1506

117. Rayment, I. (1997) Reductive alkylation of lysine residues to alter crystallization properties of proteins. *Methods Enzymol* **276**, 171-179

118. Gerken, T. A., Jentoft, J. E., Jentoft, N., and Dearborn, D. G. (1982) Intramolecular interactions of amino groups in 13C reductively methylated hen egg-white lysozyme. *J Biol Chem* **257**, 2894-2900

119. Walter, T. S., Meier, C., Assenberg, R., Au, K. F., Ren, J. S., Verma, A., Nettleship, J. E., Owens, R. J., Stuart, D. I., and Grimes, J. M. (2006) Lysine methylation as a routine rescue strategy for protein crystallization. *Structure* **14**, 1617-1622

120. Gao, G. H., Prasad, R., Lodwig, S. N., Unkefer, C. J., Beard, W. A., Wilson, S. H., and London, R. E. (2006) Determination of lysine pK values using [5-C-13]lysine: Application to the lyase domain of DNA pol beta. *J Am Chem Soc* **128**, 8104-8105

121. Nixon, B. R., Liu, B., Scellini, B., Tesi, C., Piroddi, N., Ogut, O., John Solaro, R., Ziolo, M. T., Janssen, P. M., Davis, J. P., Poggesi, C., and Biesiadecki, B. J. (2012) Tropomyosin Ser-283 pseudo-phosphorylation slows myofibril relaxation. *Arch Biochem Biophys*

122. Schulz, E. M., Correll, R. N., Sheikh, H. N., Lofrano-Alves, M. S., Engel, P. L., Newman, G., Schultz Jel, J., Molkentin, J. D., Wolska, B. M., Solaro, R. J., and Wieczorek, D. F. (2012) Tropomyosin dephosphorylation results in compensated cardiac hypertrophy. *J Biol Chem* **287**, 44478-44489

123. Sagawa, K., Suga, H., Shoukas, A. A., and Bakalar, K. M. (1977) End-systolic pressure/volume ratio: a new index of ventricular contractility. *Am J Cardiol* **40**, 748-753

124. Suga, H., Sagawa, K., and Kostiuk, D. P. (1976) Controls of Ventricular Contractility Assessed by Pressure-Volume Ratio, Emax. *Cardiovasc Res* **10**, 582-592

125. de Tombe, P. P., Mateja, R. D., Tachampa, K., Ait Mou, Y., Farman, G. P., and Irving, T. C. (2010) Myofilament length dependent activation. *J Mol Cell Cardiol* **48**, 851-858

126. Nowak, G., Pena, J. R., Arteaga, G. M., Geenen, D. L., Pieples, K., Wieczorek, D. F., Solaro, R. J., and Wolska, B. M. (2001) Correlations between alterations in length-dependent Ca2+ activation of cardiac myofilaments and the end systolic pressure-volume relation. *Circulation* **104**, 313-313

127. Nadal-Ginard, B., and Mahdavi, V. (1989) Molecular basis of cardiac performance. Plasticity of the myocardium generated through protein isoform switches. *J Clin Invest* **84**, 1693-1700

128. Linderstrom-Lang, K. (1950) Structure and enzymatic break-down of proteins. *Cold Spring Harb Symp Quant Biol* **14**, 117-126

129. Fontana, A., Polverino de Laureto, P., De Filippis, V., Scaramella, E., and Zambonin, M. (1997) Probing the partly folded states of proteins by limited proteolysis. *Fold Des* **2**, R17-26

130. Hubbard, S. J. (1998) The structural aspects of limited proteolysis of native proteins. *Bba-Protein Struct M* **1382**, 191-206

131. Park, C., and Marqusee, S. (2004) Probing the high energy states in proteins by proteolysis. *J Mol Biol* **343**, 1467-1476

132. Mo, J., Holtzer, M. E., and Holtzer, A. (1992) Kinetics of folding and unfolding of beta beta-tropomyosin. *Biopolymers* **32**, 1581-1587

133. Ly, S., and Lehrer, S. S. (2012) Long-range effects of familial hypertrophic cardiomyopathy mutations E180G and D175N on the properties of tropomyosin. *Biochemistry* **51**, 6413-6420

134. Chen, Y., and Lehrer, S. S. (2004) Distances between tropomyosin sites across the muscle thin filament using luminescence resonance energy transfer: evidence for tropomyosin flexibility. *Biochemistry* **43**, 11491-11499

135. Nitanai, Y., Minakata, S., Maeda, K., Oda, N., and Maeda, Y. (2007) Crystal structures of tropomyosin: flexible coiled-coil. *Adv Exp Med Biol* **592**, 137-151

136. Lancellotti, P., Tribouilloy, C., Hagendorff, A., Moura, L., Popescu, B. A., Agricola, E., Monin, J. L., Pierard, L. A., Badano, L., and Zamorano, J. L. (2010) European Association of Echocardiography recommendations for the assessment of valvular regurgitation. Part 1: aortic and pulmonary regurgitation (native valve disease). *Eur J Echocardiogr* **11**, 223-244

137. Suga, H., and Sagawa, K. (1974) Instantaneous pressure-volume relationships and their ratio in the excised, supported canine left ventricle. *Circ Res* **35**, 117-126

138. Kass, D. A., Yamazaki, T., Burkhoff, D., Maughan, W. L., and Sagawa, K. (1986) Determination of left ventricular end-systolic pressure-volume relationships by the conductance (volume) catheter technique. *Circulation* **73**, 586-595

139. Rajan, S., Ahmed, R. P., Jagatheesan, G., Petrashevskaya, N., Boivin, G. P., Urboniene, D., Arteaga, G. M., Wolska, B. M., Solaro, R. J., Liggett, S. B., and Wieczorek, D. F.

(2007) Dilated cardiomyopathy mutant tropomyosin mice develop cardiac dysfunction with significantly decreased fractional shortening and myofilament calcium sensitivity. *Circ Res* **101**, 205-214

140. Du, C. K., Morimoto, S., Nishii, K., Minakami, R., Ohta, M., Tadano, N., Lu, Q. W., Wang, Y. Y., Zhan, D. Y., Mochizuki, M., Kita, S., Miwa, Y., Takahashi-Yanaga, F., Iwamoto, T., Ohtsuki, I., and Sasaguri, T. (2007) Knock-in mouse model of dilated cardiomyopathy caused by troponin mutation. *Circ Res* **101**, 185-194

141. Robinson, P., Griffiths, P. J., Watkins, H., and Redwood, C. S. (2007) Dilated and hypertrophic cardiomyopathy mutations in troponin and alpha-tropomyosin have opposing effects on the calcium affinity of cardiac thin filaments. *Circ Res* **101**, 1266-1273

142. Hibberd, M. G., and Jewell, B. R. (1982) Calcium- and length-dependent force production in rat ventricular muscle. *J Physiol* **329**, 527-540

143. Smith, S. H., and Fuchs, F. (1999) Effect of ionic strength on length-dependent Ca(2+) activation in skinned cardiac muscle. *J Mol Cell Cardiol* **31**, 2115-2125

144. Solaro, R. J., Henze, M., and Kobayashi, T. (2013) Integration of Troponin I Phosphorylation With Cardiac Regulatory Networks. *Circulation Research* **112**, 355-366

145. Dubois, E., Richard, V., Mulder, P., Lamblin, N., Drobecq, H., Henry, J. P., Amouyel, P., Thuillez, C., Bauters, C., and Pinet, F. (2011) Decreased serine207 phosphorylation of troponin T as a biomarker for left ventricular remodelling after myocardial infarction. *Eur Heart J* **32**, 115-123

146. Scruggs, S. B., and Solaro, R. J. (2011) The significance of regulatory light chain phosphorylation in cardiac physiology. *Archives of Biochemistry and Biophysics* **510**, 129-134

147. James, J., and Robbins, J. (2011) Signaling and Myosin-binding Protein C. *Journal of Biological Chemistry* **286**, 9913-9919

148. McNally, E. M., Kraft, R., Bravo-Zehnder, M., Taylor, D. A., and Leinwand, L. A. (1989) Full-length rat alpha and beta cardiac myosin heavy chain sequences. Comparisons suggest a molecular basis for functional differences. *J Mol Biol* **210**, 665-671

149. van der Velden, J., Moorman, A. F., and Stienen, G. J. (1998) Age-dependent changes in myosin composition correlate with enhanced economy of contraction in guinea-pig hearts. *J Physiol* **507 (Pt 2)**, 497-510

150. Rundell, V. L., Manaves, V., Martin, A. F., and de Tombe, P. P. (2005) Impact of beta-myosin heavy chain isoform expression on cross-bridge cycling kinetics. *Am J Physiol Heart Circ Physiol* **288**, H896-903

151. Locher, M. R., Razumova, M. V., Stelzer, J. E., Norman, H. S., Patel, J. R., and Moss, R. L. (2009) Determination of rate constants for turnover of myosin isoforms in rat myocardium: implications for in vivo contractile kinetics. *Am J Physiol Heart Circ Physiol* **297**, H247-256

152. Locher, M. R., Razumova, M. V., Stelzer, J. E., Norman, H. S., and Moss, R. L. (2011) Effects of low-level α-myosin heavy chain expression on contractile kinetics in porcine myocardium. *Am J Physiol Heart Circ Physiol* **300**, H869-878

153. Reiser, P. J., and Kline, W. O. (1998) Electrophoretic separation and quantitation of cardiac myosin heavy chain isoforms in eight mammalian species. *Am J Physiol* **274**, H1048-1053

154. Krenz, M., and Robbins, J. (2004) Impact of beta-myosin heavy chain expression on cardiac function during stress. *J Am Coll Cardiol* **44**, 2390-2397

155. Korte, F. S., Herron, T. J., Rovetto, M. J., and McDonald, K. S. (2005) Power output is linearly related to MyHC content in rat skinned myocytes and isolated working hearts. *Am J Physiol Heart Circ Physiol* **289**, H801-812

156. Lehman, W., Hatch, V., Korman, V., Rosol, M., Thomas, L., Maytum, R., Geeves, M. A., Van Eyk, J. E., Tobacman, L. S., and Craig, R. (2000) Tropomyosin and actin isoforms modulate the localization of tropomyosin strands on actin filaments. *Journal of Molecular Biology* **302**, 593-606

157. Geeves, M. A., and Lehrer, S. S. (1994) Dynamics of the muscle thin filament regulatory switch: the size of the cooperative unit. *Biophys J* **67**, 273-282

APPENDICES

APPENDIX A

UIC UNIVERSITY OF ILLINOIS AT CHICAGO

January 18, 2012

Sumeyye Yar
Physiology & Biophysics
M/C 901

Dear Dr. Yar:

Office of Animal Care and
Institutional Biosafety Committees (MC 672)
Office of the Vice Chancellor for Research
206 Administrative Office Building
1737 West Polk Street
Chicago, Illinois 60612-7227

The protocol indicated below was reviewed at a convened ACC meeting in accordance with the Animal Care Policies of the University of Illinois at Chicago on **1/17/2012**. *The protocol is approved for a period of* ***3*** years with annual continuation.

Title of Application: Mechanism of Control of Cardiac Dynamics by the Mobile Domain of Cardiac Troponin-1 in Health and Disease

ACC Number: 11-227

Initial Approval Period: 1/17/2012 to 1/17/2013

Current Funding: ***Portions of this protocol are supported by the funding sources indicated in the table below.***
Number of funding sources: 1

Funding Agency	**Funding Title**			**Portion of Proposal Matched**
AHA- American Heart Association	*Mechanism of Control of Cardiac Dynamics by the Mobile Domain of Cardiac Troponin-l in health and disease*			*Matched*
Funding Number	**Current Status**	**UIC PAF NO.**	**Performance Site**	**Funding PI**
12PRE9260034	*Funded*	*2012-00130*	*UIC*	*Sumeyye Yar*

This institution has Animal Welfare Assurance Number A3460.01 on file with the Office of Laboratory Animal Welfare (OLAW), NIH. **This letter may only be provided as proof of IACUC approval for those specific funding sources listed above in which all portions of the funding proposal are matched to this ACC protocol.**

In addition, all investigators are responsible for ensuring compliance with all federal and institutional policies and regulations related to use of animals under this protocol and the funding sources listed on this protocol. Please use OLAW's "*What Investigators Need to Know about the Use of Animals*" (http://grants.nih.gov/grants/olaw/InvestigatorsNeed2Know.pdf) as a reference guide. Thank you for complying with the Animal Care Policies and Procedures of UIC.

Sincerely yours,

Bradley Merrill, PhD
Chair, Animal Care Committee
BM/*SS*
cc: BRL, ACC File, Beata M. Wolska, Lindsey Duncan, R. John Solaro, **PAF # 2012-00130**

APPENDIX B

UIC UNIVERSITY OF ILLINOIS AT CHICAGO

Office of Animal Care and Institutional
Biosafety Committee (OACIB) (M/C 672)
Office of the Vice Chancellor for Research
206 Administrative Office Building
1737 West Polk Street
Chicago, Illinois 60612

7/19/2013

R. John Solaro
Physiology & Biophysics
M/C 901

Dear Dr. Solaro:

The protocol indicated below was reviewed in accordance with the Animal Care Policies and Procedures of the University of Illinois at Chicago and **will be renewed on 7/19/2013.**

Title of Application: **Combined Mice Breeding Colonies**
ACC NO: **11-112**
Original Protocol Approval: **8/15/2011 (3 year approval with annual continuation required).**
Current Approval Period: **7/19/2013 to 7/19/2014**

Funding: ***Portions of this protocol are supported by the funding sources indicated in the table below.***
Number of funding sources: 2

Funding Agency	**Funding Title**			**Portion of Funding Matched**
NIH	*Troponin Modulation In Heart Failure*			*Protocol is linked to form G 12-054*
Funding Number	**Current Status**	**UIC PAF NO.**	**Performance Site**	**Funding PI**
RO1 HL064035 (years 11-15)	*Funded*	*2009-01189*	*UIC*	*R. John Solaro*

Funding Agency	**Funding Title**			**Portion of Funding Matched**
NIH	*Integrated Mechanisms Of Cardiac Maladaptation*			*Protocol is linked to form G 13-055*
Funding Number	**Current Status**	**UIC PAF NO.**	**Performance Site**	**Funding PI**
PO1 HL062426 (years 11-15)	*Funded*	*2009-06478*	*UIC*	*R. John Solaro*

This institution has Animal Welfare Assurance Number A3460.01 on file with the Office of Laboratory Animal Welfare, NIH. **This letter may only be provided as proof of IACUC approval for those specific funding sources listed above in which all portions of the grant are matched to this ACC protocol.**

Thank you for complying with the Animal Care Policies and Procedures of the UIC.

Sincerely,

Bradley Merrill, PhD
Chair, Animal Care Committee

BM/*kg*
cc: BRL, ACC File, Corey McCoy, Catherine Osborn

Phone (312) 996-1972 • Fax (312) 996-9088

APPENDIX C

UIC UNIVERSITY OF ILLINOIS AT CHICAGO

April 9, 2012

R. John Solaro
Physiology & Biophysics
M/C 901

Office of Animal Care and
Institutional Biosafety Committees (MC 672)
Office of the Vice Chancellor for Research
206 Administrative Office Building
1737 West Polk Street
Chicago, Illinois 60612-7227

Dear Dr. Solaro:

The protocol indicated below has been reviewed in accordance with the Institutional Biosafety Committee Policies of the University of Illinois at Chicago on 3/8/2012. *The protocol was not initiated until final clarifications were reviewed and approved on* ***3/26/2012 with the following condition. Protocol expires 3 years from the date of review (3/8/2015).***

Title of Application: Modulation of Cardiac Filament Activity

IBC Number: 12-012

Highest Biosafety Level: 2

Condition of Approval: The enclosed report indicates the training status for bloodborne pathogen (BBP) training. Only those personnel who have been trained and whose training has not expired are approved for work that may involve exposure to bloodborne pathogens. Please note that federal regulations require yearly training for BBP.

You may forward this letter of acceptable IBC verification of your research protocol to the funding agency considering this proposal. **Please be advised that investigators must report significant changes in their research protocol to the IBC office via a letter addressed to the IBC chair prior to initiation of the change. If a protocol changes in such a manner as to require IBC approval, the change may not be initiated without IBC approval being granted.**

Thank you for complying with the UIC's Policies and Procedures.

Sincerely,

Randal C. Jaffe, Ph.D.
Chair, Institutional Biosafety Committee

RCJ/mbb

Enclosures

Cc: IBC file, Chad Warren, Madhu Gupta

APPENDIX D

ASBMB Journals - Copyright Permission Policy

Copyright Permission Policy

These guidelines apply to the reuse of articles, figures, charts and photos in the *Journal of Biological Chemistry*, *Molecular & Cellular Proteomics* and the *Journal of Lipid Research*.

For authors reusing their own material:

Authors need **NOT** contact the journal to obtain rights to reuse their own material. They are automatically granted permission to do the following:

- Reuse the article in print collections of their own writing.
- Present a work orally in its entirety.
- Use an article in a thesis and/or dissertation.
- Reproduce an article for use in the author's courses. (If the author is employed by an academic institution, that institution also may reproduce the article for teaching purposes.)
- Reuse a figure, photo and/or table in future commercial and noncommercial works.
- Post a copy of the paper in PDF that you submitted via BenchPress.
- Link to the journal site containing the final edited PDFs created by the publisher.

EXCEPTION: If authors select the Author's Choice publishing option:

- The final version of the manuscript will be covered under the Creative Commons Attribution license (CC BY), the most accommodating of licenses offered. Click here for details.
- The final version of the manuscript will be released immediately on the publisher's website and PubMed Central.

Please note that authors must include the following citation when using material that appeared in an ASBMB journal:

"This research was originally published in Journal Name. Author(s). Title. *Journal Name*. Year; Vol:pp–pp. © the American Society for Biochemistry and Molecular Biology."

For other parties using material for noncommercial use:

Other parties are welcome to copy, distribute, transmit and adapt the work — at no cost and without permission — for noncommercial use as long as they attribute the work to the original source using the citation above.

Examples of noncommercial use include:

- Reproducing a figure for educational purposes, such as schoolwork or lecture presentations, with attribution.
- Appending a reprinted article to a Ph.D. dissertation, with attribution.

VITA

NAME **Sumeyye YAR**

e-mail **yar.sumeyye@gmail.com**

EDUCATION

University of Illinois at Chicago, Chicago-IL
Ph.D. Biochemistry and Molecular Genetics, 2013

Rush University, Chicago-IL
M.S. Biotechnology, 2009

Sabanci University, Istanbul, TURKEY
B.S. Biological Sciences and Bioengineering, 2007

HONORS/ AWARDS

Honorable mention in poster competition, College of Medicine Research Forum, UIC, Chicago-IL (2012)

Best abstract award, Center for Cardiovascular Research day, UIC, Chicago-IL (2012)

Outstanding poster award, Myofilament Meeting, Madison-WI (2012)

Pre-doctoral fellowship, American Heart Association (2011-2013)

Chancellor's graduate fellowship, UIC, Chicago-IL (2011-2013)

The Arthur V. Prancan award for excellence in biotechnology program, Rush University, Chicago-IL (2009)

3rd Best Poster Prize, European Molecular Biology Organization (EMBO) young scientists forum, Istanbul, TURKEY (2008)

PUBLICATIONS/ PRESENTATIONS

Refereed Journal Articles

Yar, S., Chowdhury, S. A., Davis, R. T., 3rd, Kobayashi, M., Monasky, M. M., Rajan, S., Wolska, B. M., Gaponenko, V., Kobayashi, T., Wieczorek, D. F., and Solaro, R. J. (2013) Conserved Asp-137 Is Important for both Structure and Regulatory Functions of Cardiac alpha-Tropomyosin (alpha-TM) in a Novel Transgenic Mouse Model Expressing alpha-TM-D137L. *J Biol Chem* 288, p.16235-16246

Aydin, M., Bal, E., Yesilirmak, F., Dinler, G., **Yar, S.**, Konarev, P.V., Petoukhov, M.V., Roessle, M., Kikhney, A.G., Shang, W., Svergun, D.I., Sayers, Z. Comparative Characterization of Apo-, Reconstituted- and *in vivo*-Folded forms of a durum Wheat Metallothionein**.** *J Biol Chem* (In revision)

Yar, S., Solaro, R.J., Myofilament function in heart failure. *Pflugers Archiv, European Journal of Physiology, Special issue "Heart Failure"*. Review. (In preparation)

Refereed Conference Proceedings

Yar, S., Chowdhury, S. A.,Mathew, T., Rajan, S., Wolska, B. M., Gaponenko, V., Debold, E.P., Kobayashi, T., Wieczorek, D. F., and Solaro, R. J. (2013) Altered flexibility affects regulatory functions of cardiac α-tropomyosin (α-Tm) in a novel transgenic mouse model expressing α-Tm-D137L. *Biohys J.* 104 (2) pp.448a (Suppl. 1)

Dinler, G., Yesilirmak, F., **Yar, S.,** Collak, F., Sayers, Z. (2008) Plant Type 1 Metallothioneins: Candidates for Intrinsically Unstructured Proteins. *Biohys J.*, 94 (2) pp.917

Poster Presentations (*Selected*)

Yar, S., Chowdhury, S. A., Rajan, S., Wolska, B. M., Gaponenko, V., Kobayashi, T., Wieczorek, D. F., and Solaro, R. J. (2012) Effects of decreased flexibility on structure and regulatory functions of cardiac α-tropomyosin (α-Tm) in a novel transgenic mouse model expressing α-Tm-D137L. *College of Medicine Research Forum, UIC, Chicago, IL* **(Honorable Mention)**

Yar, S., Chowdhury, S. A., Wolska, B. M., Kobayashi, T., Warren, M.C., Monasky, M. M., Rajan, S., Wieczorek, D. F., and Solaro, R. J. (2012) Conserved Asp137 provides physiologically important structural flexibility to α-tropomyosin for its regulatory function in ejecting mouse hearts. *Myofilament meeting, Madison, WI* **(Outstanding Poster Award)**

Yar, S., Chowdhury, S. A., Wolska, B. M., Kobayashi, T., Warren, M.C., Monasky, M. M., Rajan, S., Wieczorek, D. F., and Solaro, R. J. (2012) Molecular and functional characterization of a novel transgenic mouse model over expressing α-Tm-D137L; a flexibility mutant. *Biophysical Society 56th Annual Meeting, San Diego, CA*

Yar, S., Dinler, G., Yesilirmak, F., Sayers, Z. (2008) Structural Study of Triticum durum metallothionein. *European Molecular Biology Organization (EMBO) young scientists' forum, Istanbul, TURKEY.* **(3rd Best Poster Award)**

Oral Presentations

Yar, S. (2012) Conserved Asp137 provides physiologically important structural flexibility to α-tropomyosin for its regulatory function in ejecting mouse hearts. *Myofilament meeting, Madison, WI* (**speaker as the recipient of the outstanding poster award**)